https://doi.org/10.15388/vu.thesis.210
https://orcid.org/ 0000-0001-5912-3652

VILNIUS UNIVERSITY

CENTRE OF PHYSICAL SCIENCES AND TECHNOLOGY

Ligita

VALEIKIENĖ

Synthesis of new layered double hydroxides, modification and investigation of properties

DOCTORAL DISSERTATION

Natural sciences,
Chemistry (N 003)

VILNIUS 2021

This dissertation was written between 2017 and 2021 at Vilnius University.

Academic Supervisor:

Prof. Habil. Dr. Aivaras Kareiva (Vilnius University, Natural Sciences, Chemistry – N 003).

Academic Consultant:

Assoc. Prof. Dr. Inga Grigoravičiūtė-Puronienė (Vilnius University, Natural Sciences, Chemistry – N 003).

This doctoral dissertation will be defended in a public meeting of the Dissertation Defence Panel:

Chairman – **Prof. Habil. Dr. Eugenijus Norkus** (Centre for Physical Sciences and Technology, Natural Sciences, Chemistry – N 003).

Members:

Dr. Jurga Juodkazytė (Centre for Physical Sciences and Technology, Natural Sciences, Chemistry – N 003).
Prof. Dr. Raimundas Šiaučiūnas (Kaunas University of Technology, Technological Sciences, Chemical Engineering – T 005).
Prof. Dr. Aušra Valiūnienė (Vilnius University, Natural Sciences, Chemistry – N 003).
Prof. Dr. Vida Vičkačkaitė (Vilnius University, Natural Sciences, Chemistry – N 003).

The dissertation shall be defended at a public/closed meeting of the Dissertation Defence Panel at 14 p.m. on 8 October 2021 in Inorganic Chemistry auditorium 141 of the Institute of Chemistry, Faculty of Chemistry and Geoscience, Vilnius University. Address: Naugarduko str. 24, LT-03225 Vilnius, Lithuania. Tel.: +370 5 2193108. Fax: +370 5 2330987.

The text of this dissertation can be accessed at the libraries of (name of the institutions granted the right to conduct doctoral studies in alphabetical order), as well as on the website of Vilnius University:
www.vu.lt/lt/naujienos/ivykiu-kalendorius

https://doi.org/10.15388/vu.thesis.210
https://orcid.org/ 0000-0001-5912-3652

VILNIAUS UNIVERSITETAS

FIZINIŲ IR TECHNOLOGIJOS MOKSLŲ CENTRAS

Ligita

VALEIKIENĖ

Naujų sluoksniuotų dvigubų hidroksidų sintezė, modifikavimas ir savybių tyrimas

DAKTARO DISERTACIJA

Gamtos mokslai,
Chemija (N 003)

VILNIUS 2021

Disertacija rengta 2017 – 2021 metais studijuojant doktorantūroje Vilniaus universiteto Chemijos ir geomokslų fakulteto Chemijos institute.

Mokslinis vadovas:

Prof. habil. dr. Aivaras Kareiva (Vilniaus universitetas, gamtos mokslai, chemija – N 003).

Mokslinė konsultantė:

Doc. dr. Inga Grigoravičiūtė-Puronienė (Vilniaus universitetas, gamtos mokslai, chemija – N 003).

Gynimo taryba:
Pirmininkas – **prof. habil. dr. Eugenijus Norkus** (Fizinių ir technologijos mokslų centras, gamtos mokslai, chemija – N 003).

Nariai:
dr. Jurga Juodkazytė (Fizinių ir technologijos mokslų centras, gamtos mokslai, chemija – N 003);
prof. dr. Raimundas Šiaučiūnas (Kauno technologijos universitetas, technologijos mokslai, chemijos inžinerija – T 005);
prof. dr. Aušra Valiūnienė (Vilniaus universitetas, gamtos mokslai, chemija – N 003);
prof. dr. Vida Vičkačkaitė (Vilniaus universitetas, gamtos mokslai, chemija – N 003).

Disertacija ginama viešame Gynimo tarybos posėdyje 2021 m. spalio mėn. 8 d. 14 val. Vilniaus universiteto Chemijos ir geomokslų fakulteto Chemijos instituto Neorganinės chemijos auditorijoje.

Adresas: Naugarduko g. 24, LT-03225 Vilnius, Lietuva. Tel.: 2193108. Faksas: 2330987.

Disertaciją galima peržiūrėti Vilniaus universiteto, Fizinių ir technologijos mokslų centro bibliotekose ir VU interneto svetainėje adresu:
www.vu.lt/lt/naujienos/ivykiu-kalendorius

CONTENTS

LIST OF ABBREVIATIONS

LDH	Layered Double Hydroxide
MMO	Mixed Metal Oxides
XRD	X – ray diffraction
TG	Termogravimetry
DTA	Differential Thermal Analysis
SEM	Scaning Electron Microscopy
FTIR	Fourier Transform Infrared
BET	Brunauer – Emmet – Teller method
BJH	Barret – Joyner – Halenda method
EDX	Energy – dispersive X – ray spectroscopy
ICP OES	Inductive coupled plasma optical emission spectroscopy
ICP	Inductive coupled plasma
PL	Photoluminescence emission
PLE	Photoluminescence emission and excitation

INTRODUCTION

Recently layered double hydroxides (LDHs) have attracted substantial attention due to a wide range of important application areas, e.g. catalysis, photochemistry, electrochemistry, magnetization, biomedical science, environmental applications, and optics [1-15]. LDHs have a large surface area, high anion exchange capacity comparable to those of anion exchange resins and good thermal stability [1, 6-8].

A general chemical formula of the LDHs can be expressed as $[M^{2+}_{1-x}M^{3+}_{x}(OH)_2]^{x+}(A^{y-})_{x/y}\cdot zH_2O$, where M^{2+} (Mg, Zn, Co, Ni, Cu, Mn, . . .) and M^{3+} (Al, Ga, Cr, Co, Fe, V, Y, Mn, . . .) are divalent and trivalent metal cations, respectively, and A^{y-} is an intercalated anion which is located in the interlayer spaces along with water molecules and compensates the positive charge created by the partial substitution of M^{2+} by M^{3+} in a positively charged metal hydroxide layers [16-19]. LDHs exhibit excellent ability to adopt organic and inorganic anions [13, 20].

LDHs can be fabricated by different synthesis methods. The most common preparation technique is co-precipitation method starting from soluble salts of the metals [21-23]. The most common second technique for the preparation of LDHs is anion-exchange [24-27]. The indirect sol-gel synthesis route for the preparation of LDHs recently was also developed [28-30]. The synthesized precursor gels were converted to the mixed metal oxides (MMO) by heating the gels at 650 °C. The LDHs were fabricated by reconstruction of MMO in deionized water at 80 °C. The proposed sol-gel synthesis route for LDHs showed some benefits over the co-precipitation method such as simplicity, high homogeneity and good crystallinity of the end synthesis products, effectiveness, cost efficiency and suitability for different systems.

Intercalation of layered double hydroxides (LDHs) with different anions is very attractive and important area, since the anion-exchange capacity can mostly be used to change chemical and physical properties of LDHs [16, 31-33]. It was demonstrated that the combination of the lanthanide elements in the layers of LDHs, the luminescent materials could be obtained [28, 34, 35]. Lanthanide doped LDH materials could be useful in many fields such as medicine, photochemistry, catalysis, environmental applications and fundamental investigations [36-41]. However, in many cases these LDHs are limited by the low emission intensity arising from the direct coordination of water molecules and hydroxyl groups to the RE centre in the layer. It was shown that intercalation of lanthanide-doped LDH materials with sensitizing anions allows to solve partially this problem [30, 42-44]. An efficient energy

transfer between host and guest organic anions in the interlayer galleries influences the luminescence properties significantly.

The aim of this PhD thesis was to synthesize new Mg-Al-based layered double hydroxides by modifying its chemical composition, to investigate cation and anion substitution effects on the formation of the end products and to investigate properties of obtained LDHs. To achieve this, the main tasks were formulated as follows:

1. To investigate transition metal substitution effects in $Mg_{3-x}M_x/Al_1$ (M = Mn, Co, Ni, Cu, Zn) LDHs synthesized using the sol-gel chemistry approach.
2. To investigate alkaline earth metal substitution effects in sol-gel derived $Mg_{2-x}M_x/Al_1$ (M = Ca, Sr, Ba) LDHs and related mixed-metal oxides. To investigate the reconstruction peculiarities of sol-gel derived $Mg_{2-x}M_x/Al_1$ (M = Ca, Sr, Ba) LDHs.
3. To investigate the influence of ultrasound and cation substitution (Mn, Co, Ni, Cu, Zn) on the intercalation of organic anions (formate ($HCOO^-$), acetate (CH_3COO^-), oxalate ($C_2O_4^{2-}$), tartrate ($C_4H_6O_4^{2-}$) and citrate ($C_6H_5O_7^{3-}$)) to the structure of Mg_3/Al_1 LDHs.
4. To synthesize the $Mg_3Al_{1-x}Cr_x$ LDH samples using an aqueous sol-gel method and investigate effect of Cr^{3+} substitution on phase purity, morphological and luminescent properties of obtained end products.

The novelty and originality of PhD thesis. The transition metal substitution effects in $Mg_{3-x}M_x/Al_1$ (M = Mn, Co, Ni, Cu, Zn) LDHs synthesized by sol-gel synthesis method were investigated. The alkaline earth metal substitution effects in $Mg_{2-x}M_x/Al_1$ (M = Ca, Sr, Ba) LDHs synthesized by sol-gel synthesis method were investigated. The reconstruction peculiarities of sol-gel derived $Mg_{2-x}M_x/Al_1$ (M = Ca, Sr, Ba) LDHs by changing proceeding conditions were investigated. The chromium-substituted $Mg_3Al_{1-x}Cr_x$ LDH samples were fabricated using an aqueous sol-gel method and luminescent properties of obtained specimens were investigated.

1. LITERATURE OVERVIEW

1.1. Basic structural aspects of layered double hydroxides

Layered double hydroxides have two-dimensional structure which consists of positively charged layers and exchangeable interlayer anions [45-48]. A general chemical formula of the LDHs can be expressed as $[M^{2+}_{1-x}M^{3+}_{x}(OH)_2]_x^+(An^-)_{x/n}\cdot yH_2O$, where M^{2+} (Mg, Zn, Ni, Co, ..) and M^{3+} (Al, Ga, Cr, ..) are divalent and trivalent metal cations, respectively. An^- is an intercalated n− valence inorganic (CO_3^{2-}, OH^-, NO_3^-, SO_4^{2-}, ClO_4^-) or even organic acid anion which is located in the interlayer spaces along with water molecules and compensates the positive charge created by the partial substitution of M^{2+} by M^{3+} in a positively charged metal hydroxide layers [18, 19, 49, 50].

The parent material of LDH class is a mineral hydrotalcite, or anionic clay, discovered in Sweden around 1842, namely hydroxycarbonate of magnesium and aluminium, $Mg_6Al_2(OH)_{16}CO_3\cdot 4H_2O$, occurs in foliated and contorted plates and/or fibrous masses. Hydrotalcites consist of a positively charged two-dimensional brucite- (magnesium hydroxide) like layer, with anionic species in the interlayer to form neutral molecules [1]. LDHs are consequently also known as hydrotalcite-like materials [45, 51]. Although the stoichiometry of hydrotalcite was first correctly determined by Manasse (University of Florence) in 1915, the main structural features of LDHs were revealed by Allmann and Taylor in the 1960s [45, 11-14] performing the single crystal X-ray diffraction studies on the mineral samples.

The basic layer structure of LDHs is based on that of brucite $Mg(OH)_2$, which is of the CdI_2 type (space group P-3m1; Z=1; Mg: 0, 0, 0; O and H: 1/3, 2/3, *z*), and is built up by (001) layers of edge-sharing octahedra occupied by magnesium cations which are 6-fold coordinated to hydroxyl groups [46, 55]. These octahedral units form infinite layers by edge-sharing, with the hydroxide (OH) ions sitting perpendicular to the plane of the layers and parallel to the c-axis (Fig. 1a) [56]. The OH ions lie alternately above and below the neighbouring layers. The layers then stack on top of one another to form the 3D structure. Both the local geometry around the metal and the close-packing of the hydroxyl anions are strongly distorted away from the idealized arrangements. However, the distortion of the brucite layers does not change the hexagonal symmetry ($a = b = 0.3142$ nm, $c = 0.4766$ nm, $\gamma = 120^\circ$) [45].

The basic structure of the LDH may be derived by substitution of a fraction of the divalent cations in the brucite-type octahedral layer by trivalent cations such that the layers gain a positive charge. This positive charge is balanced by

anionic species, which are located together with the water molecules in the interlayer gallery (Fig. 1b) [11].

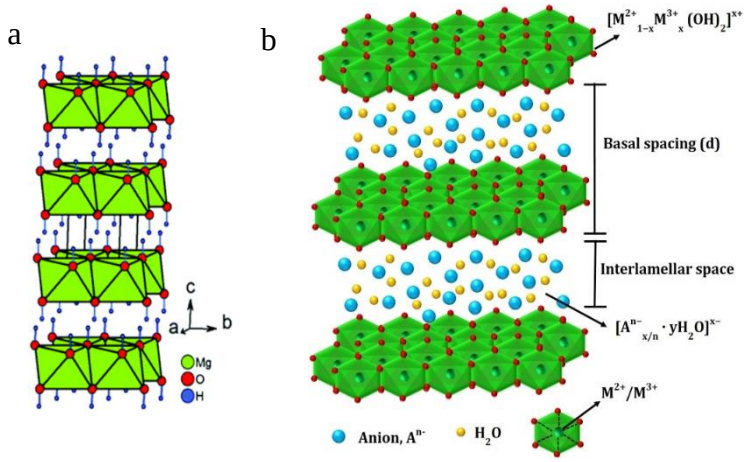

Fig. 1. Perspective view of the crystal structure of brucite (reprinted from [55]) (a) and the crystal structure of LDH (reprinted from [11]) (b).

The bonding between octahedral layers and interlayers involves a combination of electrostatic effects and hydrogen bonding [46]. LDHs have lamellar crystal structure with wide variations depending upon the identity and relative proportions of the di- and trivalent cations, as well as in the type of anions [57]. It is often said that only M^{2+} and M^{3+} ions having an ionic radius not too different from that of magnesium may be accommodated in the octahedral sites in the brucite-like layers to form LDH compounds and that cations which are too small or too large give rise to other types of compounds, and also that the most reliable composition range corresponds approximately to $0.2 \leq x \leq 0.4$ [45, 58]. LDHs are characterized by an opened structure that is suitable for physico-chemical intercalation and adsorption processes with a large variety of molecules ranging from organic molecules to biomacromolecules. Regarding the anions, their size/charge ratio is important i.e. there should be a host-guest relationship in between the host inorganic layer and the dimensions of guest species in the interlayer [11].

As a result, a large class of isostructural materials can be obtained by changing the nature of the metal cations, the molar ratios of M^{2+}/M^{3+} as well as the type of interlayer anions. Compositional diversity in the brucite-like layers and in the interlayer anions leads to widely varied physicochemical properties of materials and functional diversity which allows LDHs to be used for a variety of applications.

1.2. Synthesis methods of layered double hydroxides

LDHs can be fabricated by different synthesis methods, such as co-precipitation, sol-gel, hydrothermal, combustion synthesis and synthesis using microwave irradiation [45, 59-63]. Here only the most commonly used and described in the literature synthesis techniques will be discussed in more details.

The conventional approach for the synthesis of LDHs is co-precipitation method, which can be shortly described as follows. The addition of a base to an aqueous solution containing the salts of different metals, usually M^{2+} (or mixtures of M^{2+} species) and M^{3+} (or mixtures of M^{3+} species), and the anion that is to be incorporated into the lamellar structure gives rise the precipitation of the metal hydroxides and the subsequent formation of LDHs. Then the precipitates are collected, washed and dried to be deposited on a solid substrate, or dispersed in solution phase [21-23]. In order to ensure simultaneous precipitation of two or more cations, it is necessary to carry out the synthesis under conditions of supersaturation, which is attained by controlling the pH of the solution (as if the pH value too low does not allow the complete precipitation of all metallic ions, while a too high value leads to the leaching of one or more metallic ions) [45, 61]. Following co-precipitation, a thermal treatment process is often performed in order to increase yields and/or the crystallinity of amorphous or poorly crystallized materials [45].

The most common second an indirect technique for the preparation of LDHs (especially useful for the preparation of noncarbonate LDHs) is based on the classical anion exchange process [2, 24-27]. The method is carried out in one of two processes shown schematically as follows:

$$LDH \cdot A^{m-} + X^{n-} \rightarrow LDH \cdot (X^{n-})_{m/n} + A^{m-} \qquad (1)$$

where A^{m-} and X^{n-} represent the original anion and the anion used to exchange the original anion, respectively. Briefly, the LDH are prepared by co-precipitation (or other) method with host anions, most commonly NO_3^-, CO_3^{2-} and Cl^-, as the exchange is easier than multi charged anions [11, 64]. In the later process, anions present in the interlayer are exchanged with the specific anions by stirring the LDH precursor in a solution containing an excess of anion to be intercalated into the structure [11]. A large number of organic and inorganic anions have been incorporated in LDHs using the ion-exchange process [45].

Recently, a novel, environmentally friendly and effective sol-gel synthesis route was developed for the preparation of Mg-Al LDHs. This method was successfully applied to study the possibility of partially substituting aluminium by bismuth and cerium in LDHs [28, 29]. The synthesized precursor gels were converted to the mixed metal oxides (MMO) by heating the gels at 650 °C. The LDHs were fabricated by reconstruction of MMO in deionized water at 80 °C. Indeed, it is known that these materials benefit from the so-called "memory effect", allowing the reconstruction of the lamellar structure by rehydration of the MMO [65, 66]. The proposed sol-gel synthesis route for LDHs showed some benefits over the co-precipitation method such as simplicity, high homogeneity and good crystallinity of the end synthesis products, effectiveness, cost efficiency and suitability for different systems.

1.3. Intercalation of layered double hydroxides

The interlayer domains of LDHs contain anions, water molecules and sometimes other neutral or charged moieties [45, 58]. Relatively weak bonding occurs between the interlayer ions or molecules and the brucite-like sheets and as a consequence LDH materials exhibit excellent expanding properties. A key feature of LDHs materials is therefore their anionic exchange capacity, which makes them unique as far as inorganic materials are concerned. A great variety of anionic species can be introduced into the interlayer regions of LDHs through direct syntheses such as co-precipitation, or post-synthesis modifications, such as anion exchange [24-27, 45]. Incorporated anions can be simple ones, such as carbonate, nitrate or chloride, or larger organic anions, such as carboxylates or sulfonates or inorganic polyoxometalates such as Keggin, Finke, or Dawson-type anions [45, 67, 68].

Intercalation of layered double hydroxides with different anions is very attractive and important area, since the anion-exchange capacity can mostly be used to change chemical and physical properties of LDHs [16, 31-33]. Recently, the influence of the origin of organic anion (oxalate, laurate, malonate, succinate, tartrate, benzoate, 1,3,5-benzentricarboxylate, 4-methylbenzoate, 4-dimethylaminobenzoate and 4-biphenylacetonate) on the evolution of the chemical composition of the inorganic–organic LDHs system and on the luminescence properties of the Eu^{3+} doped LDHs containing these organic anions was investigated [13]. The X-ray diffraction analysis results showed that the positions of diffraction peaks (003) of LDHs intercalated with anions were shifted to smaller 2θ angle values in the XRD patterns. It was concluded that depending on the size these anions could have specific vertical or horizontal orientations in the LDH structure. Intercalation chemistry of

LDH materials and the advantages, disadvantages, and application possibilities of anion intercalated LDHs have been briefly summarized in [69, 70].

1.4. Applications of layered double hydroxides

LDHs have anionic exchange capacity, and the ability to capture organic and inorganic anions makes them almost unique as inorganic materials [45]. LDHs are widely used in catalysis, adsorption, pharmaceutics, photochemistry, electrochemistry and many other areas [1, 9, 11, 71-75]

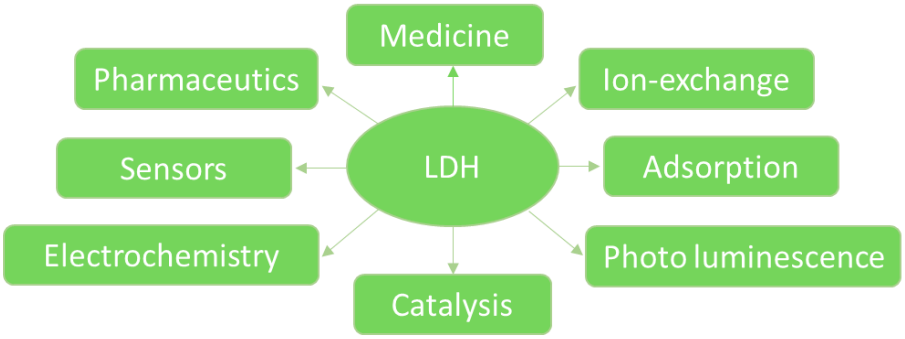

Fig. 2. Different applications of LDHs.

LDHs represent an inexpensive, versatile and potentially recyclable source of a variety of catalyst supports, catalyst precursors or actual catalysts [45, 76-79]. The application performance of LDH as photocatalyst and organic synthesis catalyst have been extensively reviewed [73, 75].

20 years ago, Aicken et al. predicted that Mg-Al LDHs can be intercalated with different guest species with the following application in medicine [81]. And soon short review articles were published on the possible application of LDHs for pharmaceutical and medical purposes [82-85]. An important feature for the biomedical application of LDH is biosafety of LDH nanoparticles [86]. In [87] it was effectively demonstrated that Mg-Al LDH nanoparticles could potentially be used in stem cell research. In the last decade the results on the application of LDHs for gen and drug delivery have been explored [88-92]. Recently, the biocompatibility of LDHs was investigated in vivo [93]. Luca et al. [94] suggested to use LDH to transfer antibiotics for therapy.

Natural or synthetic polymers and inorganic compounds including LDHs, known as bionanocomposites, show improved functional properties for

application in regenerative medicine like tissue engineering and theranostics [95-103].

It was also announced that the two-dimensional LDH based materials could possibly be used for the development of next generation biomedical devices [104-106]. Mixed metal or partially substituted LDHs bulk and thin films showed antibacterial, antimicrobial properties, high cytocompatibility and other interesting biomedical properties [107-113]. Ultrathin Ni-Fe-LDH films could possibly be used as a biomagnet [114]. LDH combined with magnetite is a suggested effective reagent for anticancer chemotherapy [115]. Mg-Fe LDH thin films were also deposited on Ti substrate [116]. Future prospects related to the application of LDHs in medicine are summarized in the review article [117].

Tran et al. [118, 119] showed that intercalated LDHs could be used as adsorbents to remove toxic metal cations and anions from aqueous media. Moreover, LDHs intercalated with succinic acid and lauric acid were used as lubricant additives [120]. Intercalated Mg-Al LDH nanosheets showed a high adsorption capability for the efficient and rapid removal of dyes [121]. LDHs intercalated with triazine-sulphonate anion showed highly efficient flame retardant performance for polypropylene [122]. The hexacyanoferrate-intercalated LDHs were used for the detection of early-stage corrosion of steel [123]. LDHs with intercalated permanganate and peroxydisulphate anions were applied for the removal of chlorinated organic solvents from the contaminated water [124].

Lanthanide doped LDH materials could be useful in many fields such as medicine, catalysis, environmental applications and fundamental investigations [125-127]. Recently it was demonstrated that the combination of the lanthanide elements in the interlayer space of LDHs, the promising luminescence materials could be obtained [28, 30, 34, 35, 44, 95, 118, 128-134]. Chromium was also used as substituent in different LDHs for the various reasons. For instance, the Cr-substituted Mg-Al LDH was successfully used as catalyst in the aldose-ketose isomerization processes [135]. Mixed oxides obtained by thermal decomposition of Cr-substituted LDHs have been studied in the reaction of hydrocarbon steam reforming for producing of hydrogen [136]. The authors [137] recently suggested to use Cr-substituted Zn-Al LDHs as UV-Vis light photocatalysts for NO gas removal from the urban environment. Finally, the spectral emission of a natural LDHs has been studied by cathodo- and photoluminescence [138]. It was concluded that the presence of Cr^{3+} ion activators induced characteristic PL emission peaks in the red-infrared region at 681, 688 and 696 nm linked to $E_2 \rightarrow {}^4A_2$ transitions.

2. EXPERIMENTAL

2.1. Materials

Aluminium nitrate nonahydrate ($Al(NO_3)_3 \cdot 9H_2O$, 98.5%, Cheaper), magnesium nitrate hexahydrate ($Mg(NO_3)_2 \cdot 6H_2O$), 99.0% Chempur), manganese nitrate tetrahydrate ($Mn(NO_3)_2 \cdot 4H_2O$, 98.0%, Chempur), cobalt nitrate hexahydrate ($Co(NO_3)_2 \cdot 6H_2O$, 99.0%, Chempur), nickel nitrate hexahydrate ($Ni(NO_3)_2 \cdot 6H_2O$, 98.0%, Chempur), copper nitrate trihydrate ($Cu(NO_3)_2 \cdot 3H_2O$, 99.0%, Chempur), zinc nitrate hexahydrate ($Zn(NO_3)_2 \cdot 6H_2O$, 99.0%, Chempur), calcium nitrate tetrahydrate ($Ca(NO_3)_2 \cdot 4H_2O$, 99.0%, Chempur), strontium nitrate ($Sr(NO_3)_2$, 99.0%, Chempur), barium nitrate ($Ba(NO_3)_2$, 99.0%, Chempur), chromium nitrate nonahydrate ($Cr(NO_3)_3 \cdot 9H_2O$, Aldrich, 99 %) were used as starting materials in the preparation of LDHs. Citric acid monohydrate ($C_6H_8O_7 \cdot H_2O$, 99.5%, Chempur) and 1,2-ethanediol ($C_2H_6O_2$, 99.8%, Chempur) were used as complexing agents in the sol-gel processing. Ammonia solution (NH_3, 25%, Chempur) was used to change pH of the solution. Sodium chloride (NaCl, 99.5%, Chempur), hydrochloric acid (HCl, 37%, Sigma-Aldrich), sodium formate (HCO_2Na), 98.0%, Alfa Aesar), ammonium oxalate monohydrate ($(NH_4)_2C_2O_4 \cdot H_2O$, 99.8%, Chempur), sodium acetate trihydrate ($CH_3COONa \cdot 3H_2O$), 99.0%, Chempur), potassium sodium tartrate tetrahydrate ($C_4H_4KNaO_6 \cdot 4H_2O$, 99.0%, Chempur) and sodium citrate dihydrate ($C_6H_5O_7Na_3 \cdot 2H_2O$, 99.0%, Chempur) were used for the intercalation of anions.

2.2. Synthesis of $Mg_{3-x}M_x/Al_1$ (M = Mn, Co, Ni, Cu, Zn) layered double hydroxides

For the synthesis of $Mg_{3-x}M_x/Al_1$ (M = Mn, Co, Ni, Cu, Zn) layered double hydroxides the stoichiometric amounts of starting materials were dissolved in distilled water under continuous magnetic stirring. Citric acid was added to the above solution and the obtained mixture was stirred for an additional 1 h at 80°C. 2 mL of 1,2-ethanediol was then added to the resulting solution. Next, the stirring was continued at 150°C for the complete evaporation of the solvent. The obtained transparent gels were dried at 105°C for 24 h. The mixed metal oxides (MMO) were obtained by heating the gels at 650°C for 4 h. The LDH powdered specimens were obtained by reconstruction of the synthesized MMO in water at 50°C for 6 h under stirring. The schematic diagram of the sol-gel processing is presented in Fig. 3.

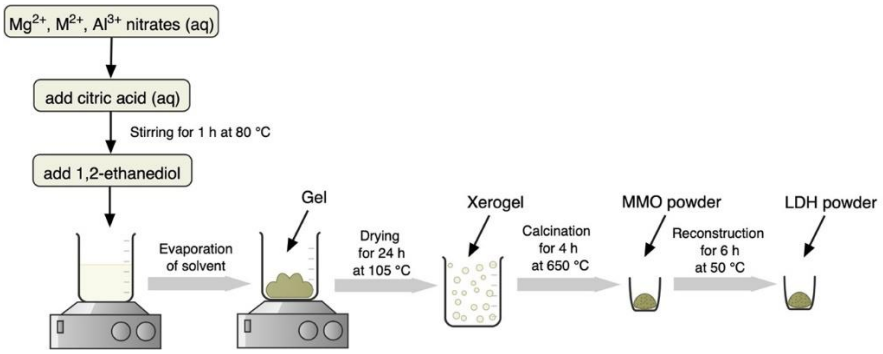

Fig. 3. Schematic diagram of sol-gel preparation of $Mg_{3-x}M_x/Al_1$ LDHs, (M = Mn, Co, Ni, Cu, Zn).

2.3. Synthesis of $Mg_{2-x}M_x/Al_1$ (M= Ca, Sr, Ba) layered double hydroxides

$Mg_{2-x}M_x/Al_1$ (M = Ca, Sr, Ba; x = 0.1) gels were synthesized by the sol-gel synthesis method depicted in Figure 3. The mixed metal oxides were obtained by heating the gels at 650°C, 800°C, and 950°C for 4 h. The $Mg_{2-x}M_x/Al_1$ (M = Ca, Sr, Ba) LDHs were obtained by reconstruction of the obtained oxides in water at 50°C for 6 h under stirring and by changing the pH of the solution to 10 with ammonia solution.

2.4. Anion exchange in Mg_3/Al_1 and $Mg_{3-x}M_x/Al_1$ (M = Mn, Co, Ni, Cu, Zn) layered double hydroxides

Mg_3/Al_1 and $Mg_{3-x}M_x/Al_1$ (M = Mn, Co, Ni, Cu, Zn) -formate, -oxalate, -acetate, tartrate and -citrate LDHs were synthesized using ion exchange method. The 0.5 g of Mg_3/Al_1 or $Mg_{3-x}M_x/Al_1$ (M = Mn, Co, Ni, Cu, Zn) LDHs was added into 500 mL of a 1 M NaCl solution containing 3.3 mM of HCl. The resultant mixture was stirred for 24 h at room temperature. The suspension was filtered, the resultant solid washed with decarbonated water and acetone for several times and dried at 40°C for 24 h. At the next step, 2 mmol of Mg_3Al_1 or $Mg_{3-x}M_x/Al_1$ (M = Mn, Co, Ni, Cu, Zn) was added in the solution of organic listed above taking 1.5 molar excess in comparison to LDH. The reaction was carried out under two different methods: (a) the mixture was mixed at room temperature for 24 h; and (b) the mixture was sonicated at room temperature for 30 min. The suspension obtained by a) or b) method was filtered, the resultant solid washed with decarbonated water and acetone for several times and dried at 40°C for 24 h.

2.5. Synthesis of $Mg_3Al_{1-x}Cr_x$ (x = 0.0, 0.01, 0.05, 0.075, 0.1 and 0.25) layered double hydroxides

The Cr-substituted $Mg_3Al_{1-x}Cr_x$ LDH samples (x = 0.0, 0.01, 0.05, 0.075, 0.1 and 0.25) were synthesized by the sol-gel synthesis method. The stoichiometric amounts of starting materials were dissolved in distilled water under continuous magnetic stirring. Citric acid was added to the above solution and the obtained mixture was stirred for an additional 1 h at 80°C. 2 mL of 1,2-ethanediol was then added to the resulting solution. Next, the stirring was continued at 150°C for the complete evaporation of the solvent. The obtained transparent gels were dried at 105°C for 24 h. The mixed metal oxides (MMO) were obtained by heating the gels at 650°C for 4 h. The LDH powdered specimens were obtained by reconstruction of the synthesized MMO in water at 50°C for 6 h under stirring.

2.6. Characterization techniques

For the characterization of phase purity of synthesized materials, the XRD analysis was performed in the 2θ range from 10 to 70° (step size of 0.02°) with a scanning speed of 2°/min using a MiniFlex II diffractometer (Rigaku, Japan) (Cu $K\alpha_1$ radiation). The FT-IR spectra were collected using an Alpha (Bruker, Inc., Germany) spectrometer. All spectra were recorded at ambient room temperature in the range of 4000–480 cm^{-1}. The morphology of synthesized LDH samples was investigated using a scanning electron microscope Hitachi SU-70 (Hitachi, Japan). Nitrogen adsorption by the BET and Barret method was used to determine the surface area and pore diameter of the materials (TriStar II 3020, Micromeritics, Norcross, GA, USA). The pore-size distribution was evaluated by the BJH procedure. Thermal analysis of synthesized samples was carried out using a simultaneous thermal analyzer STA6000 (Perkin-Elmer, Maltham, MA, USA) in air atmosphere at scan rate of 5 °C/min and the temperature range from 30°C up to 700°C. Raman scattering spectra were measured with combined Raman and SNOM microscope Alpha 300 RS (WiTec, Germany) with 532 nm excitation laser source and 20x objective. The EDX analysis of the specimens was performed using a scanning electron microscope Hitachi TM 3000 (Hitachi, Japan). Elemental analysis of the synthesized samples was also performed by ICP-OES optical emission spectrometry using Perkin-Elmer Optima 7000DV (Perkin-Elmer, Maltham, MA, USA) spectrometer. The analyzed samples were dissolved in 5% nitric acid (HNO_3, 69%, Carl Roth) and diluted to an appropriate volume. Calibration solutions were prepared by an appropriate

dilution of the stock standard solutions (single-element ICP standards 1000 mg/L, Carl Roth). The reflection, PL and PLE spectra were recorded on the Edinburg Instruments FLS980 modular spectrometer (Kirkton Campus, UK). Both excitation and emission spectra were corrected for instrument spectral response.

3. RESULTS AND DISCUSSION

3.1. Transition metal substitution effects in sol-gel derived $Mg_{3-x}M_x/Al_1$ (M = Mn, Co, Ni, Cu, Zn) layered double hydroxides

In this part, the transition metal substitution effects and limits, which could be introduced to the sol-gel derived LDHs without destroying the layered structure were investigated.

3.1.1. Characterization of synthetized $Mg_{3-x}M_x/Al_1$ (M = Mn, Co, Ni, Cu, Zn) LDHs

Fig. 4. shows XRD patterns of sol-gel derived $Mg_{3-x}Mn_x/Al_1$ LDHs. As seen, 12 mol% of manganese (II) could be introduced instead of magnesium to Mg_3Al_1 LDH without destroying the layered structure. However, with an increasing amount of transitional metal till 14 mol% the minor amount of MnO impurity phase has formed.

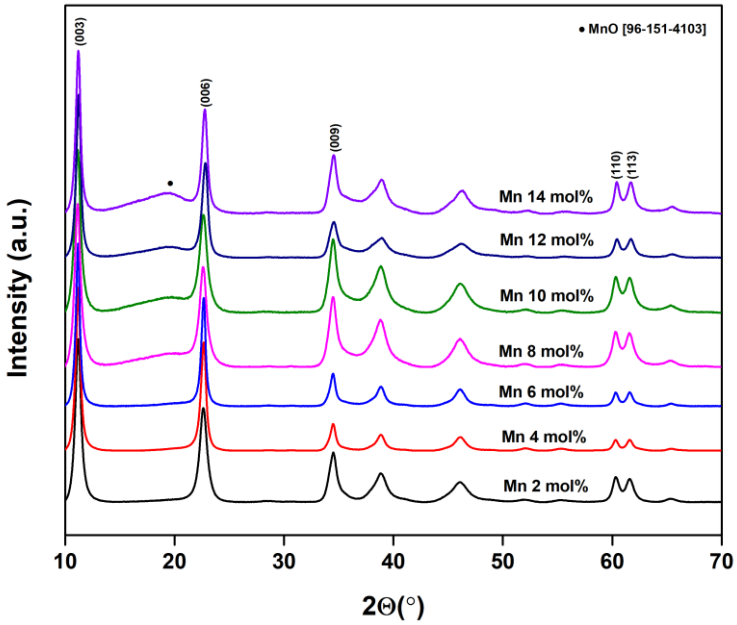

Fig. 4. XRD patterns of sol-gel derived $Mg_{3-x}Mn_x/Al_1$ LDHs

A slightly higher amount of Co (II) (14 mol%) could be introduced to the LDH structure without any structural disturbance (see Fig. 5). With futher

increase of cobalt the formation of a small amount of CoO phase was visible from the XRD pattern. The intensity of main reflections of $Mg_{3-x}Co_x/Al_1$ LDHs increases monotonically with increasing amounts of cobalt in LDHs.

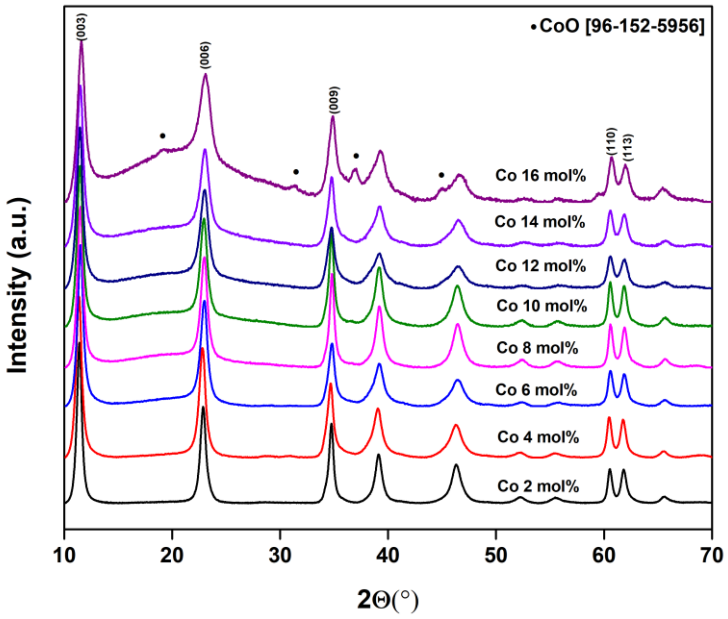

Fig. 5. XRD patterns of sol-gel derived $Mg_{3-x}Co_x/Al_1$ LDHs

As seen in Fig. 6, synthesizing Ni (II) substituted LDHs, even at low concentrations of nickel (1–5 mol%) the negligible amount of NiO phase was formed. Only 2.5 mol% of magnesium could be substituted by Cu (II) in Mg_3Al_1 LDHs without formation of impurities (see Fig. 7.).

As seen from Fig. 8, Zn (II) like manganese and cobalt substituted LDHs could be introduced to the layered structure more easily. The monophasic $Mg_{3-x}Zn_x/Al_1$ sample containing 10 mol% of zinc has been synthesized. With further increase of transition metal substituent, the formation of ZnO was not possible to avoid.

The XRD analysis results confirmed that the substitution of magnesium by transition metals in the LDHs synthesized using an aqueous sol-gel method highly depends on the nature and concentration of the transition metal. The most important parameters possibly responsible for the level of substitution of magnesium in LDHs could be an ionic crystal radius of metals and value of solubility product of appropriate metal hydroxides.

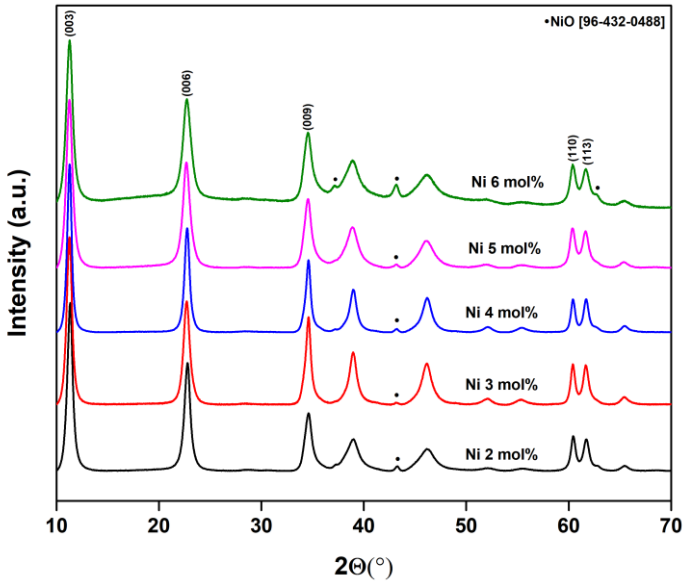

Fig. 6. XRD patterns of sol-gel derived $Mg_{3-x}Ni_x/Al_1$ LDHs

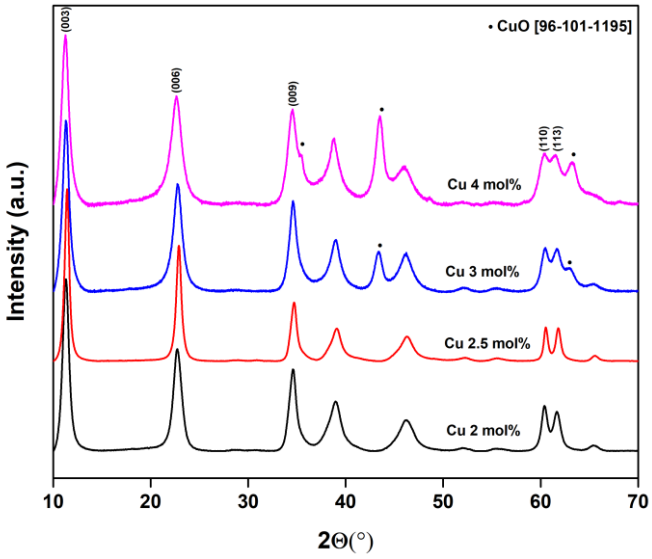

Fig. 7. XRD patterns of sol-gel derived $Mg_{3-x}Cu_x/Al_1$ LDHs

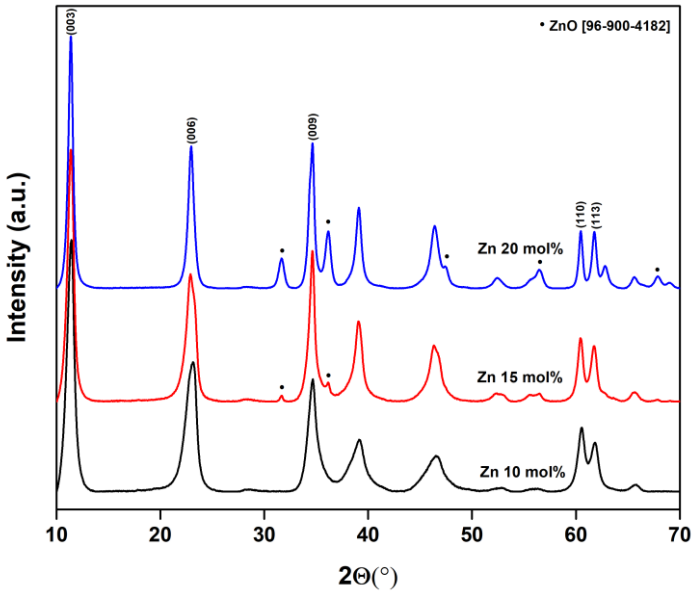

Fig. 8. XRD patterns of sol-gel derived $Mg_{3-x}Zn_x/Al_1$ LDHs

3.1.2. FT-IR spectra of $Mg_{3-x}M_x/Al_1$ (M = Mn, Co, Ni, Cu, Zn) LDHs

FT-IR spectra in the region of the representative 4000–480 cm^{-1} monophasic $Mg_{3-x}M_x/Al_1$ (M = Mn, Co, Ni, Cu and Zn) LDHs samples were almost identical independent of the nature of metal and the amount of substituent (see Fig. 9.). The broad and weak absorption bands visible in the range of wavelengths of 3600–3100 cm^{-1} and at 1630 cm^{-1} correspond to the O–H stretching vibrations in the hydroxyl layers and probably from intercalated between layers and adsorbed on the surface water molecules [130]. The narrower medium to strong absorption band visible at about 1355 cm^{-1} is attributed to the asymmetric vibration modes of ionic carbonate CO_3^{2-}. The absorption bands observed at approximately 615–610 cm^{-1} originate from the metal-oxygen stretch vibrations [130]. Thus, FT-IR spectroscopy results confirm the high reproducibility of sol-gel processing used in this study for the preparation of mixed-metal LDH samples.

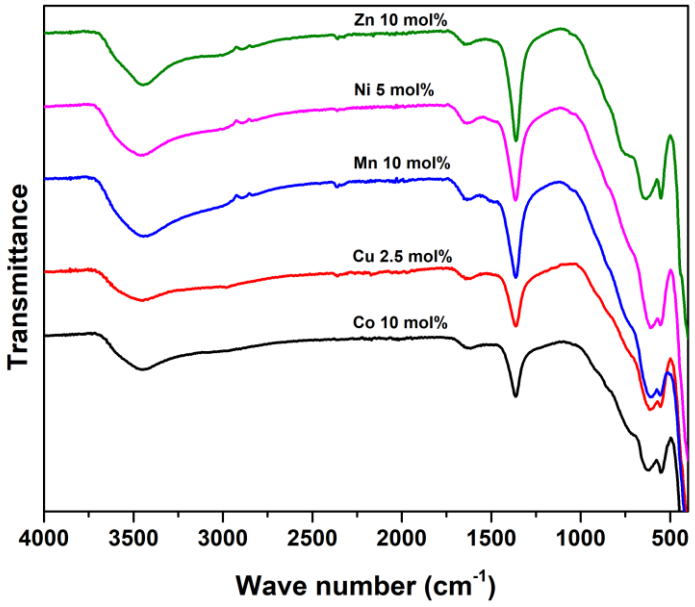

Fig. 9. FT-IR spectra of differently substituted $Mg_{3-x}M_x/Al_1$ LDHs (M = Mn, Co, Ni, Cu and Zn)

The determined N_2 adsorption-desorption isotherms for manganese- and copper-containing LDHs exhibit type IV isotherms, however, with different sub-types (see Fig. 10). At higher pressure values the H1 hysteresis characteristic for the mesoporous materials are seen [10]. However, the steep increase at relatively low pressures let us confirm the type of H4 isotherms [139] and to conclude that the adsorption-desorption isotherms obtained for copper-containing LDHs samples are qualitatively and quantitatively almost the same. The surface area of $Mg_{3-x}Mn_x/Al_1$ samples evidently depends on the amount of manganese in the specimen. The cobalt-, nickel- and zinc-containing LDHs according to the shape of isotherms could be described having only the H1 hysteresis. The surface area of $Mg_{3-x}Co_x/Al_1$, $Mg_{3-x}Ni_x/Al_1$ and $Mg_{3-x}Zn_x/Al_1$ LDHs also slightly depend on the amount of substituent. The common trend is that hysteresis increases with increasing amount of transition metal. Only in the case of cobalt was the highest adsorbed amount determined for the $Mg_{3-x}Co_x/Al_1$ sample with 8% mol of cobalt.

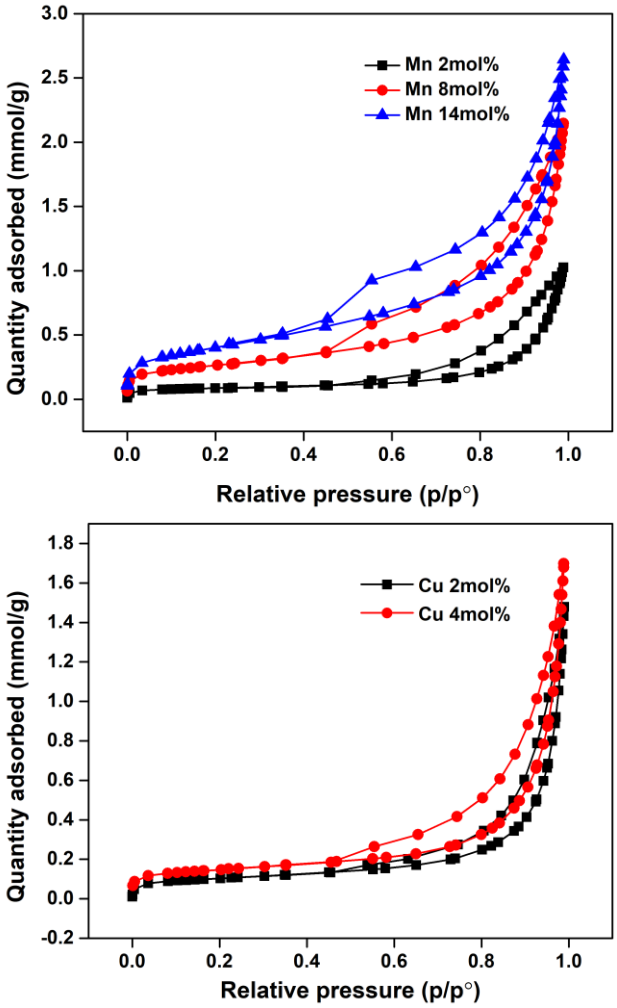

Fig. 10. N_2 adsorption-desorption isotherms of the $Mg_{3-x}Mn_x/Al_1$ and $Mg_{3-x}Cu_x/Al_1$ LDHs

3.1.3. SEM analysis of $Mg_{3-x}M_x/Al_1$ (M = Mn, Co, Ni, Cu, Zn) LDHs

The SEM micrographs of all samples clearly showed the characteristic morphology of layered double hydroxides. The morphological features of zinc-substituted $Mg_{3-x}Zn_x/Al_1$ LDHs are presented in Fig. 11.

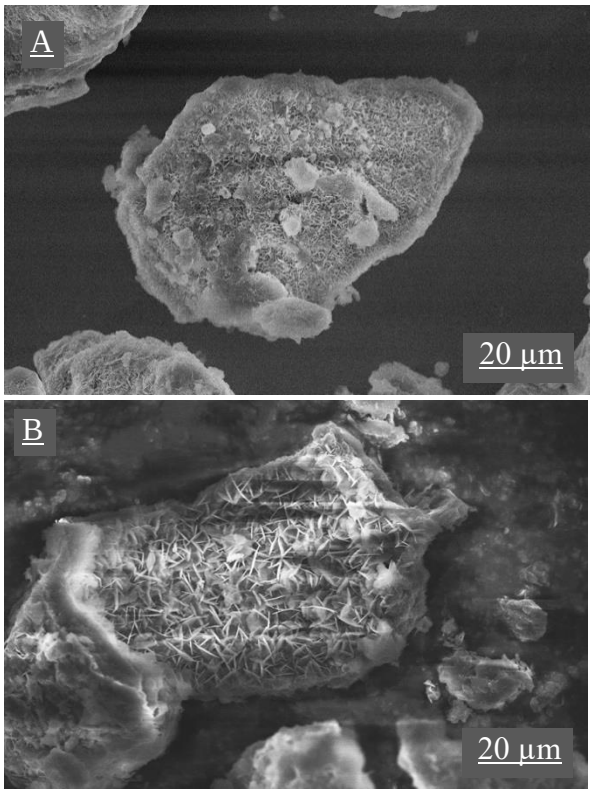

Fig. 11. SEM micrographs of the $Mg_{3-x}Zn_x/Al_1$ LDHs. Zinc content 10 mol% (A) and 20 mol% (B)

The $Mg_{3-x}Zn_x/Al_1$ sample with the 10 mol% zinc content is composed of homogeneously distributed fine plate-like nanoparticles. However, with an increasing amount of Zn from 10 to 20 mol% the increase in the size of the nanoparticles is evident. Moreover, the surface of the $Mg_{3-x}Zn_x/Al_1$ specimen with 20 mol% of Zn is covered by bigger cubic particles, which, according to XRD analysis data, could be attributed to ZnO. The surface microstructure of the $Mg_{3-x}Mn_x/Al_1$, $Mg_{3-x}Co_x/Al_1$, $Mg_{3-x}Ni_x/Al_1$ and $Mg_{3-x}Cu_x/Al_1$ samples is very similar to the zinc containing sample. Particle size and level of agglomeration slightly depend on the amount of introduced transition metals instead of magnesium to the LDH structure.

3.2. Alkaline earth metal substitution effects in sol-gel derived mixed-metal oxides and $Mg_{2-x}M_x/Al_1$ (M = Ca, Sr, Ba) layered double hydroxides

In this part of study, the alkaline earth metal substitution effects, which could be introduced to the sol-gel derived LDHs were investigated.

3.2.1. Characterization of synthetized MMO and reconstructed LDHs

Fig. 12 shows XRD patterns of sol-gel derived $Mg_{2-x}Ca_x/Al_1$ LDHs with 1 mol% of calcium reconstructed by changing the pH of the aqueous solution from 10 to 12.

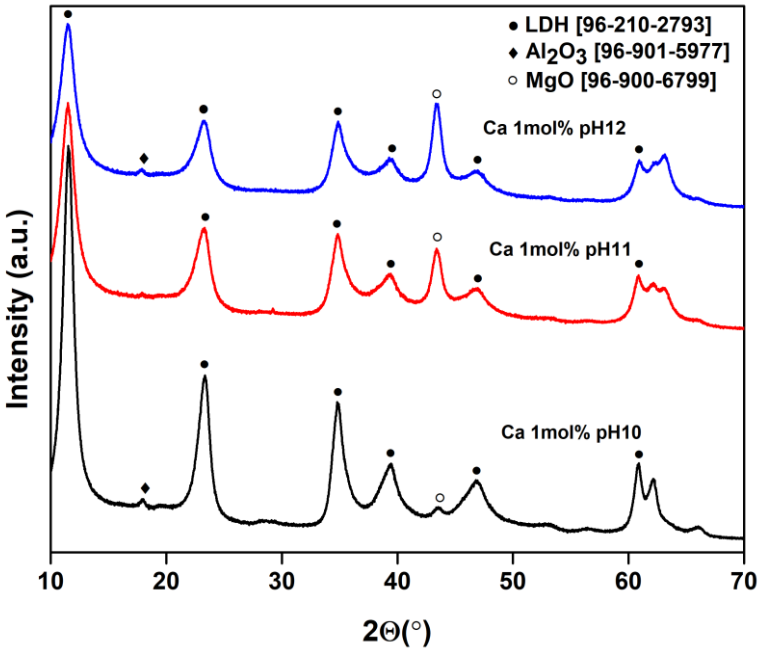

Fig. 12. XRD patterns of sol-gel derived $Mg_{2-x}Ca_x/Al_1$ (Ca = 1 mol%) LDHs obtained at different pH

As seen, 1% mol of calcium could be introduced easily instead of magnesium to Mg_2/Al_1 LDHs without destroying the layered structure [140]. However, a minor amount of alumina and magnesium oxide phase is also forming during the reconstruction approach. Besides, the reflections of LDHs were most intensive in the case when the reconstruction of sol-gel derived MMO was performed at pH = 10. Therefore, further syntheses of LDHs with higher amount of calcium were conducted at pH = 10. The XRD patterns of MMO obtained by heating the $Mg_{2-x}Ca_x/Al_1$ precursor gels at 650 °C are presented in Fig. 13. The XRD patterns of synthesis products with different substitutional level of Ca ranging from 1 to 5 mol% are almost identical and revealed in all cases the formation of poorly crystalline magnesium oxide [29].

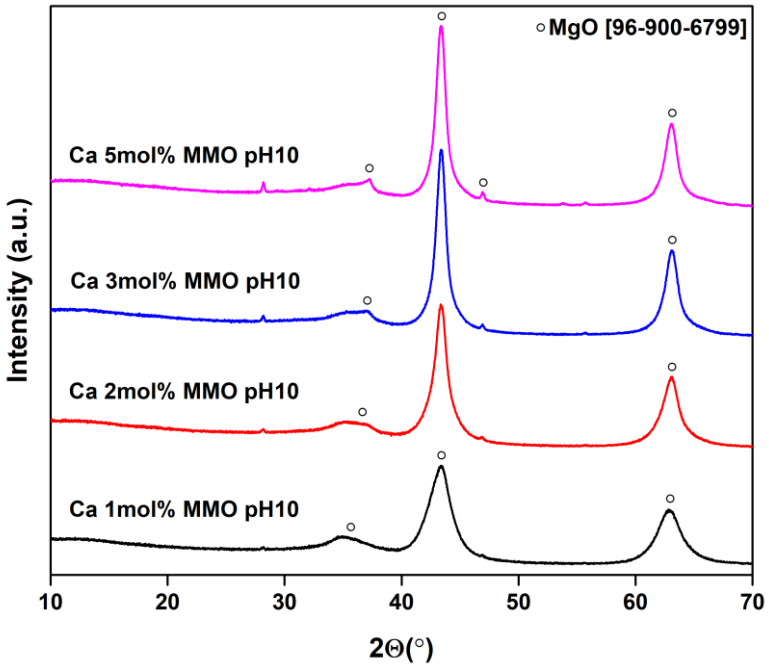

Fig. 13. XRD patterns of MMO obtained by heating the $Mg_{2-x}Ca_x/Al_1$ precursor gels at 650 °C

The phase purity of $Mg_{2-x}Ca_x/Al_1$ LDHs obtained by reconstruction of sol-gel derived MMO evidently are dependent on the amount of introduced calcium (Fig. 14). With increasing amount of Ca up to 5 mol%, the intensity of characteristic reflections of LDH monotonically decreases in the XRD patterns, and the amount of impurities, such as Al_2O_3, $CaCO_3$ and magnesium oxide phase slightly increased.

Interestingly, the phase purity of $Mg_{2-x}Sr_x/Al_1$ LDH with the 1 mol% of Sr is independent on the value of solution pH utilized during reconstruction approach. The phase purity of sol-gel–derived $Mg_{2-x}Sr_x/Al_1$ LDHs (Sr content equals to 1 and 5 mol%) also is dependent on the amount of introduced Sr. The results obtained on barium substitution in $Mg_{2-x}Ba_x/Al_1$ LDHs are very similar to the ones discussed above on the formation of $Mg_{2-x}Sr_x/Al_1$ LDHs.

The XRD analysis results confirmed that the substitution of magnesium by alkaline earth metals in the LDHs synthesized using an aqueous sol-gel method highly depends on the nature and concentration of the alkaline earth metal. The ionic crystal radius of metals possibly is not the only parameter responsible for the level of substitution of Mg by alkaline earth metals in LDHs. The second parameter that could influence the formation of LDH could be the value of the solubility product of metal hydroxides. In the case of Mg_{2-}

$_xCa_x/Al_1$ LDH which showed the highest substitutional level, the solubility products are $1.8 \cdot 10^{-11}$ for $Mg(OH)_2$ and $5.5 \cdot 10^{-6}$ for $Ca(OH)_2$. However, the hydroxides of Sr and Ba are rather soluble. On the other hand, the solubility product of $SrCO_3$ (K_{SP}= $4.59 \cdot 10^{-9}$) is slightly lower than that the solubility product of $BaCO_3$ (K_{SP} = $1.13 \cdot 10^{-8}$). This might be the reason that a small amount of barium could be introduced in the $Mg_{2-x}Ba_x/Al_1$ LDH, despite the $Ba(OH)_2$ is sufficiently soluble in water.

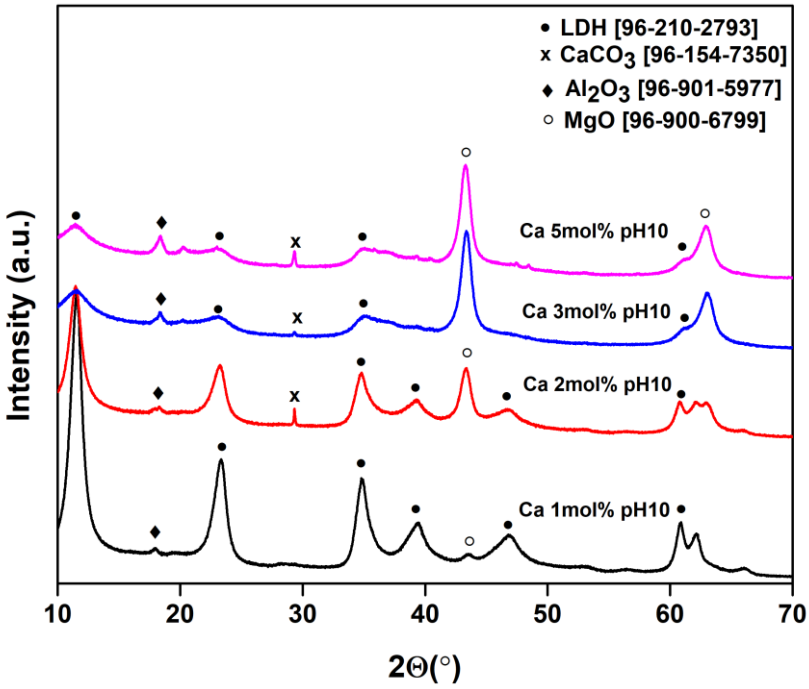

Fig. 14. XRD patterns of the sol-gel derived $Mg_{2-x}Ca_x/Al_1$ LDHs

3.2.2. N_2 adsorption-desorption isotherms and specific surface area of $Mg_{2-x}M_x/Al_1$ (M = Ca, Sr, Ba) mixed metals oxides

The BET results obtained (Fig. 15) demonstrated that the N_2 adsorption-desorption isotherms of calcium 1–4 mol% MMO samples exhibited type IV isotherms with a sharp capillary condensation step at relative pressure, 0.4–0.9 [141]. At higher pressure values clearly the H1 hysteresis loop is seen which indicates the presence of cylindrical mesopores [10, 141]. However, the increase observed at relatively low pressures let us confirm the type of H4

isotherms [139, 142]. The surface area of calcium containing MMO samples which contains 5% mol of calcium is different and dependent on the amount of calcium in the specimen.

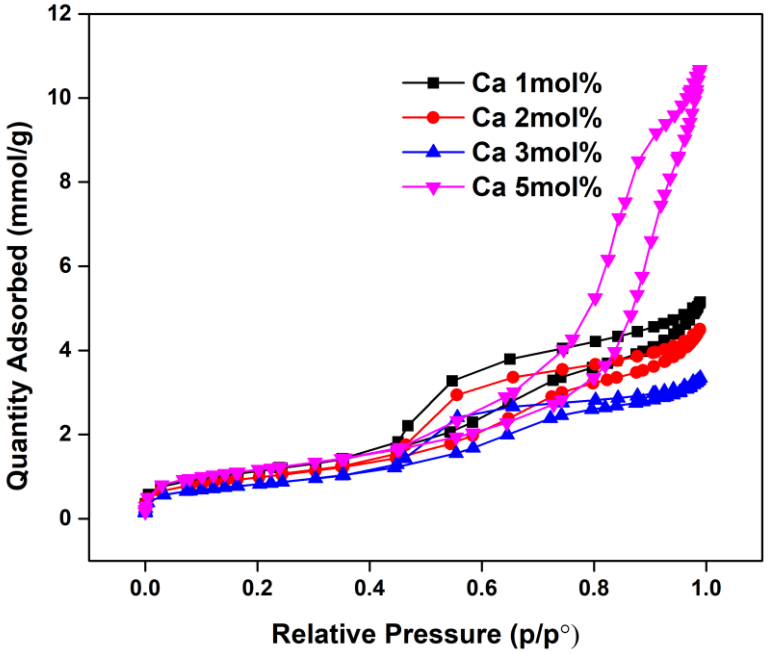

Fig. 15. N_2 adsorption-desorption isotherms of $Mg_{2-x}Ca_x/Al_1$ MMO

It was also demonstrated that N_2 adsorption-desorption isotherms of sol-gel synthesized mixed-metal oxides containing Sr and Ba are very similar to the calcium containing samples.

3.2.3. SEM analysis of $Mg_{2-x}M_x/Al_1$ (M = Ca, Sr, Ba) mixed metal oxides and layered double hydroxides

Fig. 16. shows the morphological features of calcium 1 and 5 mol% containing MMO and subsequently obtained $Mg_{2-x}Ca_x/Al_1$ LDHs. The SEM micrographs of MMO confirm that the surface of synthesized compounds is composed of large monolithic particles of about 15–20 μm in size. The randomly distributed pores on the chips-coated surface of these monoliths also are seen. The formation of plate-like crystals with size of 1.5–5 μm in the case of $Mg_{2-x}Ca_x/Al_1$ with the 1 mol% Ca content, were observed for the

reconstructed LDH. As the amount of calcium in LDH increases, the sample with more inhomogeneous morphology having larger grains has formed.

The surface microstructure of Sr and Ba containing MMO is very similar to the Ca containing ones. During the reconstruction of Sr containing MMO much larger LDHs particles have formed (5–15 μm). The formation of plate-like crystals with a size of 1.5–7.5 μm with well-pronounced connectivity between inner grains occurred for $Mg_{2-x}Ba_x/Al_1$ LDHs.

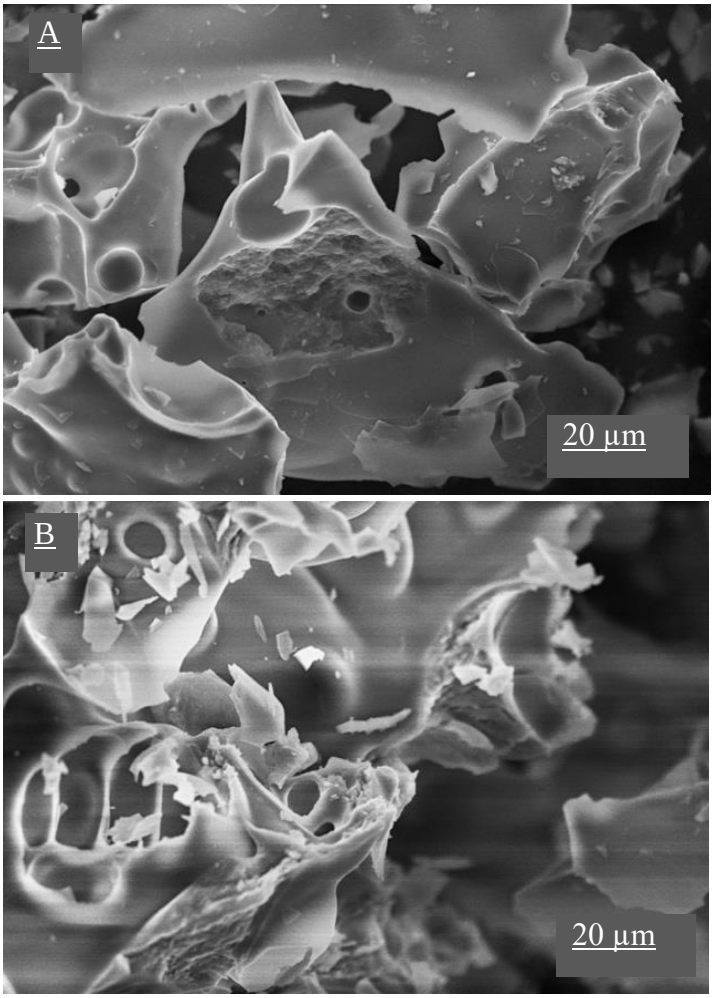

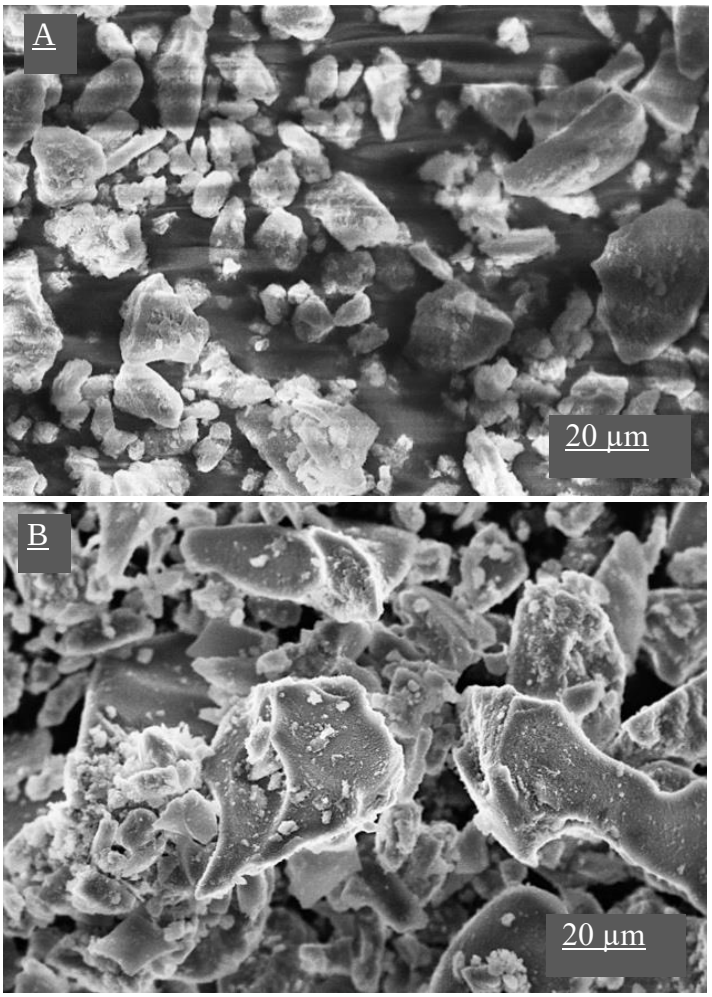

Fig. 16. SEM micrographs of the sol-gel derived $Mg_{2-x}Ca_x/Al_1$ reconstructed LDHs (bottom) and MMO obtained after calcination precursor gels at 650 ºC (top). Amount of Ca: 1 mol% (A) and 5 mol% (B).

3.3. Reconstruction peculiarities of sol-gel derived $Mg_{2-x}M_x/Al_1$ (M = Ca, Sr, Ba) layered double hydroxides

The main aim of this part of doctoral dissertation was to investigate the reconstruction peculiarities of the alkaline earth metal substituted $Mg_{2-x}M_x/Al_1$ (M = Ca, Sr, Ba; x = 0.1) LDHs.

3.3.1. Characterization of synthetized MMO and reconstructed LDHs

To study the reconstruction peculiarities of sol-gel derived $Mg_{2-x}M_x/Al_1$ (M = Ca, Sr, Ba; x = 0.1) LDHs, the precursor gels were firstly annealed at 650 °C, 800 °C, and 950 °C. The XRD patterns of MMO obtained by heating unsubstituted Mg_2/Al_1 LDH precursor gels at 650 °C show the formation of a MMO phase with an MgO-like structure [28]. Thermal treatment of the precursor gels at 800 °C resulted in the formation of MMO and a low-crystallinity spinel, $MgAl_2O_4$, phase. After heating at 950 °C the highly crystalline $MgAl_2O_4$ phase has formed along with the MgO phase. The XRD patterns of the Mg_2/Al_1 LDHs synthesized by the indirect sol-gel method show the formation of LDHs independent of the annealing temperature of the precursor gels. These results are in good agreement with those previously published elsewhere [143].

The XRD patterns of MMO obtained by heating the $Mg_{1.9}M_{0.1}/Al_1$ (M = Ca, Sr, Ba) precursor gels at 800 °C and 950 °C are almost identical and revealed in all cases the formation of crystalline MgO, magnesium spinel phase $MgAl_2O_4$ and an appropriate spinel of alkaline earth metal. During the partial reconstruction process, the phase purity of LDHs evidently is dependent on the nature of introduced metal. The spinel phases remained almost unchanged during the reconstruction process. Moreover, a negligible amount of appropriate alkaline earth metal carbonates has formed as well. The XRD patterns of $Mg_{2-x}Ca_x/Al_1$ (x = 0.1) LDHs obtained from MMO annealed at different temperatures are presented in Figure 17.

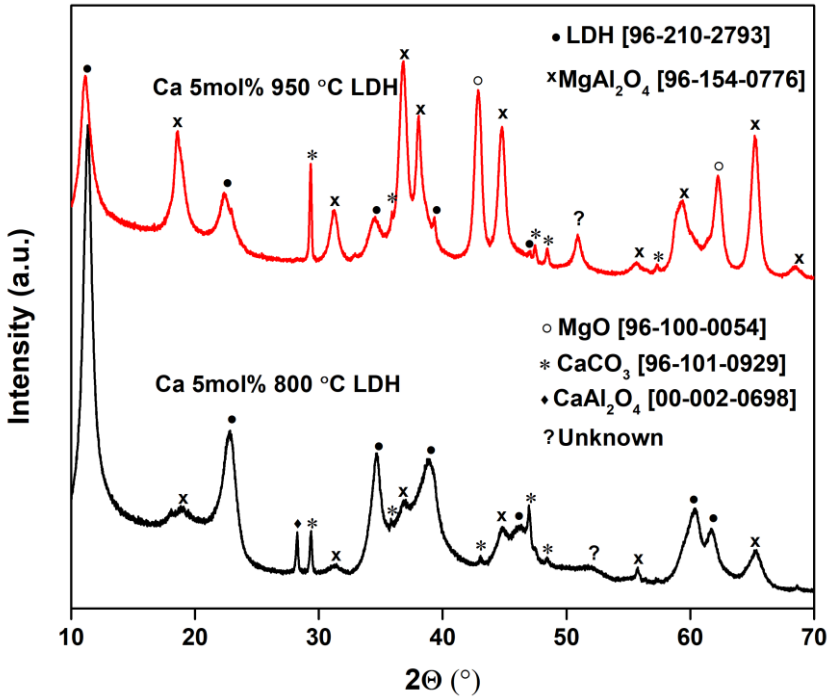

Fig. 17. XRD patterns of reconstructed $Mg_{2-x}Ca_x/Al_1$ (Ca = 5 mol%) LDHs obtained by reconstruction of MMO annealed at different temperatures.

The obtained $Mg_{2-x}M_x/Al_1$ LDH samples were repeatedly heated at different temperatures to obtain MMO and compare the phase composition, morphology, and surface properties with the ones obtained after initial annealing. The XRD patterns of mixed MMO obtained by heating the Mg_2/Al_1 precursor gels and obtained by heating the Mg_2/Al_1 LDHs are very similar, confirming the same phase composition. However, the reflections of just obtained MMO are more intense in comparison with ones presented in the repeatedly obtained MMO from LDHs. The second time obtained Ca and Sr substituted MMO samples contain much more side phases (see Figure 18). However, this is not the case for the Ba-substituted MMO samples. Both synthesis products obtained from precursor gels and by heating LDHs were composed of several crystalline phases.

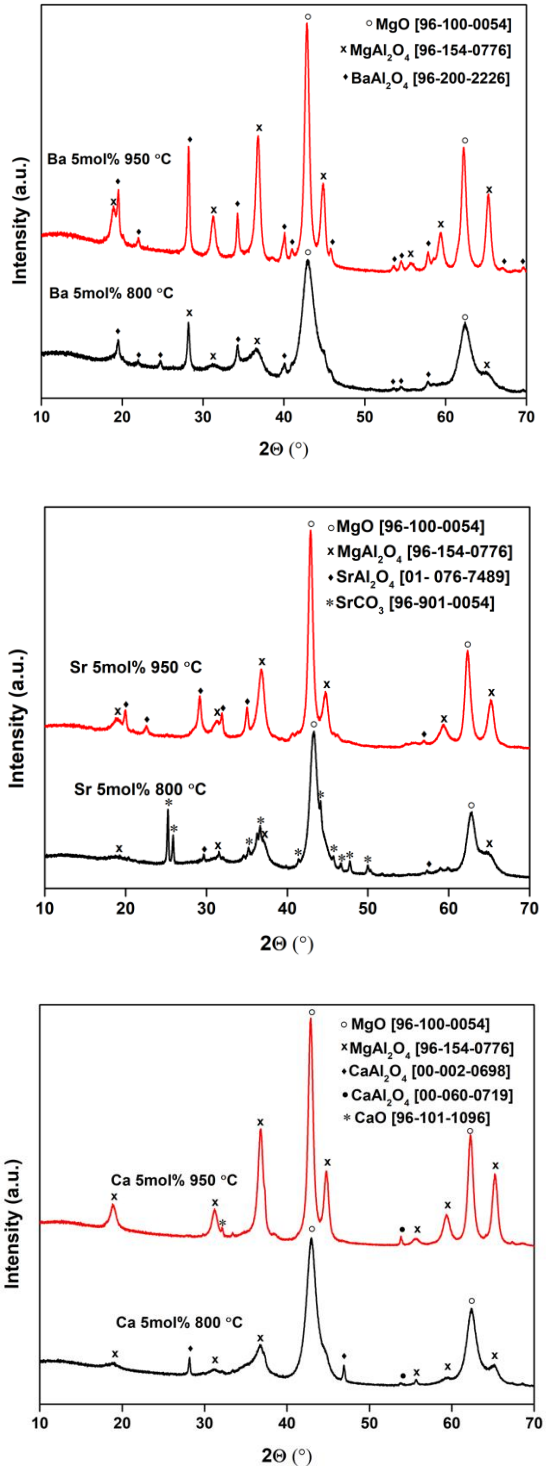

Fig. 18. XRD patterns of MMO obtained by heating the $Mg_{1.9}Ca_{0.1}/Al_1$ LDHs (bottom), $Mg_{1.9}Sr_{0.1}/Al_1$ LDHs (middle), and $Mg_{1.9}Ba_{0.1}/Al_1$ LDHs (top) at different temperatures.

3.3.2. N_2 adsorption-desorption isotherms and specific surface area of $Mg_{2-x}M_x/Al_1$ (M = Ca, Sr, Ba) MMO and LDHs

The results received by the BET method on Mg_2/Al_1 MMO obtained from Mg_2/Al_1 LDHs are comparable with those determined for the Mg_3/Al_1 LDH samples.

The samples exhibit type IV isotherms independent of the annealing temperature. At higher pressure values, the H1 hystereses are seen. However, in the case of the MMO obtained by heating Mg_2/Al_1 precursor gel, the steep increase at relatively low pressures let us predict the type of H4 hystereses, especially for the MMO samples obtained at lower temperature. The surface area of these MMO samples evidently depends on the synthesis temperature. N_2 adsorption-desorption results obtained for the MMO containing Ca, Sr and Ba demonstrated that the N_2 adsorption-desorption isotherms show very similar trends. However, in the case of Ba-MMO samples synthesized at 800 °C, the determined N_2 adsorption-desorption isotherms exhibited same type of isotherms independent of the synthesis method. The results of the BET analysis of MMO samples are summarized in Table 1.

Table 1. BET surface area of sol-gel derived $Mg_{1.9}M_{0.1}/Al_1$ (M = Ca, Sr and Ba) MMO.

Precursor compound	**Temperature**	**BET Surface Area m^2/g**
Mg_2Al_1 precursor gels	800 °C	87.47
Mg_2Al_1	800 °C	65.45
Mg_2Al_1 precursor gels	950 °C	27.75
Mg_2Al_1	950 °C	40.53
$Mg_{1.9}Ca_{0.1}/Al_1$ precursor gels	800 °C	46.46
$Mg_{1.9}Ca_{0.1}/Al_1$	800 °C	129.16
$Mg_{1.9}Ca_{0.1}/Al_1$ precursor gels	950 °C	34.79
$Mg_{1.9}Ca_{0.1}/Al_1$	950 °C	46.08
$Mg_{1.9}Sr_{0.1}/Al_1$ precursor gels	800 °C	53.85
$Mg_{1.9}Sr_{0.1}/Al_1$	800 °C	104.54
$Mg_{1.9}Sr_{0.1}/Al_1$ precursor gels	950 °C	36.29

Precursor compound	Temperature	BET Surface Area m^2/g
$Mg_{1.9}Sr_{0.1}/Al_1$	950 °C	51.96
$Mg_{1.9}Ba_{0.1}/Al_1$ precursor gels	800 °C	63.22
$Mg_{1.9}Ba_{0.1}/Al_1$	800 °C	122.49
$Mg_{1.9}Ba_{0.1}/Al_1$ precursor gels	950 °C	32.50
$Mg_{1.9}Ba_{0.1}/Al_1$	950 °C	40.58

The pore size distributions obtained by the BJH method for the MMO specimens obtained by heating Mg_2/Al_1 precursor gels and Mg_2/Al_1 LDHs show that both samples demonstrate narrow pore size distributions (PSD) almost at the mesoporous level, however close to micropores domain. Surprisingly, the PSD width does not depend neither on the synthetic procedure nor on the annealing temperature. The determined average pore diameter in the mesopore region is approximately 3.0–5.5 nm. The PSD results obtained for the MMO containing Sr are shown in Figure 19. Apparently, various surface properties could be detected for the MMO samples synthesized by two different methods. The pore size distribution of directly obtained MMO by heating precursor gels depends on the heating temperature and less on the nature of alkaline earth metal. The determined average pore diameter in the mesopore region for the Ca-MMO, Sr-MMO, and Ba-MMO samples, respectively, synthesized at 800 °C. The pore size distribution is wider for the MMO synthesized at 950 °C. The pore size distributions obtained by the BJH method for the MMO specimens synthesized from the reconstructed Mg_2/Al_1 LDHs depends on both synthesis temperature and nature of substituent. In general, the gain in the volume of mesopores is detected for the MMO samples synthesized at lower temperature. However, the pore diameter, wall thickness, and pore size distribution depend on the used synthesis method, heating temperature, and nature of alkali earth metal in the MMO host matrix, indicating that these MMO could have the potential for the application as catalysts, catalyst supports, and adsorbents.

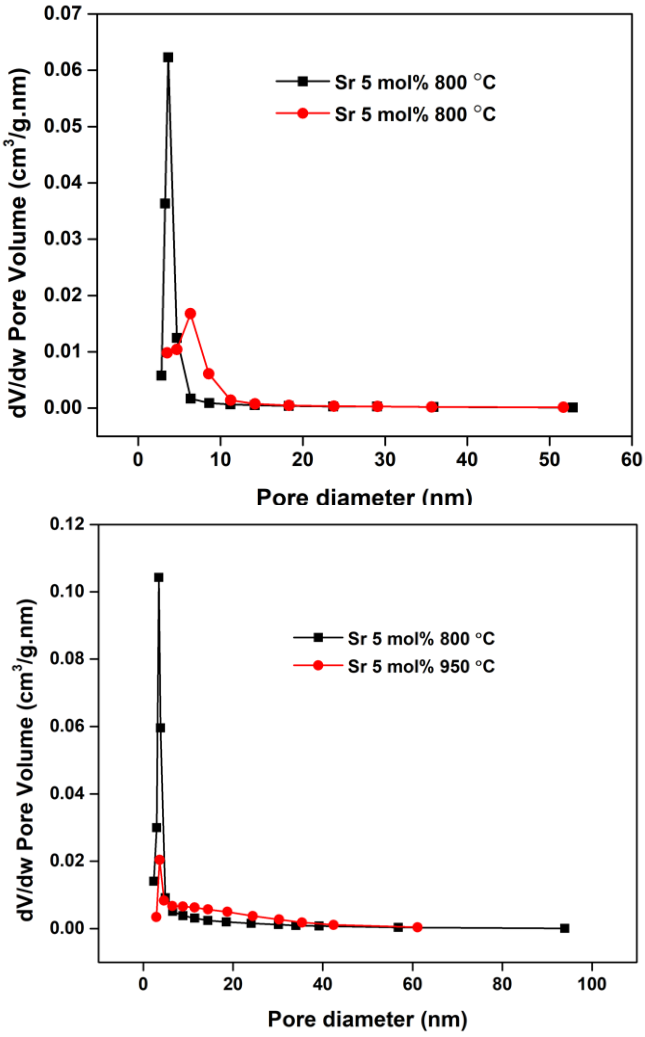

Fig. 19. The pore size distribution of MMO obtained by heating the $Mg_{1.9}Sr_{0.1}/Al_1$ LDHs (bottom) and by heating the $Mg_{1.9}Sr_{0.1}/Al_1$ precursor gels (top) at 800 °C and 950 °C.

3.3.3. Morphological investigation of synthesized samples

The SEM micrographs of Mg_2/Al_1 MMO obtained by heating precursor gel confirm that the surface of synthesized compounds is composed of large monolithic particles at about 15–20 μm in size independent of the annealing temperature (800 °C and 950 °C). The surface of these monoliths is randomly covered with smaller needle-like particles, and some pores also could be detected. The SEM micrographs of reconstructed from MMO Mg_2/Al_1 LDH samples showed the formation of round particles (3–15 μm) composed of nanosized plate-like crystallites. The most interesting observation is that the surface morphology of MMO samples obtained by heating Mg_2/Al_1 LDH specimens show "memory effect". In this case, the surface morphology of MMO is almost identical to the morphology of primary Mg_2/Al_1 LDHs. On the other hand, the morphological features of differently obtained MMO (MMO obtained by heating Mg_2/Al_1 precursor gel and MMO obtained by heating Mg_2/Al_1 LDHs) differ considerably (see Figure 20).

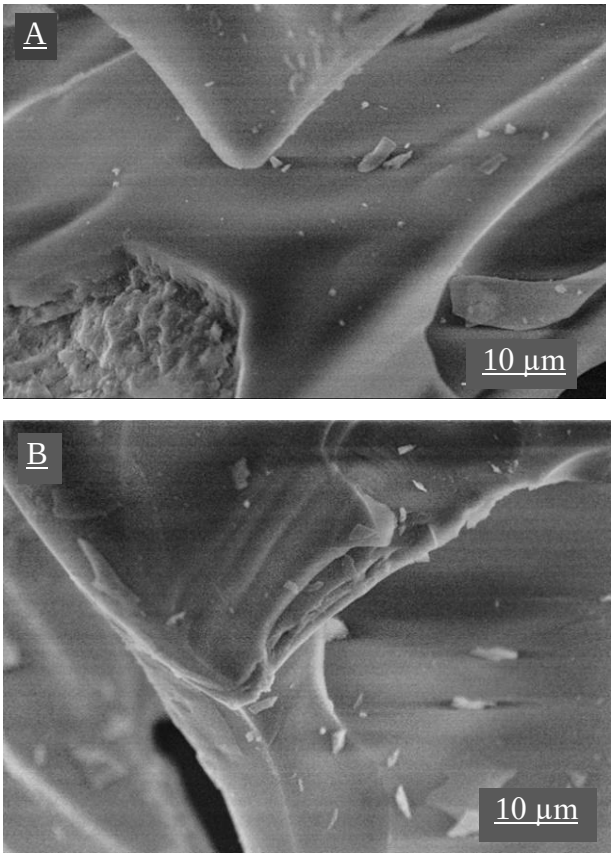

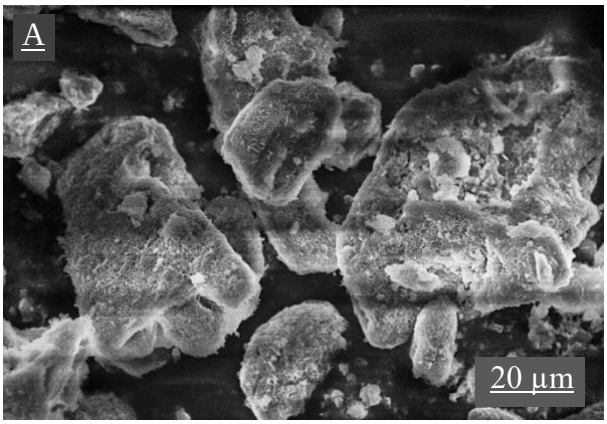
A
20 µm

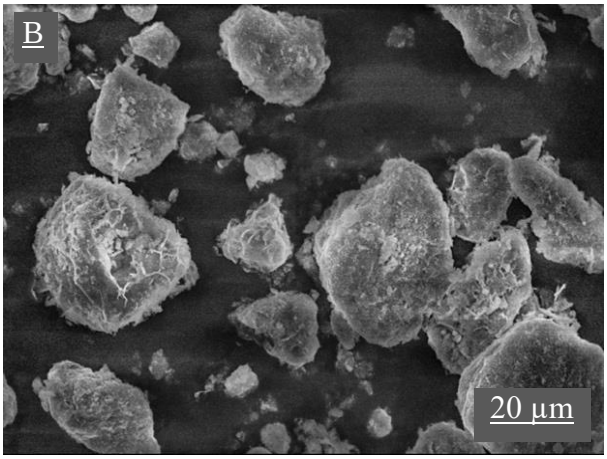
B
20 µm

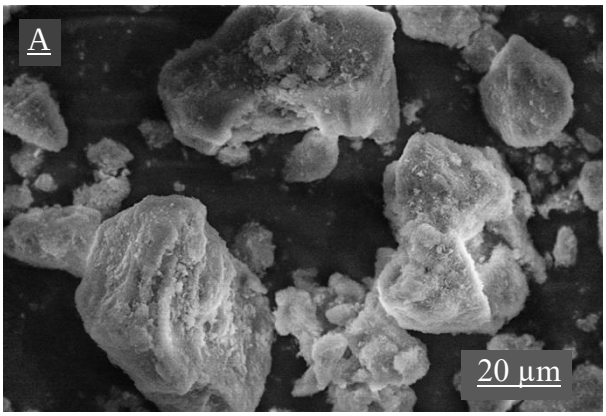
A
20 µm

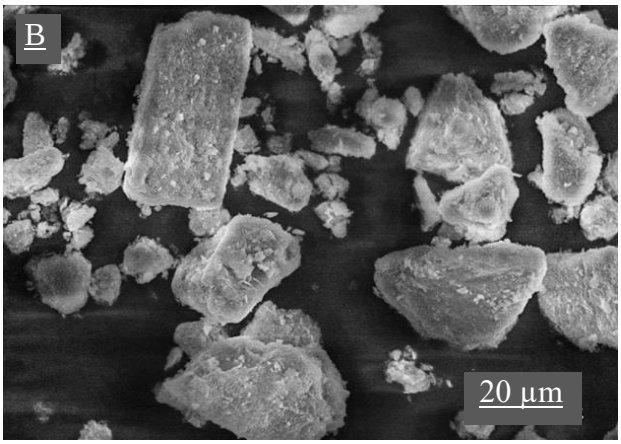

Fig. 20. SEM micrographs of MMO obtained by heating the Mg_2/Al_1 LDHs (bottom) sol-gel derived Mg_2/Al_1 LDHs (middle) and MMO obtained by heating the Mg_2/Al_1 precursor gels (top). Annealing temperatures: 800 °C (A) and 950 °C (B).

The surface of Ca containing MMO obtained by heating the precursor gels is composed of large monolithic particles (≥20 μm). The plate-like crystals with sizes of 5–15 μm composed of nanosized plate-like crystallites have formed for the reconstructed LDH samples. Almost identical microstructure was observed for the MMO specimens obtained after heating $Mg_{1.9}Ca_{0.1}/Al_1$ LDH samples. The surface microstructure of Sr-containing MMO obtained by heating the precursor gels is very similar to the Ca-containing ones. However, on the surface of plate-like crystals of reconstructed $Mg_{2-x}Sr_x/Al_1$ LDH samples, additionally spherical particles (approximately 1 μm) were determined. These spherical particles as a "memory effect" remain on the surface of already heat-treated Sr containing LDHs. Again, the microstructure of investigated samples was not dependent on the annealing temperature. Interestingly, the barium containing $Mg_{2-x}Ba_x/Al_1$ LDH samples showed the formation of smaller LDH particles (2–5 μm). The formation of plate-like crystals of MMO with the size of 7.5–12.5 μm was observed by heating these LDHs at elevated temperatures.

3.4. Influence of ultrasound and cation substitution on the intercalation of organic anions to the Mg_3/Al_1 layered double hydroxide

In this part of doctoral thesis the influence of ultrasound and cation substitution on the intercalation of organic anions to the Mg_3/Al_1 LDH has been investigated.

3.4.1. Characterization of synthetized and intercalated LDHs

Since the LDHs containing chloride anion are the most suitable precursors for the anion-exchange process [13, 144], the intercalation of organic anions formate, oxalate, acetate, tartrate and citrate in the Mg_3/Al_1 LDHs was performed from chloride containing LDHs. The XRD patterns of the LDH phases obtained by the anion exchange reactions without or with usage of ultrasound (us) are shown in Fig. 21. As seen, the diffraction peaks for Mg_3/Al_1-Cl, Mg_3/Al_1-oxalate-us, Mg_3/Al_1-tartrate-us and Mg_3/Al_1-citrate-us are shifted to the lower values of *2θ* angle indicating a considerable increase in the basal spacing *c* values as compared with the respective values for the main Mg_3/Al_1 LDH. These results clearly show that the treatment with ultrasound promotes the anion-exchange reactions significantly. This might be associated with increased reaction rate at such conditions [144]. On the other hand, the positions of diffraction peaks (003) of Mg_3/Al_1-formate-us and Mg_3/Al_1-acetate-us LDHs are not shifted.

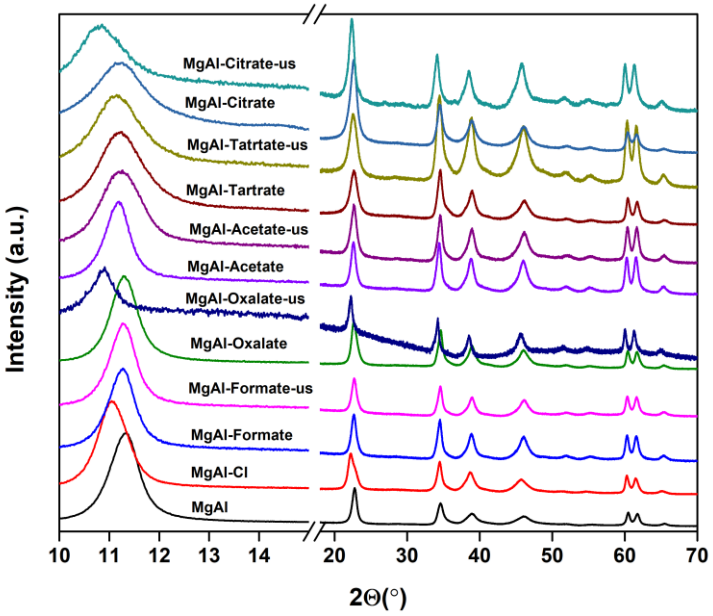

Fig. 21. XRD patterns of Mg_3/Al_1 LDHs with different intercalated anions and prepared without and with ultrasound (us).

The different manganese and cobalt substitution effects on the intercalation of above mentioned anions in $Mg_{3-x}Mn_x/Al_1$ and $Mg_{3-x}Co_x/Al_1$ LDHs could be observed in Fig. 22.

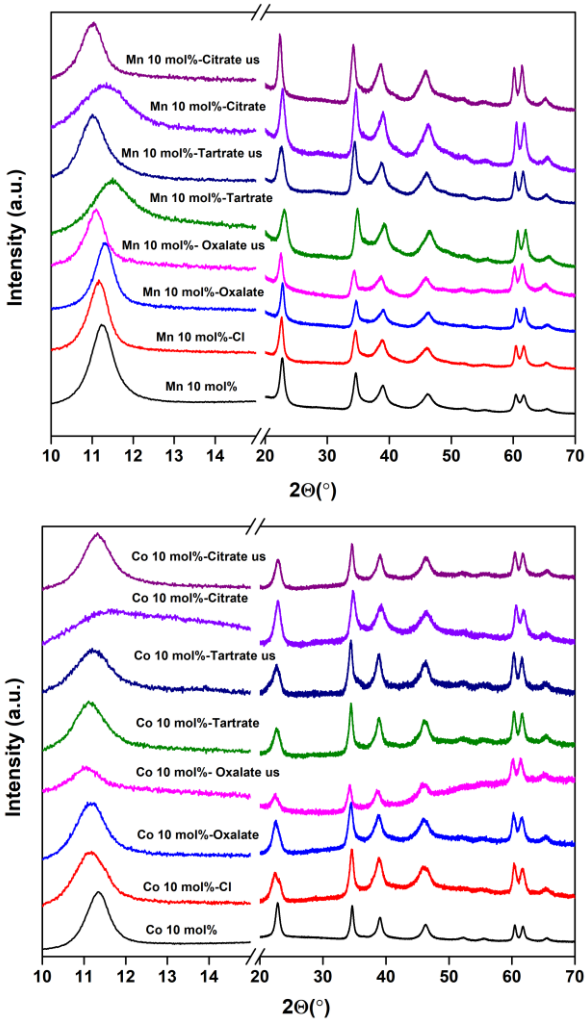

Fig. 22. XRD patterns of $Mg_{3-x}Mn_x/Al_1$ and $Mg_{3-x}Co_x/Al_1$ LDHs intercalated with different anions and prepared without and with ultrasound (us)

As seen from these results, the manganese has no influence on the intercalation process. The shift of diffraction peaks attributable only to the sonicated $Mg_{3-x}Mn_x/Al_1$-anion-us LDH samples is visible. However, the different situation is happening in the case of cobalt substitution. The XRD results confirm that cobalt promotes intercalation of oxalate and tartrate to the interlayer of $Mg_{3-x}Co_x/Al_1$ LDHs without additional sonication. It is interesting to note, that if ultrasound is not used the oxalate does not enter the interlayer of $Mg_{3-x}Ni_x/Al_1$ LDHs, but could be intercalated to the structure of $Mg_{3-x}Cu_x/Al_1$ LDHs. The behaviour of tartrate in these nickel and copper

substituted LDHs is completely opposite. The tartrate participates in the anion exchange reaction in $Mg_{3-x}Cu_x/Al_1$ LDHs, and does not enter the structure of $Mg_{3-x}Ni_x/Al_1$ LDHs. The similar shift of diffraction peaks as in $Mg_{3-x}Mn_x/Al_1$ was observed and in $Mg_{3-x}Zn_x/Al_1$ LDHs confirming that these anions could be intercalated to the zinc-substituted LDHs only under sonication (see Fig. 23).

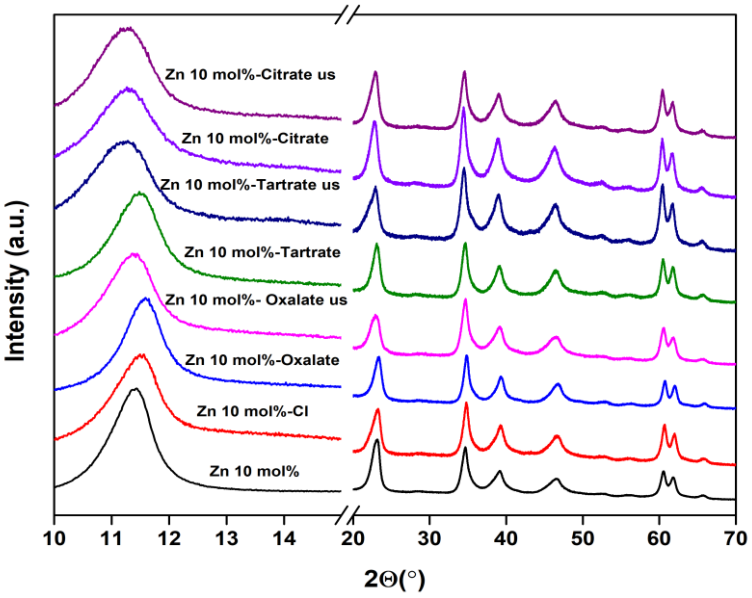

Fig. 23. XRD patterns of $Mg_{3-x}Zn_x/Al_1$ LDHs with different intercalated organic anions and prepared without and with ultrasound (us)

3.4.2. FT-IR spectra of $Mg_{3-x}M_x/Al_1$ (M = Mn, Co, Ni, Cu, Zn) LDHs intercalated with different anions

FT-IR spectra of Mg_3/Al_1 and Mg_3/Al_1-Cl LDH samples in the region of 3750–480 cm^{-1} contain the absorption bands at about 3600–3100 cm^{-1} and weaker bands at 1655–1640 cm^{-1} which could be attributed to the stretch vibration in (-OH) groups originated from the hydroxyl layers and from intercalated water molecules [13, 28, 29, 43, 145]. The strong absorption bands visible at 1360 cm^{-1} are attributed to the asymmetric vibration modes of ionic carbonate, which still exists in the interlayer of LDHs. The FT-IR spectra of Mg_3/Al_1-formate and Mg_3/Al_1-formate-us LDHs qualitatively cannot be distinguished from the spectrum of Mg_3/Al_1 LDH. However, the FT-IR spectra of Mg_3/Al_1 LDHs intercalated with oxalate ion contain the strong

absorption band at 1315 cm^{-1} which is assigned as symmetric (-COO^-) vibration in the oxalate groups.

FT-IR spectra of $Mg_{3-x}M_x/Al_1$ (M = Mn, Co, Ni, Cu and Zn) LDHs intercalated with oxalate using sonication are shown in Fig. 24. All spectra independent on the used transition metal for substitution confirms intercalation of oxalate to the structure of LDHs as was determined by XRD analysis. On the other hand, the FT-IR spectroscopy results do not support the conclusion that the tartrate anion participates in the anion exchange reaction in $Mg_{3-x}Cu_x/Al_1$ LDHs. No characteristic absorption bands of tartrate were observed in the FT-IR spectra of $Mg_{3-x}Cu_x/Al_1$-tartrate and $Mg_{3-x}Cu_x/Al_1$-tartrate-us LDHs.

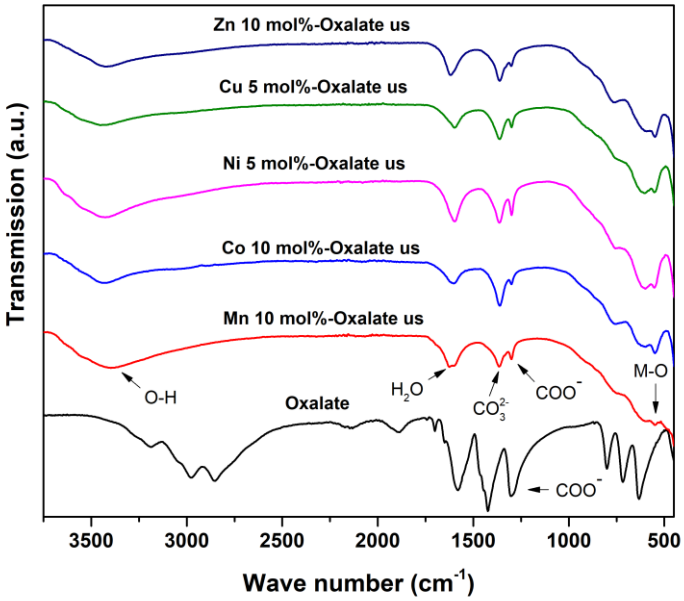

Fig. 24. FT-IR spectra of $Mg_{3-x}M_x/Al_1$ (M = Mn, Co, Ni, Cu and Zn) LDHs intercalated with oxalate using ultrasound (us) and appropriate organic compound used in ion exchange method

3.4.3. Raman spectroscopy of $Mg_{3-x}M_x/Al_1$ (M = Mn, Co, Ni, Cu, Zn) LDHs intercalated with different anions

Fig. 25 compares Raman spectra of oxalate, citrate, Mg_3/Al_1 LDH, Mg_3/Al_1 LDHs intercalated with oxalate, citrate anions and obtained without and under ultrasound conditions. The strong high frequency features located at about 1500 cm^{-1} for oxalate [146] are visible in the Raman spectra of Mg_3/Al_1-oxalate and Mg_3/Al_1-oxalate-us LDHs. The well-defined characteristic bands of citrate [147] could be determined only in sonicated Mg_3/Al_1-citrate-us (spectrum is not shown). These results are in a good agreement with previously discussed XRD and FT-IR results.

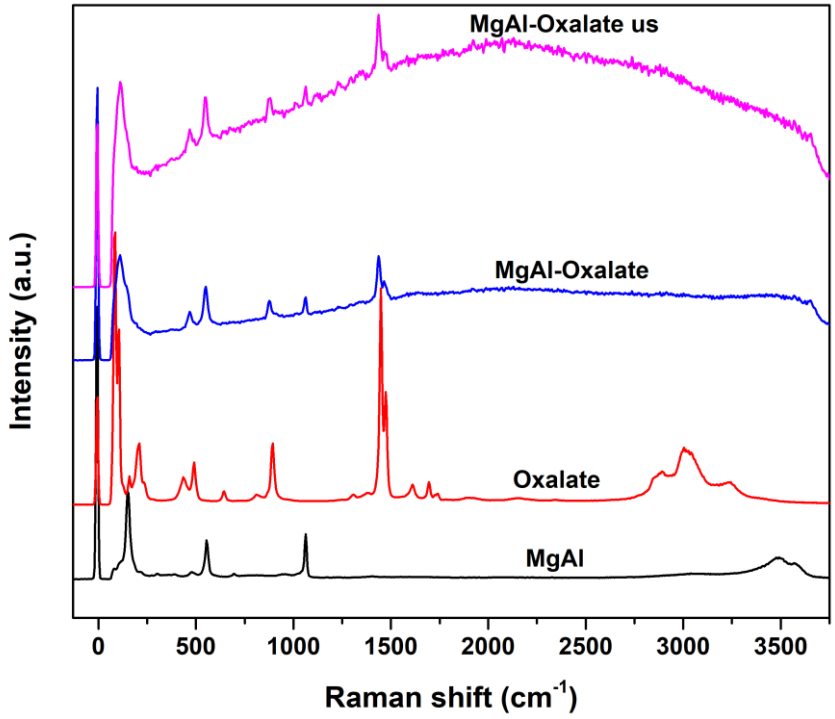

Fig. 25. Raman spectra of Mg_3/Al_1, Mg_3/Al_1 LDHs intercalated with oxalate anion without and under ultrasound (us) and appropriate organic compounds used in ion exchange method

Different spectral patterns were observed for Mg_3/Al_1 LDHs intercalated with formate and acetate anions. Interestingly, the main peak position observed for the formate [148] could be detected also in the Raman spectra of

Mg_3/Al_1 LDHs intercalated with formate. However, this feature was not confirmed by specific shift of the diffraction peaks in the XRD patterns of this compounds. On the other hand, it is clearly seen that Raman spectra of Mg_3/Al_1-acetate LDHs do not contain any specific absorption bands attributable to acetate [149]. Therefore it can be concluded that formate contrary oxalate and tartrate and citrate is only adsorbed on the surface of LDHs but does not enter the interlayer space (Fig. 26).

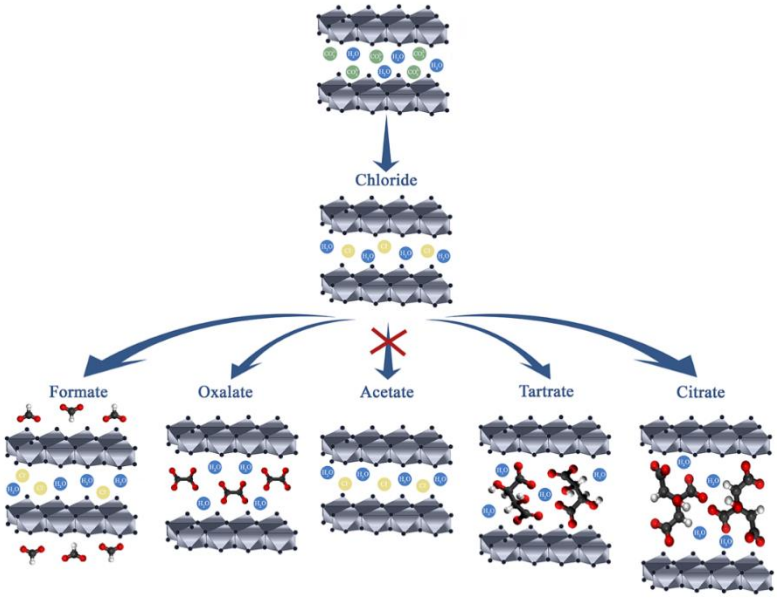

Fig. 26. The schematic representation of possible interaction of Mg_3/Al_1 LDHs with organic anions

3.4.4. TG-DTG-DCS results of $Mg_{3-x}M_x/Al_1$ (M = Mn, Co, Ni, Cu, Zn) LDHs intercalated with different anions

The TG-DTG-DCS curves of Mg_3/Al_1 and Mg_3/Al_1 LDHs intercalated with citrate under sonication are shown in Fig. 27. The initial mass loss observed in the temperature range of 30–210°C is associated with evolution of moisture and adsorbed water. The main decomposition of LDHs occurs via continuous mass loss step in the temperature range of 210–600°C. These thermal behaviour results from the loss of the coordinated water and the intercalated anions and dehydroxylation of the layers followed by collapse of the layered

structure in the higher temperature range. It could be easily observed that the total mass loss for the Mg_3/Al_1 LDH sample is about 42.5%. The increased total loss (about 48.9%) observed for the Mg_3/Al_1-citrate-us LDHs confirms once again that organic anion is intercalated in the layered structure of LDH or/and adsorbed on the surface of synthesized material. The analogous TG results were observed for the Mg_3Al_1 LDHs intercalated with formate, tartrate and oxalate.

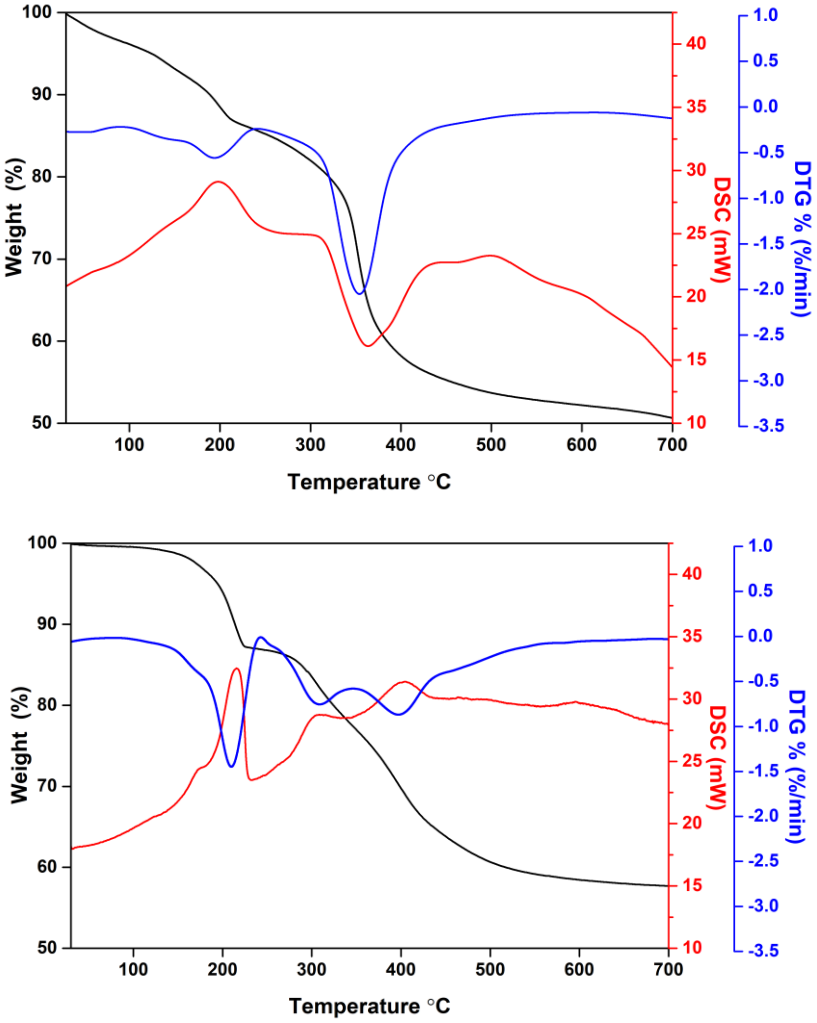

Fig. 27. TG-DTG-DCS curves of Mg_3Al_1 (bottom) and Mg_3Al_1 LDHs intercalated with citrate under sonication (top)

3.4.5. Morphological investigation of $Mg_{3-x}M_x/Al_1$ (M = Mn, Co, Ni, Cu, Zn) LDHs intercalated with different anions

The morphology of the synthesized LDHs were examined using SEM. The characteristic feature of synthesized LDHs is the formation of plate-like particles with hexagonal shape [150]. It is interesting to note that the SEM images of sol-gel derived LDH samples were almost identical independent on the nature of anion used for the intercalation, on the selected transition metal for substitution and on the used intercalation procedure. The representative SEM micrographs for the Mg_3/Al_1 LDHs intercalated with formate without and under sonication are depicted in Fig. 28. As seen, the solids are composed of differently agglomerated plate-like particles with the size about of 500 nm. The agglomerates are slightly larger in the case of sonicated LDH-formate sample.

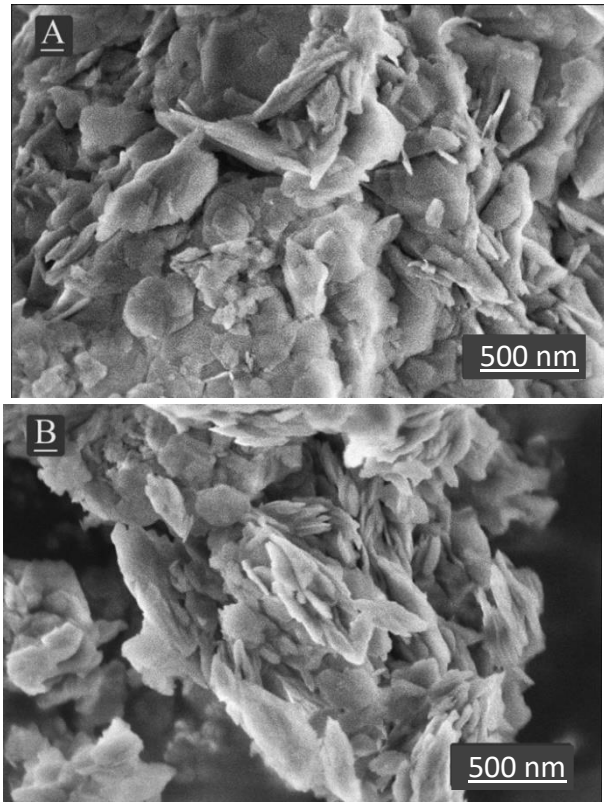

Fig. 28. SEM micrographs of Mg_3Al_1 LDHs intercalated with formate without (A) and under sonication (B).

3.5. Structural and luminescent properties of Cr-substituted $Mg_3Al_{1-x}Cr_x$ layered double hydroxides

In this part of work Cr-substituted $Mg_3Al_{1-x}Cr_x$ LDHs were synthesized through the phase conversion of sol-gel-derived mixed metal oxides in aqueous medium. Cr-substitution level in the range from 1 mol% to 25 mol% was investigated.

3.5.1. Characterization of synthetized $Mg_3Al_{1-x}Cr_x$ LDHs

The XRD patterns of Mg_3Al_1 and $Mg_3Al_{1-x}Cr_x$ LDHs with different chromium substitution levels (1 mol% – 25 mol%) are shown in Fig. 29.

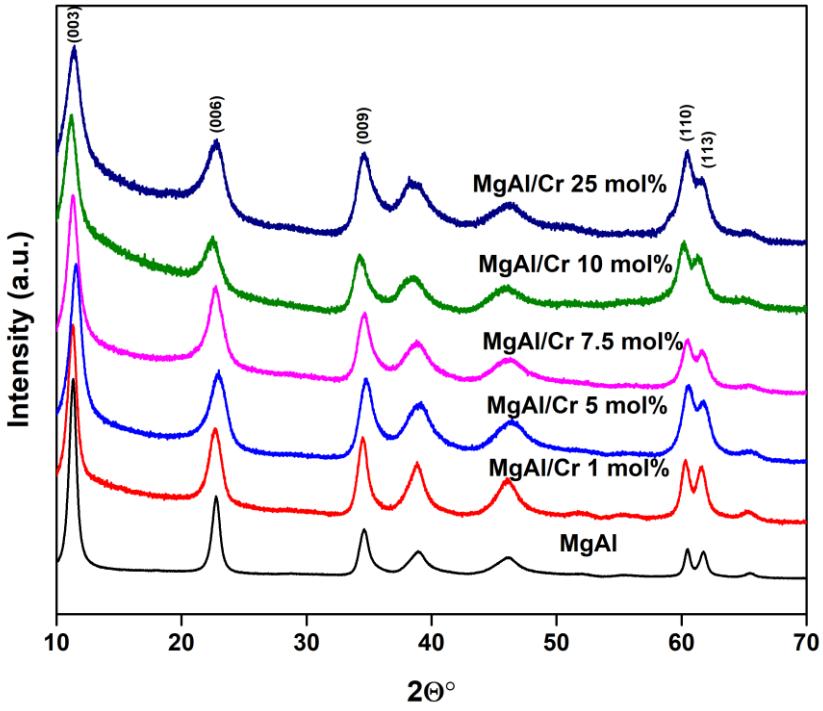

Fig. 29. XRD patterns of Cr-substituted $Mg_3Al_{1-x}Cr_x$ LDHs.

No diffraction lines attributable to the side phases could be observed in the XRD patterns of sol-gel derived LDH samples. The calculated values of d spacing and lattice parameters of $Mg_3Al_{1-x}Cr_x$ LDHs are summarized in Table 2.

Table 2. The values of d spacing and lattice parameters of $Mg_3Al_{1-x}Cr_x$ LDHs calculated by Le Bail method.

Sample	d (003), Å	d (006), Å	d (110), Å	Lattice parameters, Å	
				a	c
MgAl	7.6033	3.8017	1.5187	3.0374	22.8100
MgAl/Cr 1 mol%	7.7470	3.8735	1.5242	3.0484	23.2408
MgAl/Cr 5 mol%	7.7748	3.8876	1.5276	3.0551	23.3248
MgAl/Cr 7.5 mol%	7.8028	3.9015	1.5314	3.0627	23.4094
MgAl/Cr 10 mol%	7.8373	3.9187	1.5367	3.0733	23.5122
MgAl/Cr 25 mol%	7.8774	3.9475	1.5579	3.1158	23.6586

As seen, both d values and lattice parameters slightly increase with increasing amount of chromium in LDH structure. This was expected, since smaller Al^{3+} ion (0.535 Å, CN = 6) was monotonically replaced by larger Cr^{3+} ion (0.615 Å, CN = 6) [151].

3.5.2. ICP-OES and EDX results of elemental analysis of synthesized $Mg_3Al_{1-x}Cr_x$ LDHs

ICP-OES and EDX were used for the determination of chromium, magnesium and aluminium in Cr-substituted $Mg_3Al_{1-x}Cr_x$ LDHs samples. The summarized results (see Table 3) indicate that using both analysis methods, the molar ratio of Mg and Al and introduced amount of Cr are in a good agreement and coincide with nominal ones.

Table 3. ICP-OES and EDX results of elemental analysis of synthesized $Mg_3Al_{1-x}Cr_x$ LDHs.

Sample	ICP-OES		EDX	
	n(Cr), %	n(Mg):n(Al+Cr)	n(Cr), %	n(Mg):n(Al+Cr)
MgAl/Cr 1 mol%	1.12	3:0.994	1.43	3:0.993
MgAl/Cr 5 mol%	5.39	3:0.990	7.22	3:1.06
MgAl/Cr 7.5 mol%	7.91	3:0.988	7.77	3:1.02
MgAl/Cr 10 mol%	10.5	3:0.997	12.9	3:0.875
MgAl/Cr 25 mol%	25.8	3:1.01	26.3	3:1.02

3.5.3. Luminescent properties of synthesized $Mg_3Al_{1-x}Cr_x$ LDHs

The reflection spectra of $Mg_3Al_{1-x}Cr_x$ LDHs as a function of Cr^{3+} concentration is given in Fig. 30a. All the spectra contain two broad absorption bands with maxima at ca. 550 and 380 nm. These bands can be assigned to the Cr^{3+} optical transitions of $^4A_{2g} \rightarrow {}^4T_{2g}(^4F)$ and $^4A_{2g} \rightarrow {}^4T_{1g}(^4F)$, respectively [152, 153]. The increase of Cr^{3+} concentration in the samples resulted in increased absorption. Similarly, to the reflection spectra, there are several broad bands in excitation spectra (see Fig. 30b) as well. One band possesses the maximum at ca. 545 nm and is attributed to the $^4A_{2g} \rightarrow {}^4T_{2g}(^4F)$ optical transition, whereas the other band peaks at ca. 420 nm and can be assigned to the $^4A_{2g} \rightarrow {}^4T_{1g}(^4F)$ optical transition of Cr^{3+} ions. It is interesting to note that excitation spectrum of 1% Cr^{3+} doped sample (MgAl/Cr 1 mol%) contains the third band at ca. 310 nm. This band arises from the $^4A_{2g} \rightarrow {}^4T_{1g}(^4P)$ transitions of Cr^{3+} ions.

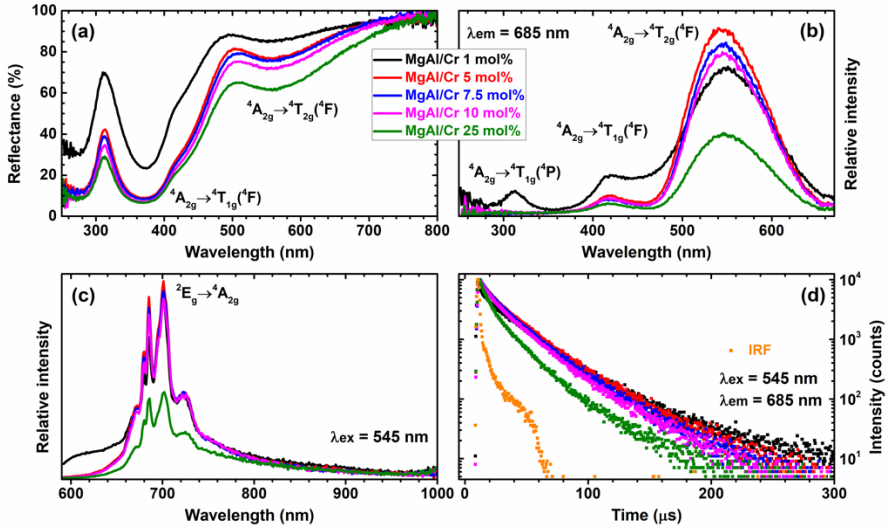

Figure 30. Reflection (a), excitation (b), emission (c), and PL decay curves (d) of $Mg_3Al_{1-x}Cr_x$ LDHs as a function of Cr^{3+} concentration. IRF in section (d) stands for Instrument Response Function.

Emission spectra of $Mg_3Al_{1-x}Cr_x$ LDHs samples are depicted in Fig. 30c. There are several relatively sharp emission lines in the range of 660 – 740 nm that can be assigned to the $^2E_g \rightarrow {}^4A_{2g}$ optical transition of Cr^{3+} ions. The strongest emission was observed for the sample doped with 5% Cr^{3+} ions. However, the emission intensity of samples doped with 1% – 10% Cr^{3+} is

relatively similar. Further increase of Cr^{3+} concentration to 25% has resulted in a severe concentration quenching. These results go hand in hand with $Mg_3Al_{1-x}Cr_x$ LDHs PL decay curves given in Fig. 30d. The PL decay curves of samples doped with 1% to 10% Cr^{3+} are packed very close together indicating the similar PL lifetime values. This is not, however, true for the PL decay curve of sample doped with 25% Cr^{3+}. Its curve is much steeper indicating lower PL lifetime values. Therefore, the effective PL lifetime values (τ_{eff}) were calculated for the analyzed samples [154]. It was found that the τ_{eff} values gradually decrease with increasing Cr^{3+} concentration what indicates that the internal efficiency of Cr^{3+} ions is decreasing as well.

4. CONCLUSIONS

1. The $Mg_{3-x}M_x/Al_1$ (M = Mn, Co, Ni, Cu, Zn) LDHs were successfully synthesized by an aqueous sol-gel method. It was demonstrated that different amount of Mn, Co, Ni, Cu, and Zn could be introduced to the sol-gel derived LDHs without destroying the layered structure. The XRD results showed that 12% mol of manganese, 14% mol of cobalt, 5% mol of nickel, 2.5% mol of copper and about 20% mol of zinc could be substituted in the magnesium positions in the Mg_3Al_1 LDHs without formation of impurities. It was demonstrated that the nature and the amount of transition metal affect the surface properties, morphological features and porosity of end products.

2. An indirect sol-gel synthesis method was also applied to prepare alkaline earth metal substituted LDHs of $Mg_{2-x}M_x/Al_1$ (M = Ca, Sr, Ba). The mixed metal oxides (MMO) were synthesized by two different routes and reconstructed in water at 50 °C for 6 h (pH 10). The obtained results confirmed that the substitution of magnesium by Ca, Sr, Ba in the MMO and LDHs obtained highly depends on the nature and concentration of the alkaline earth metal. It was demonstrated for the first time that the microstructure of reconstructed MMO from sol-gel derived LDHs showed a “memory effect”, i.e., the microstructural features of MMO were almost identical as was determined for LDHs.

3. The synthesized Mg(M)–Al (M = Ca, Sr, Ba) MMO samples exhibited type IV isotherms independent of the synthesis temperature. It was found that the pore size distributions obtained by the BJH method for the MMO specimens synthesized from the reconstructed Mg_2/Al_1 LDHs depended on both the synthesis temperature and nature of the substituent.

4. The sol-gel derived Mg_3/Al_1 and $Mg_{3-x}M_x/Al_1$ (M = Mn, Co, Ni, Cu, Zn) LDHs were intercalated with different organic anions (formate ($HCOO^-$), acetate (CH_3COO^-), oxalate ($C_2O_4^{2-}$), tartrate ($C_4H_6O_4^{2-}$) and citrate ($C_6H_5O_7^{3-}$)) using ion exchange approach. The influence of ultrasound and cation substitution on the intercalation of organic anions to the Mg_3/Al_1 LDH has been investigated. The results demonstrated that ultrasound had a positive effect in some cases for the intercalation of organic anions into the Mg_3/Al_1 LDH system. The substitution of magnesium by transition metals had only negligible effect on the intercalation process. It was concluded that formate

contrary oxalate, tartrate and citrate was only adsorbed on the surface of LDHs but did not enter the interlayer space.

5. The chromium substituted $Mg_3Al_{1-x}Cr_x$ LDHs within the substitution range of chromium from 1 mol% to 25 mol% were successfully synthesized for the first time by an aqueous sol-gel processing route The calculated values of *d* spacing and lattice parameters of $Mg_3Al_{1-x}Cr_x$ LDHs slightly increased with increasing amount of chromium. The results of elemental analysis showed that the molar ratio of Mg, Al and introduced amount of chromium were in a good agreement with the nominal ones.

6. The sol-gel-derived $Mg_3Al_{1-x}Cr_x$ LDHs consisted of characteristic hexagonally shaped nanoparticles 200–300 nm in size regardless of the chromium substitution level. All Cr-containing powders exhibited characteristic emission in the red region of the visible spectrum. The major emission lines of $Mg_3Al_{1-x}Cr_x$ LDHs excited at 545 nm peaked in the red spectral region at 680–695 nm, originating from the $^2E_g \rightarrow {}^4A_2$ transition. The highest intensity of emission was observed for the $Mg_3Al_{1-x}Cr_x$ LDH specimen containing 5% of Cr^{3+}. With further increasing the chromium content up to 25%, concentration quenching was observed.

CONFERENCES

1. L. Valeikiene, R. Paitian, I. Grigoraviciute-Puroniene, A. Kareiva, “Sol-gel synthesis and characterization of Mg(X)/Al (X = Ca, Sr, Ba, Ni, Cu, Zn) layered double hydroxides”, 6th ISGS Summer School, Alghero, Italy, 2018 09 16-19
2. L. Valeikiene, R. Paitian, I. Grigoraviciute-Puroniene, A. Kareiva, “Sol-gel synthesis of Mg(X)/Al (X = Ca, Sr, Ba, Ni, Cu, Zn) layered double hydroxides”, Ecobalt 2018, P8, Lietuva, Vilnius, 2018 10 25-27.
3. L. Valeikiene, I. Grigoraviciute-Puroniene, A. Kareiva, “Sol-gel synthesis of Mg(x)/Al (x = Mn, Co, Ni, Cu, Zn) layered double hydroxides”, Chemistry & Chemical technology 2019, P3, Lietuva, Vilnius 2019 05 16
4. Ligita Valeikiene, Inga Grigoraviciute-Puroniene, Aivaras Kareiva, “Study of Transition Metal Substitution Effects in Sol-Gel Derived $Mg_{3-x}M_x/Al_1$ (M = Mn, Co, Ni, Cu, Zn) Layered Double Hydroxides”, Advanced Materials and tehnologies 2019, P4, Lietuva, Palanga, 2019 08 19-23
5. Ligita Valeikiene, Marina Roshchina, Inga Grigoraviciute-Puroniene, Vladimir Prozorovich, Aleksej Zarkov, Andrei Ivanets, Aivaras Kareiva, “Investigation of the Reconstruction of Sol–Gel Derived $Mg_{2-x}M_x/Al_1$ (M = Ca, Sr, Ba) Layered Double Hydroxides”, Advanced Materials and tehnologies 2020, P9, Lietuva, Palanga, 2020 08 24-28.
6. L. Valeikiene, I. Grigoraviciute-Puroniene, A. Kareiva, “Study of alkaline earth metal substitution effects in sol-gel derived mixed-metal oxides and Mg2-xMx/Al1 (M = Ca, Sr, Ba) layered double hydroxides”, Functional Materials and Nanotechnologies FM&NT-2020, P73, Lietuva, Vilnius, 2020 11 23-26
7. Ligita Valeikiene, Marina Roshchina, Inga Grigoraviciute-Puroniene, Vladimir Prozorovich, Aleksej Zarkov, Andrei Ivanets, Aivaras Kareiva, “Sol–gel synthesis of $Mg_{2-x}M_x/Al_1$ (M = Ca, Sr, Ba) Layered Double Hydroxides”, Nanoctructured Bioceramic Materials 2020, P76, Lietuva, Vilnius, 2020 12 1-3.

ACKNOWLEDGEMENTS

Firstly and mostly I want to thank my supervisor Prof. Aivaras Kareiva for invaluable knowledge and all kind of help. I am immensely grateful for the opportunity to work together, for the great working atmosphere and support I had throughout my doctoral years. You are not only a great scientist, but also an amazing leader. Thank you very much.

Moreover a big thank you to the consultant and beloved friend Assoc. Prof. Inga Grigoravičiūtė–Puronienė for endless support and assistance. Thank you for your sincere help, and advices solving difficulties, also for moral support in the moments of weakness.

Very grateful to the colleagues who helped with the scientific research, especially to Rokas Vargalis, Andrius Pakalniškis, dr. Aleksej Zarkov, dr. Anton Popov, dr. Andrius Laurikėnas, prof. Artūras Katelnikovas. Thanks assoc. prof. Ramūnas Skaudžius and dr. Denis Sokol for assistance resolving scientific issues. Thanks to Justina Gaidukevič for the knowledge passed on during the measurements.

I also want to thank my husband and parents for their endless support and faith in me.

REFERENCES

1. F. Cavani, F. Trifiro, A. Vaccari **Hydrotalcite-type anionic clays: Preparation, properties and applications** Catal. Today, 11 (1991), pp. 173-301.
2. S. P. Newman, W. Jones **Synthesis, characterisation and applications of layered double hydroxides containing organic guests** New J. Chem. 22 (1998) pp. 105-115.
3. M. J. Holgado, V. Rives, M.S. San Roman **Characterization of Ni-Mg-Al mixed oxides and their catalytic activity in oxidative dehydrogenation of n-butane and propene** Appl. Catal. A-General 214 (2001) pp. 219-228.
4. L. Shi, D.Q. Li, J.R. Wang, S.F. Li, D.G. Evans, X. Duan **Synthesis, flame-retardant and smoke-suppressant properties of a borate-intercalated layered double hydroxide** Clays Clay Miner. 53 (2005) pp. 294-300.
5. D.G. Evans, X. Duan **Preparation of layered double hydroxides and their applications as additives in polymers, as precursors to magnetic materials and in biology and medicine** Chem. Commun. 5 (2006) pp. 485-496.
6. D.L. Bish **Anion-exchange in takovite-Applications to other hydroxide minerals** Bull. Mineralogie 103 (1980) pp. 170-175.
7. A. Vaccari **Preparation and catalytic properties of cationic and anionic clays** Catal. Today 41 (1998) pp. 53-71.
8. N. Das, A. Samal **Synthesis, characterisation and rehydration behaviour of titanium (IV) containing hydrotalcite like compounds** Micropor. Mesopor. Mater. 72 (2004) pp. 219-225.
9. F. Li, X. Duan **Applications of layered double hydroxides** Struct. Bond 119 (2006) pp. 193-223.
10. D. Sokol, K. Klemkaite-Ramanauske, A. Khinsky, K. Baltakys, A. Beganskiene, A. Baltusnikas, J. Pinkas, A. Kareiva **Reconstruction effects on surface properties of Co/Mg/Al layered double hydroxide** Mater. Sci. (Medžiagotyra) 23 (2017) pp. 144–149.
11. G. Mishra, B. Dash, S. Pandey **Layered double hydroxides: A brief review from fundamentals to application as evolving biomaterials** Appl. Clay Sci. 1539 (2018) pp. 172-186.
12. D.E.L. Vieira, D. Sokol, A. Smalenskaite, A. Kareiva, M.G.S. Ferreira, J.M. Vieira, C.M.A. Brett, A.N. Salak **Cast iron corrosion protection**

with chemically modified Mg-Al layered double hydroxides synthesized using a novel approach Surf. Coat. Technol. 375 (2019) pp. 158-163.

13. A. Smalenskaite, L. Pavasaryte, T.C.K. Yang, A. Kareiva **Undoped and Eu^{3+} doped magnesium-aluminium layered double hydroxides: Peculiarities of intercalation of organic anions and investigation of luminescence properties**. Materials 12 (2019) pp. 736.
14. Y.L. Li, J. Ma, Y.X. Yuan **Enhanced adsorption of chromium by stabilized Ca/Al-Fe layered double hydroxide decorated with ferric nanoparticles** Sci. Adv. Mater. 12 (2020) pp. 441-448.
15. Z.D. Zhang, J.Y. Qin, W.C. Zhang, Y.T. Pan, D.Y. Wang, R.J. Yang **Synthesis of a novel dual layered double hydroxide hybrid nanomaterial and its application in epoxy nanocomposites** Chem. Eng. J. 381 (2020) pp. 122777.
16. S. Miyata **Anion-exchange properties of hydrotalcite-like compounds** Clay. Clay. Miner. 31 (1983) pp. 305-314.
17. K. Klemkaite, A. Khinsky, A. Kareiva **Reconstitution effect of Mg/Ni/Al layered double hydroxide** Mater. Lett. 65 (2011) pp. 388-391.
18. A. Jaiswal, M.C. Chattopadhyaya **Synthesis and characterization of novel Co/Bi-layered double hydroxides and their adsorption performance for lead in aqueous solution** Arab. J. Chem. 10 (2017) pp. S2457-S2463.
19. S. M. Auerbache, K.A. Corrdado, P.K. Dutta **Hand Book of Layered Materials** Marcel Dekker Inc, New York (2014) pp. 378-474.
20. K. Klemkaite-Ramanauske, A. Zilinskas, R. Taraskevicius, A. Khinsky, A. Kareiva **Preparation of Mg/Al layered double hydroxide (LDH) with structurally embedded molybdate ions and application as a catalyst for the synthesis of 2- adamantylidene(phenyl)amine schiff base** Polyhedron 68 (2014) pp. 340-345.
21. T. Sato, H. Fujita, T. Endo, M. Shimada, A. Tsunashima **Synthesis of hydrotalcite-like compounds and their physic-chemical properties** Reactiv. Solids 5 (1998) pp. 219-228.
22. K. Klemkaite, I. Prosycevas, R. Taraskevicius, A. Khinsky, A. Kareiva **Synthesis and characterization of layered double hydroxides with different cations (Mg, Co, Ni, Al), decomposition and reformation of mixed metal oxides to layered structures** Centr. Eur. J. Chem. 9 (2011) pp. 275-282.
23. A.N. Salak, J. Tedim, A.I. Kuznetsova, J.L. Ribeiro, L.G. Vieira, M.L. Zheludkevich, M.G.S. Ferreira **Comparative X-ray diffraction and**

infrared spectroscopy study of Zn-Al layered double hydroxides: Vanadate vs nitrate Chem. Phys. 397(2012) pp. 102-108.

24. M. Meyn, K. Beneke, G. Lagaly **Anion exchange reactions of layered double hydroxides** Inorg. Chem. 29 (1990) pp. 5201-5206.
25. H.W. Olfs, L.O. Torres-Dorante, R. Eckelt, H. Kosslick **Comparison of different synthesis routes for Mg-Al layered double hydroxides (LDH): Characterization of the structural phases and anion exchange properties** Appl. Clay Sci. 43 (2009) pp. 459-464.
26. D. Scarpellini, C. Falconi, P. Gaudio, A. Mattoccia, P.G. Medaglia, A. Orsini, R. Pizzoferrato, M. Richetta **Morphology of Zn/Al layered double hydroxide nanosheets grown onto aluminum thin films** Microelectr. Eng. 126 (2014) pp. 129-133.
27. C. Jaubertie, M.J. Holgado, M.S. San Román, V. Rives **Structural characterization and delamination of lactate-intercalated Zn,Al-layered double hydroxides** Chem. Mater. 18 (2006) pp. 3114-3121.
28. A. Smalenskaite, D.E.L. Vieira, A.N. Salak, M.G.S. Ferreira, A. Katelnikovas, A. Kareiva **A comparative study of co-precipitation and sol-gel synthetic approaches to fabricate cerium-substituted Mg/Al layered double hydroxides with luminescence properties** Appl. Clay Sci. 143 (2017) pp. 175-183.
29. D. Sokol, A.N. Salak, M.G.S. Ferreira, A. Beganskiene, A. Kareiva **Bi-substituted Mg_3Al-CO_3 layered double hydroxides** J. Sol-Gel Sci. Technol. 85 (2018) pp. 221-230.
30. A. Smalenskaite, A. N. Salak, A. Kareiva **Induced neodymium luminescence in sol-gel derived layered double hydroxides** Mendeleev Commun. 28 (2018) pp. 493-494.
31. A.I. Khan, D. O'Hare **Intercalation chemistry of layered double hydroxides: recent developments and applications recent developments and applications** J. Mater. Chem. 12 (2002) pp. 3191-3198.
32. W.Y. Nie **Dynamics analysis of anion exchange in layered double hydroxides** Brazil. J. Chem. Eng. 37 (2020) pp. 795-803.
33. X.J. Zhao, Y.Q. Zhu, S.M. Xu, H.M. Liu, P. Yin, Y.L. Feng, H. Yan **Anion exchange behavior of $M^{II}Al$ layered double hydroxides: a molecular dynamics and DFT study** Phys. Chem. Chem. Phys. 22 (2020) pp.19758-19768.
34. A. Smalenskaite, S. Sen, A.N. Salak, M.G.S. Ferreira, A. Beganskiene, A. Kareiva **Sol-gel derived lanthanide-substituted layered double hydroxides $Mg_3/Al_{1-x}Ln_x$** A. Phys. Pol. A 133 (2018) pp. 884-886.

35. N. Sonoyama, K. Takagi, S. Yoshida, T. Ota, P.D. Kimilita, Y. Ogasawara **Optical properties of the europium (II) and (III) ions doped metal oxides obtained from sintering layered double hydroxides, and their fine structures** Appl. Clay Sci. 186 (2020) pp. 105440.
36. F.L. Sousa, M. Pillinger, R.A.S. Ferreira, C.M. Granadeiro, A.M.V. Cavaleiro, J. Rocha, L.D. Carlos, T. Trindade, H.I.S. Nogueira **Luminescent polyoxotungstoeuropate anion-pillared layered double hydroxides** Eur. J. Inorg. Chem. (2006) pp. 726-734.
37. R.A.S. Ferreira, M. Nolasco, A.C. Roma, R.L. Longo, O.L. Malta, L.D. Carlos **Dependence of the lifetime upon the excitation energy and intramolecular energy transfer rates: The $^{5}D_{0}$ Eu^{III} emission case** Chem.-A Eur. J. 18 (2012) pp. 12130-12139.
38. Y.Q. Jia, S. Zhao, Y.F. Song **The application of spontaneous flocculation for the preparation of lanthanide-containing polyoxometalates intercalated layered double hydroxides: highly efficient heterogeneous catalysts for cyanosilylation** Appl. Catal. A-Gener. 487 (2014) pp. 172-180.
39. Y. Fu, F.Y. Ning, S.M. Xu, H.L. An, M.F. Shao, M. Wei **Terbium doped ZnCr-layered double hydroxides with largely enhanced visible light photocatalytic performance** J. Mater. Chem. A 4 (2016) pp. 3907-3913.
40. T.L. Wang, M.T. Liu, H.W. Ma, D.F. Cao **Synthesis and characterization of La-doped luminescent multilayer films** J. Chem. 2017 (2017) pp. 8203581.
41. K.N. Andrade, G.G.C. Arizaga, J.A.R. Mayorga **Effect of Gd and Dy concentrations in layered double hydroxides on contrast in magnetic resonance imaging**. Processes 8 (2020) pp. 462.
42. P. Gunawan, R. Xu **Lanthanide-doped layered double hydroxides intercalated with sensitizing anions: Efficient energy transfer between host and guest layers** J. Phys. Chem. C 113 (2009) pp. 17206-17214.
43. L. Liu**,** Q. Wang**,** C. Gao**,** H. Chen**,** W. Liu**,** Y. Tang **Dramatically enhanced luminescence of layered terbium hydroxides as induced by the synergistic effect of Gd3+ and organic sensitizers** J. Phys. Chem. C. 118 (2014) pp. 14511-14520.
44. A. Smalenskaite, A.N. Salak, M.G.S. Ferreira, R. Skaudzius, A. Kareiva **Sol-gel synthesis and characterization of hybrid inorganic-organic Tb(III)-terephthalate containing layered double hydroxides** Opt. Mater. 80 (2018) pp. 186-196.

45. D.G. Evans, R.C.T. Slade **Structural aspects of layered double hydroxides** Struct. Bond 119 (2006) pp. 1-87.
46. M. Catti, G. Ferraris, S. Hull, A. Pavese **Static compression and H-disorder in brucite, $Mg(OH)_2$, to 11 GPA-A powder neutron-diffraction study** Phys. Chem. Miner 22 (1995) pp. 200-206.
47. Z. Wang, P. Fongarland, G.Z. Lu, N. Essayem **Reconstructed La-, Y-, Ce-modified MgAl-hydrotalcite as a solid base catalyst for aldol condensation: Investigation of water tolerance** J. Catal 318 (2014) pp. 108-118.
48. P. Liu, K. Youa, R. Deng, Z. Chen, J. Jian, F. Zhao, P. Ai, Q. Liua, H. Luo **Hydrotalcite-derived Co-MgAlO mixed metal oxides as efficient and stable catalyst for the solvent-free selective oxidation of cyclohexane with molecular oxygen** Molec. Catal. 466 (2019) pp. 130-137.
49. S. Miyata **Anion-exchange properties of hydrotalcite-like compounds** Clay. Clay. Miner. 31 (1983) pp. 305-314.
50. K. Klemkaite, A. Khinsky, A. Kareiva **Reconstitution effect of Mg/Ni/Al layered double hydroxide.** Mater. Lett. 65 (2011) pp. 388-391.
51. S. Miyata, T. Kumura **Synthesis of new hydrotalcite-like compounds and their physico-chemical properties** Chem. Lett. (1973) pp. 843-848.
52. R. Allmann **The crystal structure of pyaurite.** Acta. Cryst. B24 (1968) pp. 972-977.
53. H.F.W. Taylor Segregation and cation-ordering in sjögrenite and pyroaurite Miner. Mag. 37 (1969) pp. 338-342.
54. H.F.W. Taylor **Crystal structures of some double hydroxide minerals** Miner. Mag. 39 (1973) pp. 377-389.
55. B. Clavier, T. Baptiste, F. Massuyeau, A. Jouanneaux, A. Guiet, F. Boucher, V. Fernandez, C. Roquesd, G. Corbel **Enhanced bactericidal activity of brucite through partial copper substitution J. Mater. Chem. B 8** (2020) pp. 100-113.
56. K. Shinoda, N. Aikawa **Interlayer proton transfer in brucite under pressure polarized IR spectroscopy to 5.3 GPa** Phys. Chem. Min. 25 (1998) pp. 197-202.
57. Z.K. Birgul, A. Ahmet **Layered double hydroxides-multifunctional nanomaterials** Chem. Pap. 66 (2012) pp. 1-10.
58. A. de Roy, C. Forano, J. P. Besse **Layered Double Hydroxides: Present and Future** Nova Science Publishers Inc, New York (2001) pp 8-87.
59. L.A. Utracki, M. Sepehr, E. Boccaleri **Polymers for Advanced. Technologies** 18 (2007) pp. 1-37.

60. M.R. Othman, Z. Helwani, Martunus, W.J.N. Fernando Synthetic hydrotalcites from different routes and their application as catalysts and gas adsorbents: a review Appl. Organomet. Chem. 23 (2009) pp. 335-346.
61. D. Chaillot, S. Bennici, J. Brendlé **Layered double hydroxides and LDH-derived materials in chosen environmental applications: a review**. Environ. Sci. Pollut. Res. Apr 1 (2020).
62. A. Karmakar, K. Karthick, S. Sam Sankar, S. Kumaravel, R. Madhu, S. Kundu **A vast exploration of improvising synthetic strategies for enhancing the OER kinetics of LDH structures: a review J. Mater. Chem. A 9 (2021) pp. 1314-1352.**
63. M.V.Bukhtiyarova **A review on effect of synthesis conditions on the formation of layered double hydroxides** J. Solid State Chem. 269 (2019) pp. 494-506.
64. V. Rives, M. Del Arco C. Martín Intercalation of drugs in layered double hydroxides and their controlled release: A review Appl. Clay. Sci. 88-89 (2014) pp. 239-269.
65. F. Prinettoa, G. Ghiottia, P. Graffinb D. Tichit **Synthesis and characterization of sol-gel Mg/Al and Ni/Al layered double hydroxides and comparison with co-precipitated samples** Micropor. Mezopor. Mater. 39 (2000) pp. 229-247.
66. K. Sato, T. Wakabayashi, M. Shimada Adsorption of various anions by magnesium aluminum oxide of (Mg0.7Al0.3O1.15) Ind. Eng. Chem. Prod. Res. Dev. 25 (1986) pp. 89-92.
67. E.A. Gardner, S.K. Yun, T. Kwon, T.J. Pinnavaia Layered double hydroxides pillared by macropolyoxometalates Appl. Clay. Sci. 13 (1998) pp. 479-494.
68. J.J. Bravo-Suárez, E.A. Páez-Mozo S.T. Oyama Intercalation of Decamolybdodicobaltate (III) Anion in Layered Double Hydroxides Chem. Mater. 16 (2004) pp. 1214-1225.
69. I. Ogino, Y. Hirayama, S.R. **Mukai Intercalation chemistry and thermal characteristics of layered double hydroxides possessing organic phosphonates and sulfonates** New J. Chem. 44 (2020) 10002-10010.
70. S. Mallakpour, M. Hatami, C.M. Hussain **Recent innovations in functionalized layered double hydroxides: Fabrication, characterization, and industrial applications** Adv. Coll. Interf. Sci. 283 (2020) pp. 102216.

71. V. Rives, M.A. Ulibarri Layered double hydroxides (LDH) intercalated with metal coordination compounds and oxometalates Coord. Chem. Rev. 181 (1991) pp. 61-120.
72. W. Kagunya, Z. Hassan, W. Jones **Catalytic properties of layered double hydroxides and their calcined derivatives** Inorg. Chem. 35 (1996) pp. 5970- 5974.
73. Z. Yang, F. Wang, C. Zhang, G. Zeng, X. Tan, Z. Yu, Y. Zhong, H. Wang, F. Cui
Utilization of LDH-based materials as potential adsorbents and photocatalysts for the decontamination of dyes wastewater: a review RSC Adv. 6 (2016) pp. 79415-79436.
74. S. Anantharajab K. Karthickab S. Kundu **Evolution of layered double hydroxides (LDH) as high performance water oxidation electrocatalysts: A review with insights on structure, activity and mechanism**, Mater. Today Energy 6 (2017) pp. 1-26.
75. Q. Wang, D. O'Hare **Recent Advances in the Synthesis and Application of Layered Double Hydroxide (LDH) Nanosheets** Chem. Rev. 112 (2012) pp. 4124-4155.
76. A.N. Salak, A.D. Lisenkov, M.L. Zheludkevich, M.G.S. Ferreira **Carbonate-free Zn-Al (1:1) layered double hydroxide film directly grown on zinc-aluminum alloy coating** ECS Electrochem. Lett. 3 (2014) C9-C11.
77. M. Serdechnova, A.N. Salak, F.S. Barbosa, D.E.L. Vieira, J. Tedim, M.L. Zheludkevich, M.G.S. Ferreira Interlayer intercalation and arrangement of 2-mercaptobenzothiazolate and 1,2,3-benzotriazolate anions in layered double hydroxides: *In situ* X-ray diffraction study J. Solid State Chem. 233 (2016) pp. 158-165.
78. H.J. Li, X.Y. Su, C.H. Bai, Y.Q. Xu, Z.C. Pei, S.G. Sun Detection of carbon dioxide with a novel HPTS/NiFe-LDH nanocomposite Sens. Actuators B. Chem. 225 (2016) pp. 109-114.
79. P. Lu, S. Liang, L. Qiu, Y.S. Gao, Q. Wang, Thin film nanocomposite forward osmosis membranes based on layered double hydroxide nanoparticles blended substrates J. Membr. Sci. 504 (2016) pp. 196-205.
80. J. Qu, L. Sha, C. Wu, Q. Zhang **Applications of Mechanochemically Prepared Layered Double Hydroxides as Adsorbents and Catalysts: A Mini-Review** *Nanomaterials* 9 (2019) pp. 80.
81. A.M. Aicken, I.S. Bell, P.V. Coveney, W. Jones **Simulation of layered double hydroxide intercalates** Adv. Mater. 9 (1997) pp. 496-500.
82. J. Tronto, E.L. Crepaldi, P.C. Pavan, C.C. De Paula, J.B. Valim **Organic anions of pharmaceutical interest intercalated in magnesium**

aluminum LDHs by two different methods Molec. Cryst. Liquid Cryst. 356 (2001) pp. 227-237.
83. J. Tronto, M.J. dos Reis, F. Silverio, V.R. Balbo, J.M. Marchetti, J.B. **Valim In vitro release of citrate anions intercalated in magnesium aluminium layered double hydroxides** J. Phys. Chem. Solids 65 (2004) pp. 475-480.
84. J.H. Choy, S.J. Choi, J.M. Oh, T. Park **Clay minerals and layered double hydroxides for novel biological applications** Appl. Clay Sci. 36 (2007) pp. 122-132.
85. Z. P. Xu, Q.H. Zeng, G.Q. Lu, A.B. Yu **Inorganic nanoparticles as carriers for efficient cellular delivery** Chem. Eng. Sci. 61 (2006) pp. 1027-1040.
86. Z. Gu, S.Y. Yan, S. Cheong, Z.B. Cao, H.L. Zuo, A.C. Thomas, B.E. Rolfe, Z.P. Xu **Layered double hydroxide nanoparticles: Impact on vascular cells, blood cells and the complement system** J. Coll. Interf. Sci. 512 (2018) pp. 404-410.
87. Y.J. Wu, R.R. Zhu, Y. Zhou, J. Zhang, W.R. Wang, X.Y. Sun, X.Z. Wu, L.M. Cheng, J. Zhang, S.L. Wang **Layered double hydroxide nanoparticles promote self-renewal of mouse embryonic stem cells through the PI3K signaling pathway** Nanoscale 7 (2015) pp. 11102-11114.
88. K. Ladewig, Z.P. Xu, G.Q. Lu, Gao **Layered double hydroxide nanoparticles in gene and drug delivery** Exp. Opin. Drug Deliv. 6 (2009) pp. 907-922.
89. E. Ruiz-Hitzky, P. Aranda, M. Darder, G. Rytwo **Hybrid materials based on clays for environmental and biomedical applications** J. Mater. Chem. 20 (2010) pp. 9306-9321.
90. G. Choi, H. Piao, M.H. Kim, J.H. Choy **Enabling nanohybrid drug discovery through the soft chemistry telescope** Industr. Eng. Chem. Res. 55 (43) (2016) pp. 11211-11224.
91. K.R. Rakhimol, R. Augustine, S. Thomas, N. Kalarikkal **In Nanomedicine and tissue engineering: State of the art and recent trends** Apple Academic Press, Oakville (2016).
92. N.B. Allou, P. Saikia, A. Borah, R.L. Goswamee **Hybrid nanocomposites of layered double hydroxides: an update of their biological applications and future prospects** Coll. Polym. Sci. 295 (2017) pp. 725-747.
93. V.R.R. Cunha, R.B. de Souza, A.M.C.R.P.D.F. Martins, I.H.J. Koh, V.R.L. Constantino **Accessing the biocompatibility of layered double**

hydroxide by intramuscular implantation: histological and microcirculation evaluation Scient. Reports 6 (2016) Art. No. 30547.

94. A.C. Luca, L.D. Duceac, G. Mitrea, M.I. Ciuhodaru, D.L. Ichim, G. Baciu, E.A. Banu, A.C. **Iordache Antibiotic encapsulated nanomaterials with application in medical area** Mater. Plast. 55 (2018) pp. 552-554.
95. A. Smalenskaite, L. Pavasaryte, Thomas C.K. Yang, A. Kareiva **Undoped and Eu3+ doped magnesium-aluminium layered double hydroxides: Peculiarities of intercalation of organic anions and investigation of luminescence properties** Mater. 12 (5) 736 (2019) pp. 1-14.
96. M. Darder, P. Aranda, E. Ruiz-Hitzky **Bionanocomposites: A new concept of ecological, bioinspired, and functional hybrid materials** Adv. Mater. 19 (10) (2007) pp. 1309-1319.
97. E. Ruiz-Hitzky, M. Darder, B. Wicklein, F.M. Fernandes, F.A. Castro-Smirnov, M.A.M. del Burgo, G. del Real, P. Aranda **Advanced biohybrid materials based on nanoclays for biomedical applications** Nanosyst. Eng. Med. 8548 (2012) Art. No. 85480D.
98. M. Ghadiri, W. Chrzanowski, R. Rohanizadeh **Biomedical applications of cationic clay minerals** RSC Adv. 5 (2015) pp. 29467-29481.
99. D.H. Park, G. Choi, J.H. Choy **Bio-layered double hydroxides nanohybrids for theranostics applications. In: Photofunctional Layered Materials** Springer International Publishing, Switzerland (2015).
100. H.Q. Huang, J.B. Xu, K.C. Wei, Y.J. Xu, C.K.K. Choi, M.L. Zhu, L.M. Bian **Bioactive nanocomposite poly (ethylene glycol) hydrogels crosslinked by multifunctional layered double hydroxides nanocrosslinkers** Macromolec. Biosci. 16 (7) (2016) pp. 1019-1026.
101. I.C. Radu, E. Vasile, C.M. Damian, H. Iovu, P.O. Stanescu, C. Zaharia **Influence of the double bond LDH clay on the exfoliation/intercalation mechanism of polyacrylamide nanocomposite hydrogels** Mater. Plast. 55 (2018) pp. 263-268.
102. P. Win, C. G. Lin, Y. Long, W. Chen, G.M. Chen, Y.F. Song **Covalently cross-linked layered double hydroxide nanocomposite hydrogels with ultrahigh water content and excellent mechanical properties** Chem. Eng. J. 335 (2018) pp. 409-415.
103. B. Galateanu, I.C. Radu, E. Vasile, A. Hudita, M.V. Serban, M. Costache, H. Iovu, C. Zaharia **Fabrication of novel silk fibroin-LDHs composite arhitectures for potential bone tissue engineering** Mater. Plast. 54 (2017) pp. 659-665.

104. P. Zhang, Y.H. Hu, R.L. Ma, L. Lia, J. Lu **Enhanced green fluorescence protein/layered double hydroxide composite ultrathin films: bio-hybrid assembly and potential application as a fluorescent biosensor** J. Mater. Chem. B. 5 (2017) pp. 160-166.
105. M. Z. Li, Y.Y. Fu, L. Jin **A dual-signal sensing system based on organic dyes-LDHs film for fluorescence detection of cysteine** Dalt. Trans. 46 (2017) pp. 7284-7290.
106. A. Jayakumar, A. Surendranath, P.V. Mohanan **2D materials for next generation healthcare applications** Int. J. Pharmaceut. 551 (1-2) (2018) pp. 309-321.
107. P.D. Marcato, N.V. Parizotto, D.S.T. Martinez, A.J. Paula, I.R. Ferreira, P.S. Melo, N. Duran, O.L. Alves **New hybrid material based on layered double hydroxides and biogenic silver nanoparticles: Antimicrobial activity and cytotoxic effect** J. Braz. Chem. Soc. 24 (2) (2013) pp. 266-272.
108. A. Matei, R. Birjega, A. Vlad, C. Luculescu, G. Epurescu, F. Stokker-Cheregi, M. Dinescu, R. Zavoianu, O.D. Pavel **Pulsed laser deposition of Mg-Al layered double hydroxide with Ag nanoparticles** Appl. Phys. A-Mater. Sci. Process. 110 (4) (2013) pp. 841-846.
109. S. Saha, S. Ray, R. Acharya, T.K. Chatterjee, J. Chakraborty **Magnesium, zinc and calcium aluminium layered double hydroxide-drug nanohybrids: A comprehensive study** Appl. Clay Sci. 135 (2017) pp. 493-509.
110. M. Richetta, A. Varone, A. Mattoccia, P. G. Medaglia, S. Kaciulis, A. Mezzi, P. Soltani, R. Pizzoferrato **Preparation, intercalation, and characterization of nanostructured (Zn, Al) layered double hydroxides (LDHs)** Surf. Interf. Anal. 50 (11) (2018) pp. 1094-1098.
111. T.M.T. Nguyen, S. Ippili, J.H. Eom, V. Jella, D.V. Tran, S.G. Yoon **Enhanced output performance of nanogenerator based on composite of poly vinyl fluoride (PVDF) and Zn:Al layered-double hydroxides (LDHs) nanosheets** Transact. Electr. Electron. Mater. 19 (6) (2018) pp. 403-411.
112. F. Peng, D.H. Wang, D.D. Zhang, B.C. Yan, H.L. Cao, Y.Q. Qiao, X.Y. Liu **PEO/Mg-Zn-Al LDH composite coating on Mg alloy as a Zn/Mg ion-release platform with multifunctions: Enhanced corrosion resistance, osteogenic, and antibacterial activities** ACS Biomater. Sci. Eng. 4 (12) (2018) pp. 4112-4121.
113. F. Peng, D.H. Wang, D.D. Zhang, H.L. Cao, X.Y. Liu **The prospect of layered double hydroxide as bone implants: A study of mechanical**

properties, cytocompatibility and antibacterial activity Appl. Clay Sci. 165 (2018) pp. 179-187.

114. G. Abellan, J.A. Carrasco, E. Coronado, J.P. Prieto-Ruiz, H. Prima-Garcia **In-situ growth of ultrathin films of NiFe-LDHs: Towards a hierarchical synthesis of bamboo-like carbon nanotubes** Adv. Mater. Interf. 1 (6) (2014) Art. No. 1400184.
115. E.P. Komarala, S. Nigam, M. Aslam, D. Bahadur **In-vitro evaluation of layered double hydroxide-Fe_3O_4 magnetic nanohybrids for thermo-chemotherapy** New J. Chem. 40 (2016) pp. 423-433.
116. Q.W. Li, D.H. Wang, J.J. Qiu, F. Peng, X.Y. Liu **Regulating the local pH level of titanium via Mg-Fe layered double hydroxides films for enhanced osteogenesis** Biomater. Sci. 6 (2018) pp. 1227-1237.
117. C. Taviot-Gueho, V. Prevot, C. Forano, G. Renaudin, C. Mousty, F. Leroux **Tailoring hybrid layered double hydroxides for the development of innovative applications** Adv. Funct. Mater. 28 (27) (2018) Art. No. 1703868.
118. H.N. Tran, C.C. Lin, S.H. Woo, H.P. Chao **Efficient removal of copper and lead by Mg/Al layered double hydroxides intercalated with organic acid anions: Adsorption kinetics, isotherms, and thermodynamics** Appl. Clay Sci. 154 (2018) pp. 17-27.
119. S.T. Lin, H.N. Tran, H.P. Chao, J.F. Lee **Layered double hydroxides intercalated with sulfur-containing organic solutes for efficient removal of cationic and oxyanionic metal ions** Appl. Clay Sci. 162 (2018) pp. 443-453.
120. S. Li, H. Qin, R. Zuo, Z. Bai **Intercalation of methotrexatum into layered double hydroxides via exfoliation-reassembly process** Appl. Surf. Sci. 353 (2015) pp. 643-650.
121. S.Q. Lei, S.N. Wang, B.X. Gao, Y.L. Zhan, Q.C. Zhao, S.S. Jin, G.X. Song, X.C. Lyu, Y.H. Zhang, Y. Tang **Ultrathin dodecyl-sulfate-intercalated Mg-Al layered double hydroxide nanosheets with high adsorption capability for dye pollution** J. Coll. Interf. Sci. 577 (2020) pp. 181-190.
122. S. Xu, M. Zhang, S.Y. Li, H.Y. Zeng, X.Y. Tian, K. Wu, J. Hu, C.R. Chen, Y. Pan **Intercalation of a novel containing nitrogen and sulfur anion into hydrotalcite and its highly efficient flame retardant performance for polypropylene** Appl. Clay Sci. 191 (2020) pp. 105600.
123. M. Wilhelm, M.C. Quevedo, A. Sushkova, T.L.P. Galvao, A. Bastos, M. Ferreira, J. Tedim, **Hexacyanoferrate-intercalated layered double hydroxides as nanoadditives for the detection of early-stage**

corrosion of steel: The revival of Prussian blue Eur. J. Inorg. Chem. 2020 (2020) pp. 2063-2073.

124. K.M. Dietmann, T. Linke, M. d. Nogal Sanchez, J.L. Perez Pavon, V. Rives **Layered double hydroxides with intercalated permanganate and peroxydisulphate anions for oxidative removal of chlorinated organic solvents contaminated water** Minerals 10 (2020) pp. 462.
125. D. Karoblis, K. Mazeika, D. Baltrunas, G. Niaura, A. Zarkov, A. Beganskiene, A. Kareiva, **Sol-gel synthesis, structural, morphological and magnetic properties of BaTiO3-BiMnO3 solid solutions** Ceramics Int. 46 (2020) pp. 16459-16464.
126. J. Grigorjevaite, M. Janulevicius, A. Kruopyte, E. Ezerskyte, R. Vargalis, S. Sakirzanovas, A. Katelnikovas **Synthesis and optical properties of efficient orange emitting $GdB_5O_9:Sm^{3+}$ phosphors** J. Sol-Gel Sci. Technol. 94 (2020) pp. 80-87.
127. A. Pakalniskis, A. Marsalka, R. Raudonis, V. Balevicius, A. Zarkov, R. Skaudzius, A. Kareiva **Sol-gel synthesis and study of praseodymium substitution effects in yttrium aluminium garnet $Y_{3-x}Pr_xAl_5O_{12}$** Optic. Mater. 111 (2021) pp. 110586.
128. X. Hu, X. Gao **Multilayer coating of goldnanorods for combined stability and biocompatibility** Phys. Chem. Chem. Phys. 13 (2011) pp. 10028-10035.
129. Y. Sohn **Structural and spectroscopic characteristics of terbium hydroxide/oxide nanorods and plate** Ceramics Int. 40 (2014) pp. 13803-13811.
130. A. Smalenskaite, S. Sen, A.N. Salak, M.G.S. Ferreira, R. Skaudzius, A. Katelnikovas, A. Kareiva **Sol-Gel Synthesis and Characterization of Non-Substituted and Europium- Substituted Layered Double Hydroxides Mg3/Al1-xEux** Curr. Inorg. Chem. 6 (2016) pp. 149-154.
131. T. Posati, F. Costantino, L. Latterini, M. Nocchetti, M. Paolantoni, L. Tarpani **New insights on the incorporation of lanthanide ions into nanosized layered double hydroxides** Inorg. Chem. 51 (2012) pp. 13229-13236.
132. Z. Zhang, G.M. Chen, J.G. Liu **Tunable photoluminescence of europium-doped layered double hydroxides intercalated by coumarin-3-carboxylate** RSC Adv. 4 (2014) pp. 7991-7997.
133. X.R. Gao, L.X. Lei, L.W. Kang, Y.Q. Wang, Y.W. Lian, K.L. Jiang **Synthesis, characterization and optical properties of a red organic-inorganic phosphor based on terephthalate intercalated Zn/Al/Eu layered double hydroxide** *J. All. Compd.* 585 (2014) pp. 703-707.

134. P. Vicente, M.E. Perez-Bernal, R.J. Ruano-Casero, D. Ananias, P.A.A. Paz, J. Rocha, V. Rives **Luminescence properties of lanthanide-containing layered double hydroxides** Micropor. Mezopor. Mater. 226 (2016) pp. 209-220.
135. M. Shirotori, S. Nishimura, K. Ebitani **Genesis of a bi-functional acid-base site on a Cr-supported layered double hydroxide catalyst surface for one-pot synthesis of furfurals from xylose with a solid acid catalyst** Catal. Sci. Technol. 6 (2016) pp. 8200-8211.
136. F. Melo, N. Morlanes **Study of the composition of ternary mixed oxides: Use of these materials on a hydrogen production process** Catal. Today. 133 (2008) pp. 374-382.
137. F. Rodriguez-Rivas, A. Pastor, G. de Miguel, M. Cruz-Yusta, I. Pavlovic, L. Sanchez **Cr^{3+} substituted Zn-Al layered double hydroxides as UV-Vis light photocatalysts for NO gas removal from the urban environment** Sci. Total Env. 706 (2020) pp. 136009.
138. V. Correcher, J. Garcia-Guinea, **Cathodo- and photoluminescence emission of a natural Mg-Cr carbonate layered double hydroxide** Appl. Clay Sci. 161 (2018) pp. 127-131.
139. X. Yan, T. T. Tsotsis, M. Sahimi **Fabrication of high-surface area nanoporous SiOC materials using pre-ceramic polymer blends and a sacrificial template** Micropor. Mesopor. Mater. 210 (2015) pp. 77-85.
140. L. Valeikiene, R. Paitian, I. Grigoraviciute-Puroniene, K. Ishikawa, A. Kareiva **Transition metal substitution effects in sol-gel derived $Mg_{3-x}M_x/Al_1$ (M = Mn, Co, Ni, Cu, Zn) layered double hydroxides** Mater. Chem. Phys. 237 (2019) pp. 121863.
141. F. Sakina, R.T. Baker **Metal- and halogen-free synthesis of ordered mesoporous carbon materials** Micropor. Mesopor. Mater. 289 (2019) pp. 109622.
142. V. Claude, J.G. Mahy, F. Micheli, J. Geens, S.D. Lambert **Sol-gel Ni/γ-Al_2O_3 material as secondary catalyst for toluene reforming: Tailoring the γ-Al_2O_3 substrate with stearic acid** Micropor. Mesopor. Mater. 291 (2020) pp. 109681.
143. Y. Zhao, J.-G. Li, F. Fang, N. Chu, H. Ma, X. Yang **Structure and luminescence behaviour of as-synthesized, calcined, and restored MgAlEu-LDH with high crystallinity**. *Dalton Trans.* 41 (2012) pp. 12175-12184.
144. N.A.G. Gomez, G.M. Silva, H.M. Wilhelm, F. Wypych **Zn_2Al layered double hydroxides intercalated with nitrate and p-aminobenzoate as ultraviolet protective agents in low-density polyethylene**

nanocomposites and natural insulating oils J. Braz. Chem. Soc. 31 (2020) pp. 971-981.

145. D. Sokol, D. Vieira, A. Zarkov, M. Ferreira, A. Beganskiene, V. Rubanik, A. Shilin, A. Kareiva, A. Salak **Sonication accelerated formation of Mg-Al-phosphate layered double hydroxide via sol-gel prepared mixed metal oxides** Scient. Reports 9 (2019) pp. 10419.
146. K.I. Peterson, D.P. Pullman **Determining the structure of oxalate anion using infrared and Raman spectroscopy coupled with gaussian calculations** J. Chem. Educ. 93 (2016) pp. 1130-1133.
147. H. Tada, J. Bronkema, A.T. Bell **Application of in situ surface-enhanced Raman spectroscopy (SERS) to the study of citrate oxidation on silica-supported silver nanoparticles** Catal. Lett. 92 (2004) pp. 93-99.
148. J. Su, X.L. Yu, J.L. You, S.T. Yin **Raman spectroscopy studies on the aqueous solutions of sodium formate and lithium formate** Guang Pu Xue Yu Guang Pu Fen Xi 25 (2005) pp. 532-536.
149. H. Noma, Y. Miwa, I. Yokoyama, K. Machida **Infrared and Raman intensity parameters of sodium acetate and their intensity distributions** J. Molec. Struct. 242 (1991) pp. 207-219.
150. Z.P. Xu, P.S. Braterman **Synthesis, structure and morphology of organic layered double hydroxide (LDH) hybrids: Comparison between aliphatic anions and their oxygenated analogs** Appl. Clay Sci. 48 (2010) pp. 235-242.
151. R.D. Shannon **Revised Effective Ionic Radii and Systematic Studies of Interatomic Distances in Halides and Chalcogenides** Acta Crystallogr. A32 (1976), pp. 751-767, doi:10.1107/S0567739476001551.
152. G. Blasse, B.C. Grabmaier **Luminescent Materials; Springer-Verlag**: Berlin, (1994) pp. x 232 p.
153. W.M. Yen, S. Shionoya, H. Yamamoto **Fundamentals of Phosphors**; CRC Press: Boca Raton (2007) pp. 335 p.
154. F. Lahoz, I.R. Martín, J. Méndez-Ramos, P. Núñez **Dopant distribution in a Tm^{3+}-Yb^{3+} codoped silica based glass ceramic: An infrared-laser induced upconversion study** J. Chem. Phys. 120 (2004) 6180-6190, doi:10.1063/1.1652016.

SUMMARY IN LITHUANIAN

ĮVADAS

Sluoksniuoti dvigubi hidroksidai (SDH) sulaukia didelio mokslininkų bendruomenės susidomėjimo dėl plačių taikymo galimybių katalizėje, fotochemijoje, elektrochemijoje, biomedicinos moksle, aplinkos apsaugoje, optikoje ir kt.. SDH priklauso anijoninių molžemių šeimai. Yra žinomi kaip hidrotalcito tipo junginiai, susidedantys iš teigiamą krūvį turinčių brusito ($Mg(OH)_2$) tipo sluoksnių. SDH bendra cheminė formulė gali būti užrašyta $[M^{2+}_{1-x}M^{3+}_x(OH)_2]^{x+}(A^{y-})_{x/y}\cdot zH_2O$, kurioje M^{2+} ir M^{3+} yra atitinkamai metalų katijonai, kurių oksidacijos laipsnis yra +2 ir +3. A^{y-} yra neorganinis (pvz., karbonatas, hidroksidas, nitratas, halogenidas, sulfatas, chromatas, vanadatas) arba organinis (pav. karbokslilatai ir kt.) anijonai, tarpsluoksnyje išsidėstęs kartu su vandens molekulėmis.

Termiškai skaidant SDH susidaro M^{2+} ir M^{3+} mišrūs metalų oksidai arba tų oksidų mišinys (MMO). MMO pasižymi dideliu paviršiaus plotu ir "atminties efektu" – unikalia savybe, kurios dėka, pašildžius MMO vandenyje, atsistato prieš terminį skaidymą buvusi sluoksniuota dvigubo hidroksido struktūra.

SDH sintetinamas įvairiais metodais. Dažniausiai naudojamas bendrojo nusodinimo metodas, kuris vykdomas sumaišant tirpiąsias metalų, sudarančių sluoksniuotą hidroksidą, druskas. Kita plačiai taikoma SDH sintezės technika yra anijonų mainų metodas, kurio metu tarpsluoksnyje esantis anijonas pakeičiamas kitu (vyksta intrerkaliacija). Dėl savo prigimtimi skirtingų anijonų įterpimo į SDH kristalinę struktūrą, keičiasi sluoksniuoto hidroksido cheminės ir fizikinės savybės. Daugybėje mokslinių publikacijų parodyta, kad zolių-gelių metodas yra labai patrauklus preparatyvinis sintezės būdas daugiakomponentėms medžiagoms gauti. Neseniai buvo sukurtas netiesioginis zolių-gelių sintezės metodas, leidžiantis pagaminti aukšto grynumo SDH. Sintezės zolių-gelių metodu gauti pradiniai pirmtakų geliai yra kaitinami 650 °C temperatūroje, o susidarę MMO yra atstatomi (rekonstruojami) dejonizuotame vandenyje 80 °C temperatūroje. Šis zolių-gelių sintezės metodas, palyginti su bendrojo nusodinimo metodu, yra paprastesnis, gauti produktai yra homogeniškesni ir pasižymi aukštu kristališkumu.

Eksperimentiškai buvo įrodyta, kad įterpus retųjų žemių elementą (RŽE) į SDH brusito tipo sluoksnius, galima gauti liuminescencines medžiagas, kurios gali būti panaudojamos daugybėje sričių, pav., medicinoje, katalizėje, aplinkosaugoje ir kt. Deja, šių medžiagų panaudojimą riboja žemas emisijos intensyvumas, atsirandantis dėl vandens molekulių ir hidroksilinių grupių

tiesioginės sąveikos su RŽE, esančiu brusito tipo sluoksnyje. Buvo įrodyta, kad RŽE legiruotų SDH interkaliavimas tam tikrais sensibilizuojančiais anijonais leidžia iš dalies išspręsti šią problemą ir smarkiai pagerinti galutinių produktų liuminescencines savybes.

Šio disertacinio darbo **tikslas** yra susintetinti naujus Mg/Al sluoksniuotus dvigubus hidroksidus ir, modifikuojant jų cheminę sudėtį, ištirti katijonų ir anijonų pakaitų įtaką galutinių produktų susidarymui bei gautų SDH savybėms. Šiam tikslui pasiekti buvo iškelti tokie **uždaviniai**:

1. Ištirti zolių-gelių metodu susintetintų $Mg_{3-x}M_x/Al_1$ (M = Mn, Co, Ni, Cu, Zn) SDH pakeitimo pereinamųjų metalų jonais galimybes.
2. Ištirti zolių-gelių metodu susintetintų $Mg_{2-x}M_x/Al_1$ (M = Ca, Sr, Ba) SDH ir atitinkamų MMO pakeitimo šarminių žemių metalų jonais galimybes. Ištirti susintetintų $Mg_{2-x}M_x/Al_1$ (M = Ca, Sr, Ba) SDH rekonstrukcijos ypatumus.
3. Ištirti ultragarso ir katijonų (Mn, Co, Ni, Cu, Zn) pakeitimo įtaką organinių anijonų (formiatas ($HCOO^-$), acetatas (CH_3COO^-), oksalatas ($C_2O_4^{2-}$), tartratas ($C_4H_6O_4^{2-}$) ir citratas ($C_6H_5O_7^{3-}$) įterpimo į Mg_3/Al_1 SDH struktūrą galimybėms.
4. Susintetinti $Mg_3Al_{1-x}Cr_x$ SDH mėginius zolių-gelių metodu ir ištirti Cr^{3+} poveikį gautų mėginių faziniam grynumui, morfologinėms ir liuminescencinėms savybėms.

Šio darbo **naujumas ir originalumas:** Buvo ištirtos zolių-gelių sintezės metodu susintetintų pereinamųjų metalų $Mg_{3-x}M_x/Al_1$ (M = Mn, Co, Ni, Cu, Zn) SDH, šarminių žemių metalų $Mg_{2-x}M_x/Al_1$ (M = Ca, Sr, Ba) SDH (ir atitinkamų MMO) pakeitimo galimybės. Išanalizuoti Mg(M)–Al (M = Ca, Sr, Ba) MMO rekonstrukcijos ypatumai. Ištirta ultragarso ir katijonų (Mn, Co, Ni, Cu, Zn) pakeitimo įtaka organinių anijonų (formiato ($HCOO^-$), acetato (CH_3COO^-), oksalato ($C_2O_4^{2-}$), tartrato ($C_4H_6O_4^{2-}$) ir citrato ($C_6H_5O_7^{3-}$)) į Mg_3/Al_1 SDH struktūrą įterpimui. Pirmą kartą zolių-gelių metodu buvo susintetinti $Mg_3Al_{1-x}Cr_x$ SDH mėginiai. Ištirta Cr^{3+} įtaka gautų mėginių faziniam grynumui, morfologinėms ir liuminescencinėms savybėms.

Atlikti gausūs eksperimentiniai darbai, kurių rezultatai buvo susisteminti keturiuose straipsniuose, leido padaryti svarbias šio disertacinio darbo rezultatų išvadas.

IŠVADOS

1. $Mg_{3-x}M_x/Al_1$ (M = Mn, Co, Ni, Cu, Zn) SDH buvo susintetinti vandeniniu zolių-gelių sintezės metodu. Pradiniai geliai buvo kaitinami 650 ^oC temperatūroje, o gauti MMO rekonstruojami vandenyje, susidarant minėtiems SDH. Nustatyta, kad į $Mg_{3-x}M_x/Al_1$ SDH, nesuardant sluoksniuotos struktūros, gali būti įvedami skirtingi Mn, Co, Ni, Cu ir Zn kiekiai. Susintetinti vienfaziai pakeisti $Mg_{3-x}M_x/Al_1$ SDH, turintys iki 12 mol% mangano, 14 mol% kobalto, 5 mol% nikelio, 2,5 mol% vario ir apie 20 mol% cinko. Parodyta, kad keičiant pereinamąjį metalą ar jo kiekį, susidaro nanostruktūriniai mišrių metalų SDH, turintys skirtingą cheminę sudėtį, fazinį grynumą, porėtumą ir paviršiaus morfologiją.

2. Netiesioginis zolių-gelių sintezės metodas buvo pritaikytas $Mg_{2-x}M_x/Al_1$ (M = Ca, Sr, Ba) SDH sintetinti. Mg(M)–Al (M = Ca, Sr, Ba) MMO buvo susintetinti dviem būdais ir rekonstruoti vandenyje 50 °C temperatūroje, 6 h, esant pH=10. Nustatyta, kad dalį magnio $Mg_{2-x}M_x/Al_1$ pakeitus šarminių žemių metalų (Ca, Sr, Ba) jonais, susintetintų MMO ir SDH fazinis grynumas ir sudėtis priklausė nuo šarminių žemių metalų prigimties ir koncentracijos. Pirmą kartą buvo parodyta, kad iš $Mg_{2-x}M_x/Al_1$ (M = Ca, Sr, Ba) SDH gauti Mg(M)–Al (M = Ca, Sr, Ba) MMO pasižymi „atminties efektu“: MMO mikrostruktūra buvo beveik identiška prieš termini skaidymą buvusio sluoksniuoto hidroksido mikrostruktūrai.

3. Nustatyta, kad nepriklausomai nuo MMO sintezės temperatūros, susintetintų Mg(M)–Al MMO N_2 adsorbcijos-desorbcijos izotermos buvo IV tipo su H1 histereze (ji būdinga mezoporinėms medžiagoms). Taip pat buvo nustatyta, kad porų dydžio pasiskirstymas MMO mėginiuose, susintetintuose iš rekonstruotų Mg_2/Al_1 LDH, nustatytas BJH metodu, priklausė nuo sintezės temperatūros ir nuo magnį pakeičiančio metalo prigimties.

4. Anijonų mainų metodu zolių-gelių metodu susintetintuose Mg_3/Al_1 ir $Mg_{3-x}M_x/Al_1$ (M = Mn, Co, Ni, Cu, Zn) SDH buvo įterpiami organiniai anijonai: formiatas ($HCOO^-$), acetatas (CH_3COO^-), oksalatas ($C_2O_4^{2-}$), tartratas ($C_4H_6O_4^{2-}$) ir citratas ($C_6H_5O_7^{3-}$). Ultragarso panaudojimas tik kai kuriais atvejais turėjo teigiamą poveikį organinių anijonų interkaliacijai į Mg_3/Al_1 SDH struktūrą. Formiatas, priešingai nei oksalatas, tartratas bei citratas, adsorbavosi tik ant sluoksniuotos struktūros paviršiaus, o neįsiterpė į SDH

tarpsluoksnį. Padaryta išvada, kad interkaliacijos procesą mažai veikė magnio pakeitimas pereinamųjų metalų jonais.

5. Zolių-gelių sintezės metodas buvo sėkmingai panaudotas Cr pakeistiems $Mg_3Al_{1-x}Cr_x$ SDH, kuriuose Cr koncentracija buvo keičiama nuo 5 iki 25 mol%, sintetinti. Apskaičiuoti $Mg_3Al_{1-x}Cr_x$ SDH tarplokštuminiai atstumai ir kristalinės gardelės parametrų vertės šiek tiek padidėjo didėjant įvedamo chromo kiekiui. Elementinės analizės rezultatai parodė, kad Mg ir Al molinis santykis ir įvesto chromo kiekis buvo artimi nominaliems.

6. Zolių-gelių metodu susinteinti $Mg_3Al_{1-x}Cr_x$ SDH buvo sudaryti iš heksagoninės formos 200-300 nm dydžio nanodalelių, kurių morfologija nepriklausė nuo įvedamo chromo kiekio. Visi Cr pakeisti $Mg_3Al_{1-x}Cr_x$ SDH pasižymėjo šviesos emisija regimojo spektro raudonojoje srityje. Pagrindinės $Mg_3Al_{1-x}Cr_x$ SDH emisijos linijos, esant 545 nm sužadinimui, buvo matomos raudonojo spektro srityje prie 680–695 nm, atsirandančios dėl $^2Eg \rightarrow {}^4A_2$ perėjimo. Intensyviausia emisija pasižymėjo $Mg_3Al_{1-x}Cr_x$ junginys, turinčiame 5% of Cr^{3+}. Toliau didnant chromo koncentraciją iki 25%, dėl koncentracinio gesinimo emisijos intensyvumas mažėjo.

LIST OF PUBLICATIONS AND CONFERENCES PARTICIPATION

1. L. Valeikiene, R. Paitian, I. Grigoraviciute-Puroniene, K. Ishikawa, A. Kareiva **Transition metal substitution effects in sol-gel derived $Mg_{3-x}M_x/Al_1$ (M= Mn, Co, Ni, Cu, Zn) layered double hydroxides.** *Materials Chemistry and Physics*, 237, 121863 (2019).
2. L. Valeikiene, I. Grigoraviciute-Puroniene, A. Kareiva. **Alkaline earth metal substitution effects in sol-gel derived mixed-metal oxides and $Mg_{2-x}M_x/Al_1$ (M = Ca, Sr, Ba) layered double hydroxides.** *Journal of the Australian Ceramic Society*, 56, 1531–1541 (2020).
3. Ligita Valeikiene [1], Marina Roshchina [2], Inga Grigoraviciute-Puroniene[1], Vladimir Prozorovich [2], Aleksej Zarkov [1], Andrei Ivanets [2], Aivaras Kareiva. **On the Reconstruction Peculiarities of Sol–Gel Derived $Mg_{2-x}M_x/Al_1$ (M = Ca, Sr, Ba) Layered Double Hydroxides.** *Crystals*, 10(6), 470 (2020).
4. Ligita Valeikiene, Inga Grigoraviciute-Puroniene, Arturas Katelnikovas, Aleksej Zarkov, Aivaras Kareiva. **Structural and luminescent properties of Cr-substituted $Mg_3Al_{1-x}Cr_x$ layered double hydroxides synthesized through the conversion of sol-gel-derived mixed metal oxides.** *Molecules*, *26*(7), 1848 (2021)

1 publikacija / 1st publication

Transition metal substitution effects in sol-gel derived $Mg_{3-x}M_x/Al_1$ (M 1⁄4 Mn, Co, Ni, Cu, Zn) layered double hydroxides

L. Valeikiene, R. Paitian, I. Grigoraviciute-Puroniene, K. Ishikawa, A. Kareiva.

Materials Chemistry and Physics **237**, 12863 (2019)

DOI: 10.1016/j.matchemphys.2019.121863

2 publikacija / 2nd publication

Alkaline earth metal substitution effects in sol-gel–derived mixed metal oxides and $Mg_{2-x}M_x/Al_1$ (M = Ca, Sr, Ba)–layered double hydroxides

L.Valeikiene, I. Grigoraviciute-Puroniene, A. Kareiva.

Journal of the Australian Ceramic Society **56,** 1531–1541 (2020)

DOI: 10.1007/s41779-020-00497-7

3 publikacija / 3rd publication

On the Reconstruction Peculiarities of Sol–Gel Derived $Mg_{2-x}M_x/Al_1$ (M = Ca, Sr, Ba) Layered Double Hydroxides

L. Valeikiene, M. Roshchina, I. Grigoraviciute-Puroniene, V. Prozorovich, A. Zarkov, A. Ivanets, A. Kareiva.

Crystals **10**, 470 (2020)

DOI: 10.3390/cryst10060470

crystals

MDPI

Article

On the Reconstruction Peculiarities of Sol–Gel Derived $Mg_{2-x}M_x/Al_1$ (M = Ca, Sr, Ba) Layered Double Hydroxides

Ligita Valeikiene [1], Marina Roshchina [2], Inga Grigoraviciute-Puroniene [1], Vladimir Prozorovich [2], Aleksej Zarkov [1], Andrei Ivanets [2] and Aivaras Kareiva [1,*]

[1] Institute of Chemistry, Faculty of Chemistry and Geosciences, Vilnius University, Naugarduko 24, LT-03225 Vilnius, Lithuania; ligita.valeikiene@chgf.vu.lt (L.V.); inga.grigoraviciute@gmail.com (I.G.-P.); aleksej.zarkov@chf.vu.lt (A.Z.)

[2] Institute of General and Inorganic Chemistry of National Academy of Sciences of Belarus, st. Surganova 9/1, 220072 Minsk, Belarus; che.roschina@bsu.by (M.R.); vladimirprozorovich@gmail.com (V.P.); andreiivanets@yandex.by (A.I.)

* Correspondence: aivaras.kareiva@chgf.vu.lt; Tel.: +37061567428

Received: 6 May 2020; Accepted: 30 May 2020; Published: 2 June 2020

Abstract: In this study, the reconstruction peculiarities of sol–gel derived $Mg_{2-x}M_x/Al_1$ (M = Ca, Sr, Ba) layered double hydroxides were investigated. The mixed metal oxides (MMO) were synthesized by two different routes. Firstly, the MMO were obtained directly by heating Mg(M)–Al–O precursor gels at 650 °C, 800 °C, and 950 °C. These MMO were reconstructed to the $Mg_{2-x}M_x/Al_1$ (M = Ca, Sr, Ba) layered double hydroxides (LDHs) in water at 50 °C for 6 h (pH 10). Secondly, in this study, the MMO were also obtained by heating reconstructed LDHs at the same temperatures. The synthesized materials were characterized using X-ray powder diffraction (XRD) analysis and scanning electron microscopy (SEM). Nitrogen adsorption by the Brunauer, Emmett, and Teller (BET) and Barrett, Joyner, and Halenda (BJH) methods were used to determine the surface area and pore diameter of differently synthesized alkaline earth metal substituted MMO compounds. It was demonstrated for the first time that the microstructure of reconstructed MMO from sol–gel derived LDHs showed a "memory effect".

Keywords: layered double hydroxides; sol–gel processing; alkaline earth metals; mixed metal oxides; reconstruction effect; surface properties

1. Introduction

Layered double hydroxides ($[M^{2+}_{1-x}M^{3+}_x(OH)_2]^{x+}(A^{y-})_{x/y}\cdot zH_2O$, where M^{2+} and M^{3+} are divalent and trivalent metal cations, respectively, and A^{y-} is a intercalated anion, LDHs) are widely used in catalysis, in ion-exchange processes, as catalyst support precursors, adsorbents, anticorrosion inhibitors, anion exchangers, flame retardants, polymer stabilizers, and in pharmaceutical applications, optics, in separation science and photochemistry [1–7]. The most common preparation technique of LDHs is the co-precipitation method starting from the soluble salts of the metals [8–10]. The second synthetic technique also widely used for the preparation of LDHs is anion exchange [11–13]. Recently, for the preparation of Mg_3Al_1 LDHs, we developed the indirect sol–gel synthesis route [14–17]. In this synthetic approach, the synthesized Mg–Al–O precursor gels were converted to the mixed metal oxides (MMO) by heating the gels at 650 °C. The LDHs were fabricated by the reconstruction of MMO in deionized water at 80 °C. The proposed sol–gel synthesis route for LDHs showed some benefits over the co-precipitation and anion-exchange methods such as simplicity, high homogeneity, and good

crystallinity of the end synthesis products, effectiveness, cost efficiency, and suitability for the synthesis of different LDH compositions.

Recently, this newly developed sol–gel synthesis method has been successfully applied for the synthesis of the transition metal substituted layered double $Mg_{3-x}M_x/Al_1$ (M = Mn, Co, Ni, Cu, Zn) [18]. Calcined at temperatures higher than 600–650 °C, the M/Mg/Al LDHs form $M_xMg_{1-x}Al_2O_4$ solid solutions having the spinel structure and various cations distributions [19–23]. It was reported that these spinel structure compounds obtained at high temperatures cannot be reconstructed to the LDHs [24–29].

The investigation of mixed oxides derived from calcined LDHs prepared by direct and indirect methods is an interesting topic, since the reformation conditions could have an effect not only on the composition of a solid but also on the morphology of oxides and consequently on the properties. Usually, the calcined LDHs materials or mixed metal oxides have high surface areas. During the calcination, the dehydroxylation of LDHs with different chemical composition gave rise to the crystal deformation and interstratified structure of metal oxides, resulting in the development of mesopores and enhancement of specific surface area and enhanced sorption capacity [30–34]. Interestingly, the obtained MMO sometimes can preserve the morphology of the LDH precursor and show also the efficient recycling of the spent adsorbent [35,36]. It has been found that the nature of the partially introduced cation into the M^{2+} position influences the conditions of thermal decomposition of LDHs and also the structural and morphological features of the formed mixed metal oxides [37]. The obtained data can be used to synthesize the oxide supports with desired adsorption and other physical properties. In this study, the alkaline earth metal substituted $Mg_{2-x}M_x/Al_1$ (M = Ca, Sr, Ba) layered double hydroxides were synthesized by an indirect sol–gel method. The aim of this study was to decompose the sol–gel-derived LDHs at different temperatures and investigate the possible reconstruction of obtain mixed metal oxides to LDHs. The surface area and porosity as important characteristics of these alkaline earth metal substituted MMO materials were investigated in this study as well.

2. Experimental

Aluminium nitrate nonahydrate ($Al(NO_3)_3{\cdot}9H_2O$, 98.5%, Chempur, Plymouth, MI, USA), magnesium nitrate hexahydrate ($Mg(NO_3)_2{\cdot}6H_2O$), 99,0% Chempur, Plymouth, MI, USA), calcium nitrate tetrahydrate ($Ca(NO_3)_2{\cdot}4H_2O$, 99%, Chempur, Plymouth, MI, USA), strontium nitrate ($Sr(NO_3)_2$, 99.0%, Chempur, Plymouth, MI, USA) and barium nitrate ($Ba(NO_3)_2$, 99.0%, Chempur, Plymouth, MI, USA) were used as metal sources in the preparation of $Mg_{2-x}M_x/Al_1$ (M = Ca, Sr, Ba) layered double hydroxides. In the sol–gel processing, citric acid monohydrate ($C_6H_8O_7{\cdot}H_2O$, 99.5%, Chempur, Plymouth, MI, USA) and 1,2-ethanediol ($C_2H_6O_2$, 99.8%, Chempur, Plymouth, MI, USA) were used as complexing agents. Ammonia solution (NH_3, 25%, Chempur, Plymouth, MI, USA) was used to change pH of the solution.

For the synthesis of $Mg_{2-x}M_x/Al_1$ (M = Ca, Sr, Ba; x is a molar part of substituent metal) LDHs, the stoichiometric amounts of starting materials were dissolved in distilled water under continuous stirring. Citric acid was added to the above solution, and the obtained mixture was stirred for an additional 1 h at 80 °C. Then, 2 mL of 1,2-ethanediol was added to the resulting solution. The transparent gels were obtained by the complete evaporation of the solvent under continuous stirring at 150 °C. The synthesized precursor gels were dried at 105 °C for 24 h. The mixed metal oxides (MMO) were obtained by heating the gels at 650 °C, 800 °C, and 950 °C for 4 h. The $Mg_{2-x}M_x/Al_1$ (M = Ca, Sr, Ba) LDHs were obtained by reconstruction of the MMO in water at 50 °C for 6 h under stirring and by changing the pH of the solution to 10 with ammonia.

X-ray diffraction (XRD) analysis was performed using a MiniFlex II diffractometer (Rigaku, The Woodlands, TX, USA) (Cu Kα radiation) in the 2θ range from 10° to 70° (step of 0.02°) with the exposition time of 2 min per step. The morphological features of MMO samples were estimated using a scanning electron microscope (SEM) Hitachi SU-70, Tokyo, Japan. Nitrogen adsorption by the Brunauer, Emmett, and Teller (BET) and Barret method was used to determine the surface area

and pore diameter of the materials (Tristar II, Norcross, GA, USA). The pore-size distribution was evaluated by the Barrett–Joyner–Halenda (BJH) procedure. Prior to analysis, the calcined samples were outgassed at 523 K for 5 h.

3. Results and Discussion

To study the reconstruction peculiarities of sol–gel derived $Mg_{2-x}M_x/Al_1$ (M = Ca, Sr, Ba) layered double hydroxides (LDHs), the precursor gels were firstly annealed at 650 °C, 800 °C, and 950 °C for 4 h. The XRD patterns of mixed metal oxides (MMO) obtained by heating the Mg_2/Al_1 LDHs precursor gels at different temperatures are presented in Figure 1. The XRD pattern of the sample heated at 650 °C had two XRD peaks, which show the formation of a mixed metal oxide (MMO) phase with an MgO-like structure (JCPDS No. 96-100-0054) [14]. Thermal treatment of the precursor gels at 800 °C resulted in the formation of two phases, namely MMO and a low-crystallinity spinel phase with the composition of $MgAl_2O_4$ (JCPDS No. 96-154-0776). After heating at 950 °C, evidently, the highly crystalline $MgAl_2O_4$ phase has formed along with the MgO phase.

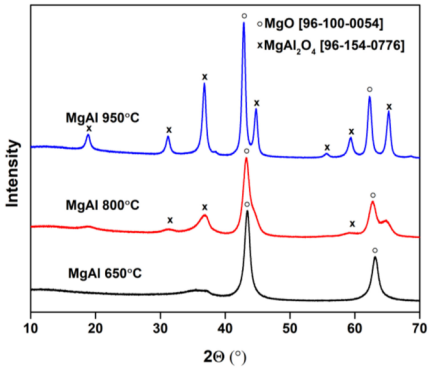

Figure 1. XRD patterns of mixed metal oxides (MMO) obtained by heating the Mg_2/Al_1 precursor gels at 650 °C, 800 °C, and 950 °C.

The XRD patterns of the Mg/Al LDH synthesized by the indirect sol–gel method (reconstruction of sol–gel derived MMO) show the formation of layered double hydroxides independent of the annealing temperature of the precursor gels (see Figure 2).

Three basal reflections typical of an LDH structure were observed: at 2θ of about 10° (003), 23° (006), and 35° (009) [14,15]. Besides, the spinel phase obtained at 800 °C and 950 °C remain almost unchanged during the reconstruction process. These results are in good agreement with those previously published elsewhere [38].

The XRD patterns of synthesis products with the same substitutional level of Ca, Sr, and Ba obtained at 800 °C and 950 °C are almost identical and revealed in all cases with the formation of crystalline magnesium oxide, magnesium spinel phase $MgAl_2O_4$ and an appropriate spinel of alkaline earth metal ($CaAl_2O_4$, $SrAl_2O_4$ and $BaAl_2O_4$). Again, during the partial reconstruction process, the phase purity of sol–gel derived $Mg_{2-x}M_x/Al_1$ LDHs evidently is dependent on the nature of introduced metal. As was expected, the spinel phases obtained at 800 °C and 950 °C remained almost unchanged during the partial reconstruction process. Moreover, during the reconstruction process, a negligible amount of metal carbonates ($CaCO_3$, $SrCO_3$, and $BaCO_3$) have formed as well. The XRD patterns of mixed metal oxides (MMO) obtained by heating the $Mg_{2-x}M_x/Al_1$ (M = Ca, Sr, Ba) precursor gels at different temperatures and reconstructed LDHs are presented in Figures 3–5, respectively. The XRD analysis results confirmed that the phase purity of alkaline earth substituted

LDHs obtained by an indirect sol–gel synthesis approach is highly dependent on both the annealing temperature of the precursor gels and that of the alkaline earth metal.

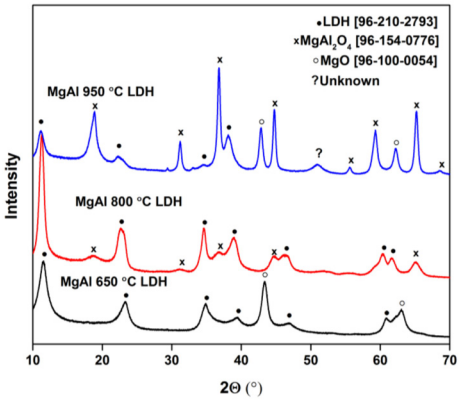

Figure 2. XRD patterns of sol–gel derived Mg_2/Al_1 layered double hydroxides (LDHs, reconstructed from MMO). The annealing temperature of the precursor gels was 650 °C, 800 °C, and 950 °C.

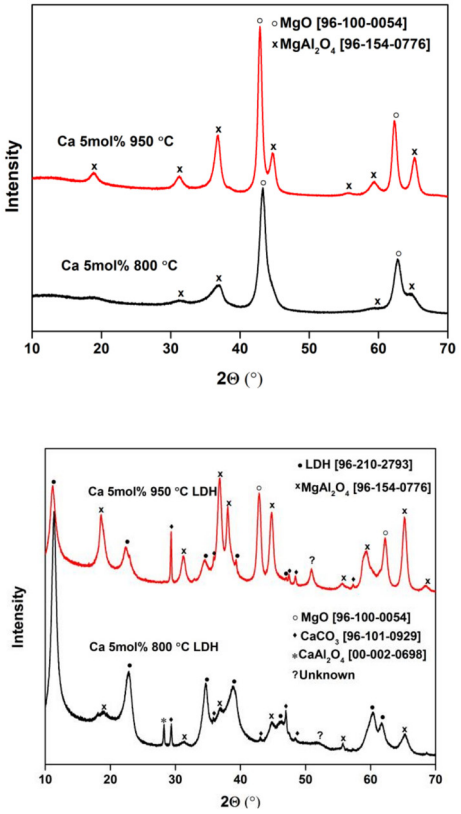

Figure 3. XRD patterns of mixed metal oxides (MMO) obtained by heating the $Mg_{1.95}Ca_{0.05}/Al_1$ precursor gels at 800 °C and 950 °C (**top**) and reconstructed $Mg_{1.95}Ca_{0.05}/Al_1$ LDHs (**bottom**).

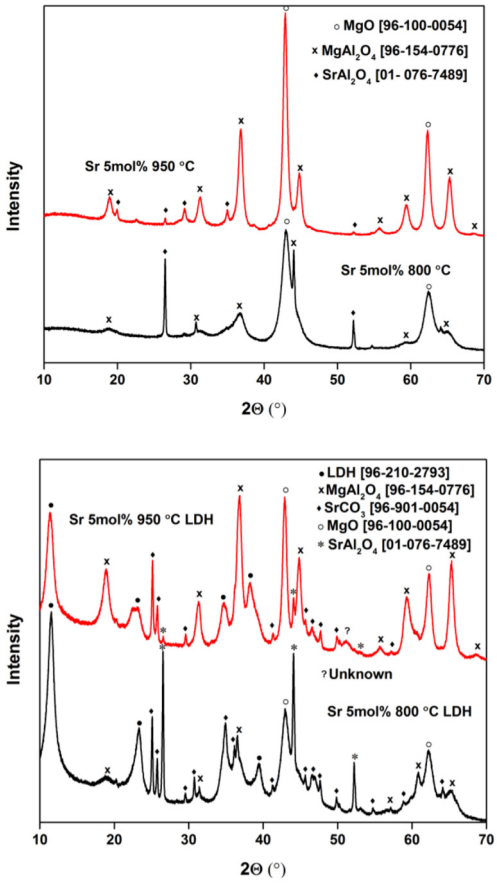

Figure 4. XRD patterns of mixed metal oxides (MMO) obtained by heating the $Mg_{1.95}Sr_{0.05}/Al_1$ precursor gels at 800 °C and 950 °C (**top**) and reconstructed $Mg_{1.95}Sr_{0.05}/Al_1$ LDHs (**bottom**).

The obtained mixed metal LDH samples were repeatedly heated at different temperatures to obtain MMO and compare the phase composition, morphology, and surface properties with obtained ones after initial annealing. The XRD patterns of non-substituted and Ca, Sr, and Ba containing MMO obtained after the heating of LDHs are shown in Figures 6 and 7, respectively. Evidently, the XRD patterns of mixed metal oxides (MMO) obtained by heating the Mg_2/Al_1 precursor gels (see Figure 1) and obtained by heating the Mg_2/Al_1 LDHs (Figure 6) are very similar, confirming the same phase composition. However, the reflections of just obtained MMO are more intense in comparison with ones presented in the repeatedly obtained MMO from LDHs. Obviously, the second time obtained Ca and Sr substituted MMO samples contain much more side phases (see Figures 3, 4 and 7). However, this is not the case for the Ba-substituted MMO samples. Both synthesis products obtained from precursor gels and by heating LDHs were composed of several crystalline phases.

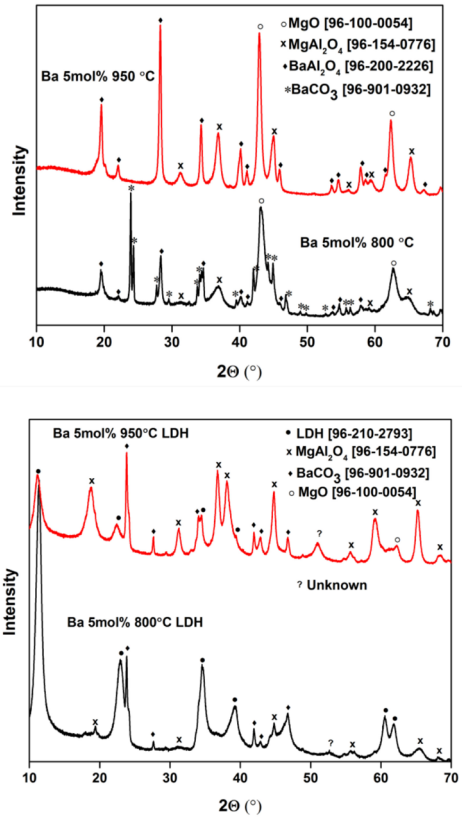

Figure 5. XRD patterns of mixed metal oxides (MMO) obtained by heating the $Mg_{1.95}Ba_{0.05}/Al_1$ precursor gels at 800 °C and 950 °C (**top**) and reconstructed $Mg_{1.95}Ba_{0.05}/Al_1$ LDHs (**bottom**).

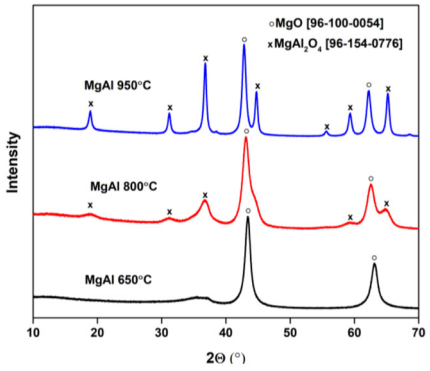

Figure 6. XRD patterns of mixed metal oxides (MMO) obtained by heating the Mg_2/Al_1 LDHs at different temperatures.

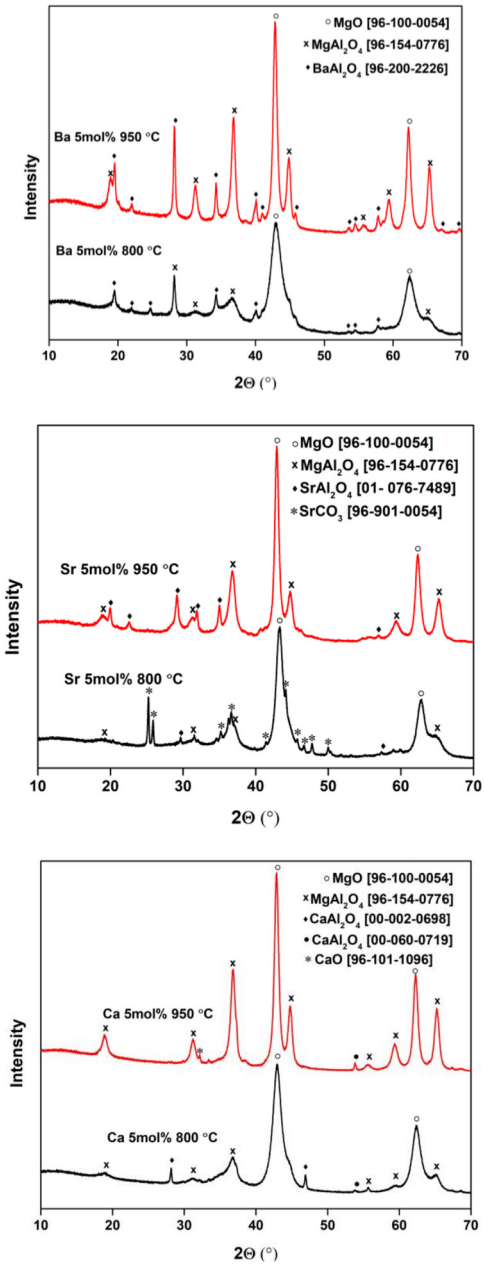

Figure 7. XRD patterns of mixed metal oxides (MMO) obtained by heating the $Mg_{1.95}Ca_{0.05}/Al_1$ LDHs (**bottom**), $Mg_{1.95}Sr_{0.05}/Al_1$ LDHs (**middle**), and $Mg_{1.95}Ba_{0.05}/Al_1$ LDHs (**top**) at different temperatures.

The interplanar spacings and lattice parameters of sol–gel derived $Mg_{2-x}M_x/Al_1$ (M = Ca, Sr and Ba) LDHs with standard deviations in parentheses are presented in Table 1.

Table 1. The interplanar spacings and lattice parameters of sol–gel derived $Mg_{1.95}M_{0.05}/Al_1$ (M = Ca, Sr and Ba) LDHs.

Compound	d(003), Å	d(006), Å	d(110), Å	c, Å	a, Å
Mg_2Al_1	7.601(5)	3.810(3)	1.511(3)	22.818(3)	3.040(2)
$Mg_{1.95}Ca_{0.05}/Al_1$	7.690(4)	3.813(4)	1.512(2)	23.027(4)	3.041(3)
$Mg_{1.95}Sr_{0.05}/Al_1$	7.697(3)	3.826(3)	1.517(3)	23.034(5)	3.039(4)
$Mg_{1.95}Ba_{0.05}/Al_1$	7.695(6)	3.828(4)	1.521(1)	23.176(5)	3.041(4)

Surprisingly, the calculated values of parameter *a* are not increasing monotonically with the increasing ionic radius of metal in $Mg_{1.95}M_{0.05}/Al_1$. On the other hand, the amount of substituent is rather small, and the obtained LDHs were not fully monophasic.

Figures 8–11 show the morphological features of non-substituted and alkaline earth metal-substituted LDHs and MMO obtained by heating the precursor gels or Mg_2/Al_1 LDHs. The SEM micrographs of Mg–Al MMO obtained by heating Mg–Al–O precursor gel (Figure 8) confirm that the surface of synthesized compounds is composed of large monolithic particles at about 15–20 μm in size independent of the annealing temperature (800 °C and 950 °C). The surface of these monoliths is randomly covered with smaller needle-like particles, and some pores also could be detected. The SEM micrographs of reconstructed from MMO Mg_2/Al_1 LDH samples showed different morphological features. The formation of round particles (3–15 μm) could be observed, and these particles are composed of nanosized plate-like crystallites. The most interesting observation is that the surface morphology of MMO samples obtained by heating Mg_2/Al_1 LDH specimens show "memory effect". In this case, the surface morphology of MMO is almost identical to the morphology of primary Mg_2/Al_1 LDHs. On the other hand, the morphological features of differently obtained MMO (MMO obtained by heating Mg–Al–O precursor gel and MMO obtained by heating Mg_2/Al_1 LDHs) differ considerably (see Figure 8).

The SEM micrographs of MMO obtained by heating the $Mg_{1.95}Ca_{0.05}/Al_1$ precursor gels, sol–gel derived $Mg_{1.95}Ca_{0.05}/Al_1$ LDHs, and MMO obtained by heating the $Mg_{1.95}Ca_{0.05}/Al_1$ LDHs are presented in Figure 9. The surface of Ca containing MMO obtained by heating the $Mg_{1.95}Ca_{0.05}/Al_1$ precursor gels is composed of large monolithic particles (≥20 μm). Apparently, the different morphological features could be determined for the reconstructed $Mg_{2-x}Ca_x/Al_1$ LDH samples. The plate-like crystals with sizes of 5–15 μm composed of nanosized plate-like crystallites have formed. An almost identical microstructure was observed for the MMO specimens obtained after heating $Mg_{2-x}Ca_x/Al_1$ LDH samples. SEM micrographs of strontium containing MMO and related $Mg_{2-x}Sr_x/Al_1$ LDHs are presented in Figure 10. The surface microstructure of Sr-containing MMO obtained by heating the $Mg_{1.95}Sr_{0.05}/Al_1$ precursor gels is very similar to the Ca-containing ones. However, on the surface of plate-like crystals of reconstructed $Mg_{2-x}Sr_x/Al_1$ LDH samples, additionally spherical particles (approximately 1 μm) were determined. These spherical particles as a "memory effect" remain on the surface of already heat-treated Sr containing LDHs. Again, the microstructure of investigated samples was not dependent on the annealing temperature. Interestingly, the barium containing $Mg_{2-x}Ba_x/Al_1$ LDH samples showed the formation of smaller LDH particles (2–5 μm) (Figure 11). The formation of plate-like crystals of MMO with the size of 7.5–12.5 μm was observed by heating these LDHs at elevated temperatures.

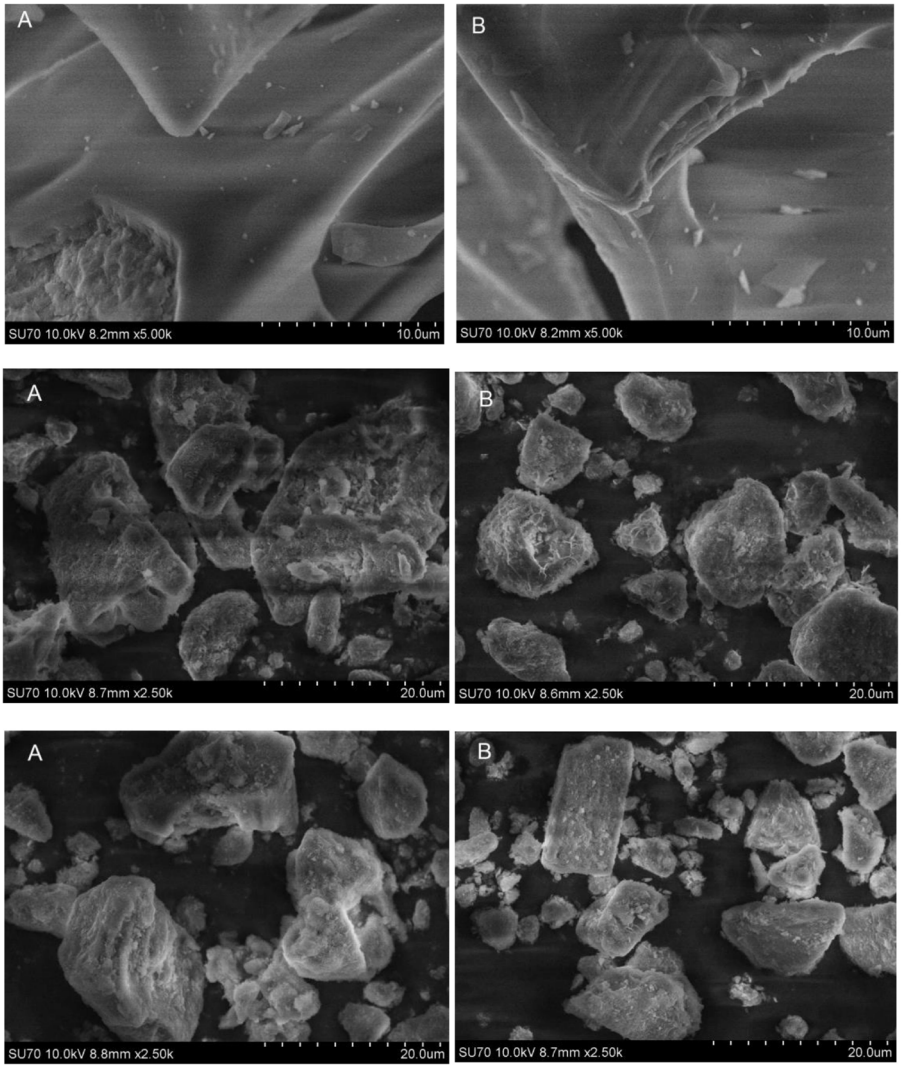

Figure 8. SEM micrographs of MMO obtained by heating the Mg_2/Al_1 precursor gels (**top**), sol–gel derived Mg_2/Al_1 LDHs (**middle**) and MMO obtained by heating the Mg_2Al_1 LDHs (**bottom**). Annealing temperatures: 800 °C (**A**) and 950 °C (**B**).

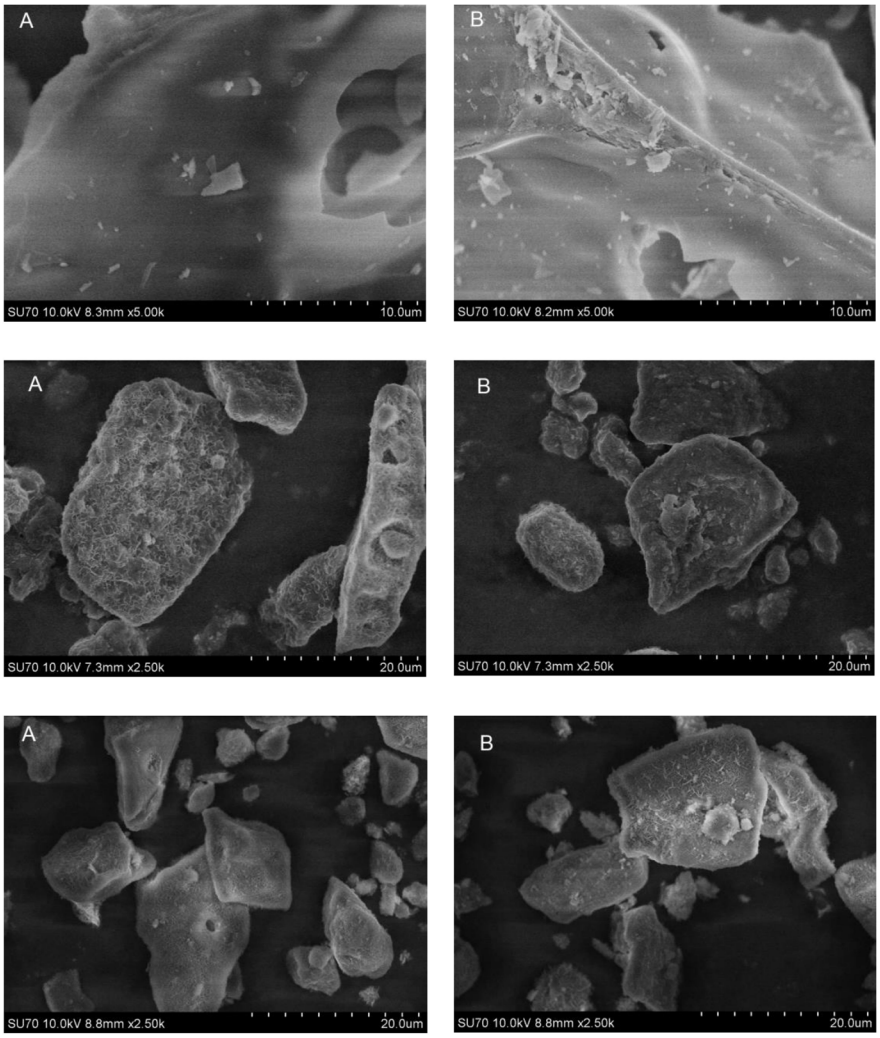

Figure 9. SEM micrographs of MMO obtained by heating the $Mg_{1.95}Ca_{0.05}/Al_1$ precursor gels (**top**), sol–gel derived $Mg_{1.95}Ca_{0.05}/Al_1$ LDHs (**middle**) and MMO obtained by heating the $Mg_{1.95}Ca_{0.05}/Al_1$ LDHs (**bottom**). Annealing temperatures: 800 °C (**A**) and 950 °C (**B**).

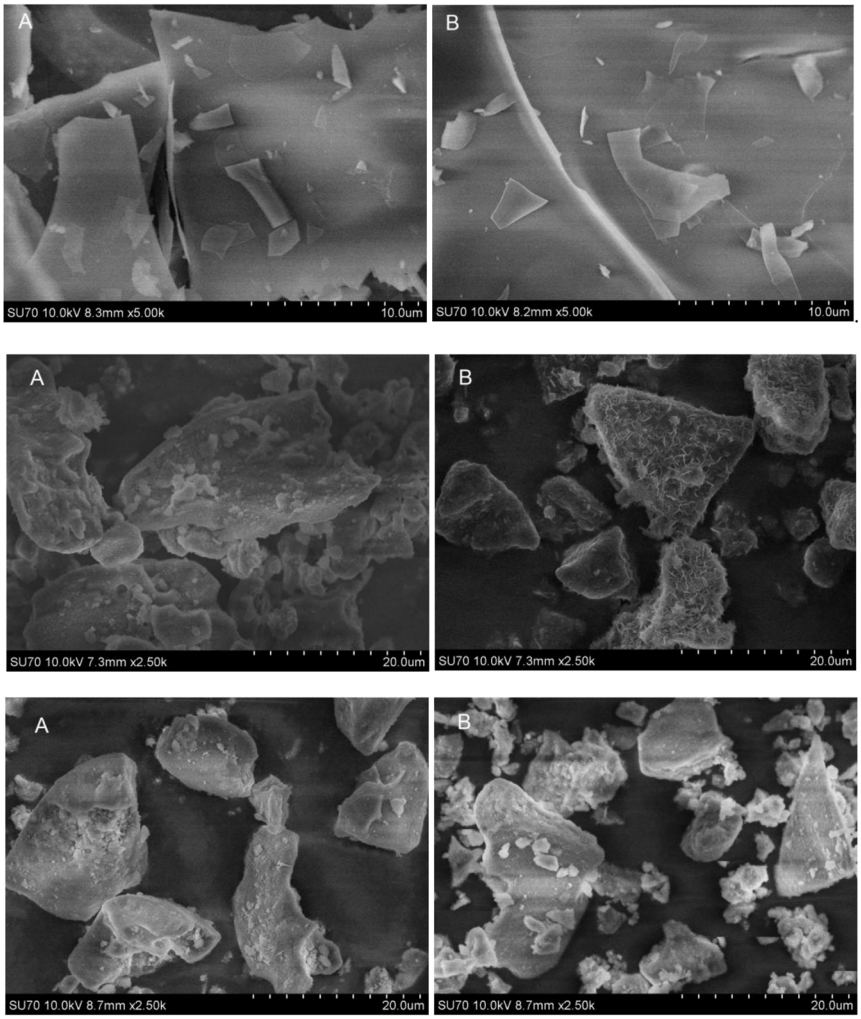

Figure 10. SEM micrographs of MMO obtained by heating the $Mg_{1.95}Sr_{0.05}/Al_1$ precursor gels (**top**), sol–gel derived $Mg_{1.95}Sr_{0.05}/Al_1$ LDHs (**middle**), and MMO obtained by heating the $Mg_{1.95}Sr_{0.05}/Al_1$ LDHs (**bottom**). Annealing temperatures: 800 °C (**A**) and 950 °C (**B**).

The results received by the BET method on Mg–Al MMO obtained by heating Mg–Al–O precursor gel and Mg_2/Al_1 LDHs are presented in Figure 12. Interestingly, these results of MMO obtained from Mg_2/Al_1 LDHs are comparable with those determined for the Mg_3/Al_1 LDH samples [18]. These samples exhibit type IV isotherms independent of the annealing temperature. At higher pressure values, the H1 hystereses are seen. This type of hysteresis is characteristic for the mesoporous (pore size in the range of 2–50 nm) materials. However, in the case of the MMO obtained by heating Mg–Al–O precursor gel, the steep increase at relatively low pressures let us predict the type of H4 isotherms, especially for the MMO samples obtained at lower temperature (800 °C). The surface area of these MMO samples evidently depends on the synthesis temperature.

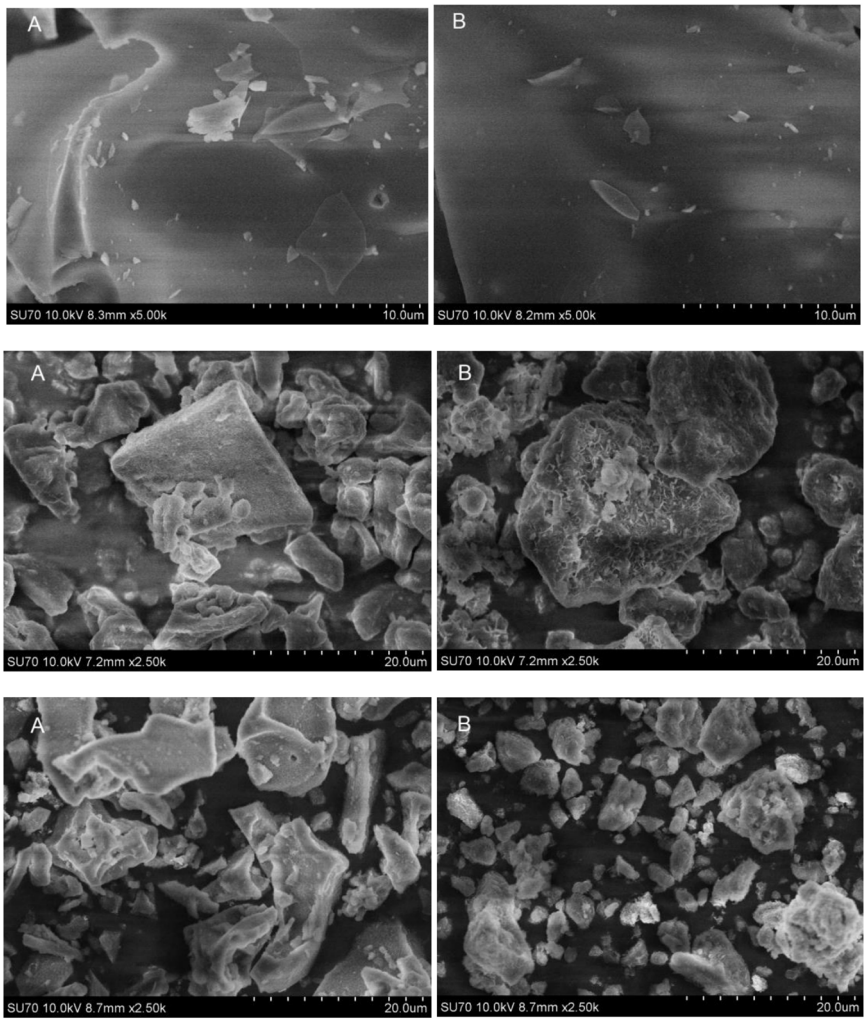

Figure 11. SEM micrographs of MMO obtained by heating the $Mg_{1.95}Ba_{0.05}/Al_1$ precursor gels (**top**), sol–gel derived $Mg_{1.95}Ba_{0.05}/Al_1$ LDHs (**middle**) and MMO obtained by heating the $Mg_{1.95}Ba_{0.05}/Al_1$ LDHs (**bottom**). Annealing temperatures: 800 °C (**A**) and 950 °C (**B**).

Thus, the isotherms and hystereses are dependent on both synthesis pathway and annealing temperature. The nitrogen adsorption–desorption results obtained for the mixed metal oxides containing Ca, Sr, and Ba (Figure 13) demonstrated that the N_2 adsorption–desorption isotherms show very similar trends.

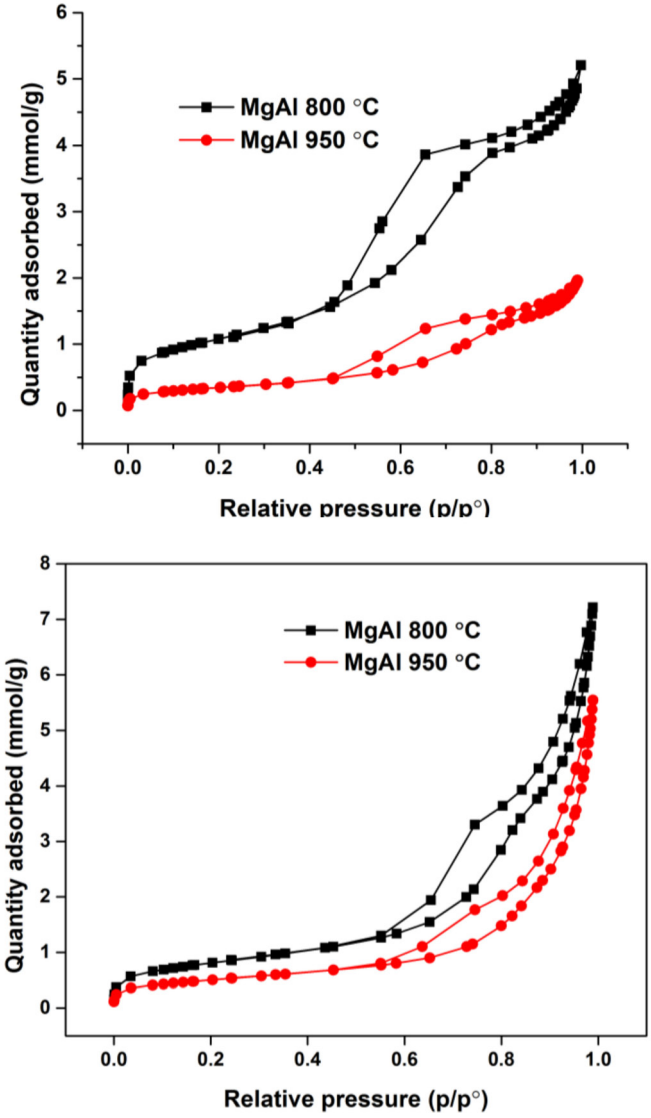

Figure 12. Nitrogen adsorption–desorption isotherms of mixed metal oxides (MMO) obtained by heating the Mg_2/Al_1 precursor gels (**top**) and obtained by heating the Mg_2Al_1 LDHs (**bottom**) at 800 °C and 950 °C.

However, in the case of barium-substituted MMO samples synthesized at 800 °C, the determined N_2 adsorption–desorption isotherms exhibited same type of isotherms independent of the synthesis method.

The results of the BET analysis of MMO samples are summarized in Table 2.

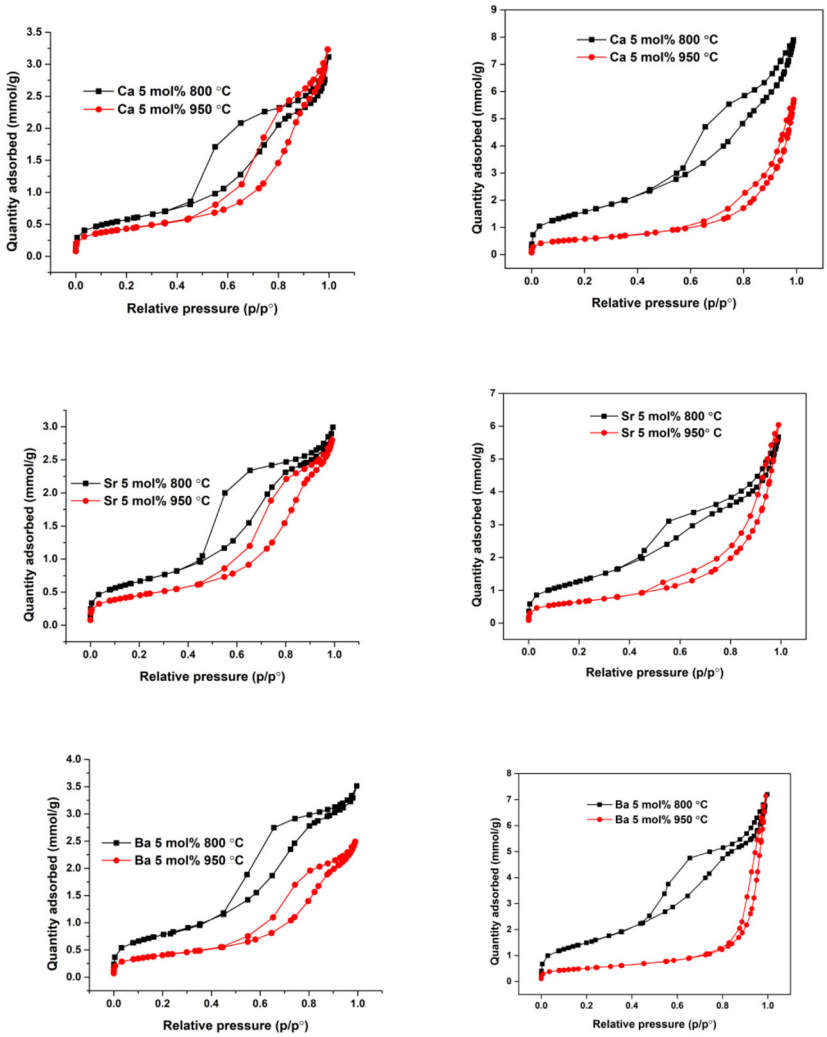

Figure 13. Nitrogen adsorption–desorption isotherms of mixed metal oxides (MMO) obtained by heating the $Mg_{1.95}Ca_{0.05}/Al_1$ precursor gels (**top, left**), by heating the $Mg_{1.95}Ca_{0.05}/Al_1$ LDHs (**top, right**), by heating the $Mg_{1.95}Sr_{0.05}/Al_1$ precursor gels (**middle, left**), by heating the $Mg_{1.95}Sr_{0.05}/Al_1$ LDHs (**middle, right**), by heating the $Mg_{1.95}Ba_{0.05}/Al_1$ precursor gels (**bottom, left**), and by heating the $Mg_{1.95}Ba_{0.05}/Al_1$ LDHs (**bottom, right**) at 800 °C and 950 °C.

Figure 14 shows the pore size distributions obtained by the BJH method for the MMO specimens obtained by heating Mg–Al–O precursor gels and Mg_2/Al_1 LDHs. Both samples demonstrate narrow pore size distributions (PSD) almost at the mesoporous level, but very close to micropores domain.

Table 2. Brunauer, Emmett and Teller (BET) surface area of sol–gel derived $Mg_{1.95}M_{0.05}/Al_1$ (M = Ca, Sr and Ba) MMO.

Precursor Compound	Temperature	BET Surface Area m^2/g
Mg_2Al_1 precursor gels	800 °C	87.470
Mg_2Al_1	800 °C	65.450
Mg_2Al_1 precursor gels	950 °C	27.749
Mg_2Al_1	950 °C	40.528
$Mg_{1.95}Ca_{0.05}/Al_1$ precursor gels	800 °C	46.461
$Mg_{1.95}Ca_{0.05}/Al_1$	800 °C	129.16
$Mg_{1.95}Ca_{0.05}/Al_1$ precursor gels	950 °C	34.791
$Mg_{1.95}Ca_{0.05}/Al_1$	950 °C	46.078
$Mg_{1.95}Sr_{0.05}/Al_1$ precursor gels	800 °C	53.847
$Mg_{1.95}Sr_{0.05}/Al_1$	800 °C	104.543
$Mg_{1.95}Sr_{0.05}/Al_1$ precursor gels	950 °C	36.292
$Mg_{1.95}Sr_{0.05}/Al_1$	950 °C	51.961
$Mg_{1.95}Ba_{0.05}/Al_1$ precursor gels	800 °C	63.217
$Mg_{1.95}Ba_{0.05}/Al_1$	800 °C	122.486
$Mg_{1.95}Ba_{0.05}/Al_1$ precursor gels	950 °C	32.498
$Mg_{1.95}Ba_{0.05}/Al_1$	950 °C	40.576

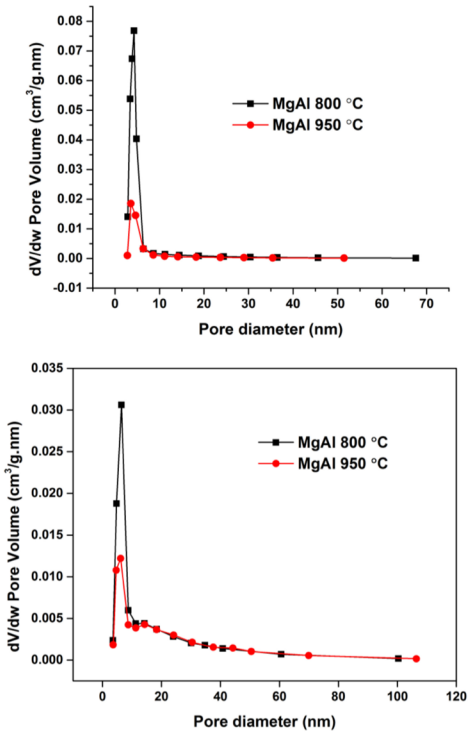

Figure 14. The pore size distribution of mixed metal oxides (MMO) obtained by heating the Mg_2/Al_1 precursor gels (**top**) and obtained by heating the Mg_2/Al_1 LDHs (**bottom**) at 800 °C and 950 °C.

Surprisingly, the PSD width does not depend neither on the synthetic procedure nor on the annealing temperature. The determined average pore diameter in the mesopore region is approximately 3.0–5.5 nm. The PSD results obtained for the mixed metal oxides containing Ca, Sr, and Ba are shown in Figure 15.

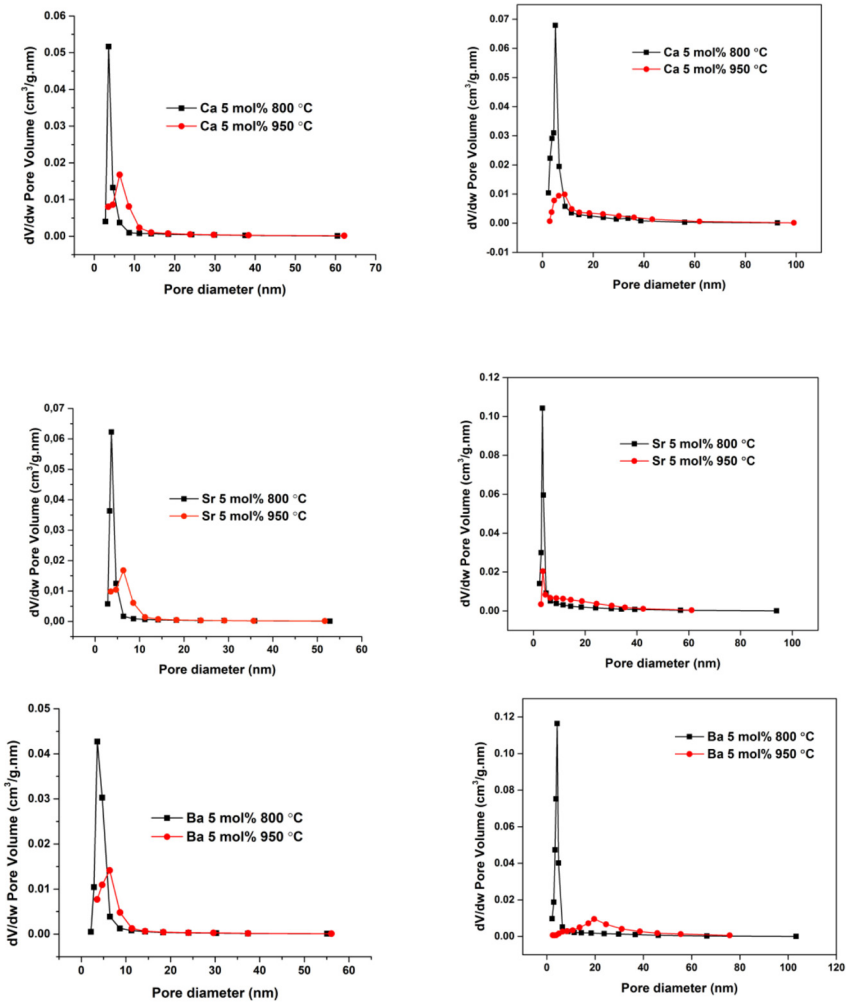

Figure 15. The pore size distribution of mixed metal oxides (MMO) obtained by heating the $Mg_{1.95}Ca_{0.05}/Al_1$ precursor gels (**top, left**), by heating the $Mg_{1.95}Ca_{0.05}/Al_1$ LDHs (**top, right**), by heating the $Mg_{1.95}Sr_{0.05}/Al_1$ precursor gels (**middle, left**), by heating the $Mg_{1.95}Sr_{0.05}/Al_1$ LDHs (**middle, right**), by heating the $Mg_{1.95}Ba_{0.05}/Al_1$ precursor gels (**bottom, left**), and by heating the $Mg_{1.95}Ba_{0.05}/Al_1$ LDHs (**bottom, right**) at 800 °C and 950 °C.

As seen, various surface properties could be detected for the MMO samples synthesized by two different methods. The pore size distribution of directly obtained MMO by heating Mg–Al–O precursor gels depends on the heating temperature and less on the nature of alkaline earth metal. The determined average pore diameter in the mesopore region is approximately 2.5–8 nm, 2.5–7 nm, and 2.5–9 nm

for the Ca-MMO, Sr-MMO, and Ba-MMO samples, respectively, synthesized at 800 °C. The pore size distribution is visible wider for the MMO synthesized at 950 °C (approximately 3–10.15 nm, 3–12.5 nm, and 3.5–10.1 nm for the Ca-MMO, Sr-MMO, and Ba-MMO samples, respectively). As seen from Figure 15, the pore size distributions obtained by the BJH method for the MMO specimens synthesized from the reconstructed Mg_2/Al_1 LDHs depends on both synthesis temperature and nature of substituent. The most narrow pore size distribution was determined for Sr-containing MMO (2.5–3.5 nm for the sample heat-treated at 800 °C). On the other hand, the sample with 5% mol of Ba and prepared at 950 °C has very broad pore size distribution. In general, the gain in the volume of mesopores is clearly visible for the MMO samples synthesized at lower temperature. However, the pore diameter, wall thickness, and pore size distribution depend on the used synthesis method, heating temperature, and nature of alkali earth metal in the MMO host matrix, indicating that these MMO could have the potential for the application as catalysts, catalyst supports, and adsorbents.

4. Conclusions

In this study, the reconstruction peculiarities of sol–gel derived $Mg_{2-x}M_x/Al_1$ (M = Ca, Sr, Ba) layered double hydroxides (LDHs) were investigated. For the synthesis of $Mg_{2-x}M_x/Al_1$ (M = Ca, Sr, Ba) LDHs, the indirect sol–gel synthesis method has been used. Citric acid and 1,2-ethanediol were used as complexing agents in sol–gel processing [39]. The mixed metal oxides (MMO) were synthesized by two different routes in this work. Firstly, the MMO were obtained directly by heating Mg(M)–Al–O precursor gels at 650 °C, 800 °C, and 950 °C. The XRD pattern of the MMO sample obtained by heating Mg–Al–O precursor gels at 650 °C showed the formation of monophasic MMO. However, with increasing annealing temperature up to 800 °C or 950 °C and upon the substitution of Mg by Ca, Sr, and Ba, highly crystalline spinel ($MgAl_2O_4$, $CaAl_2O_4$, $SrAl_2O_4$ and $BaAl_2O_4$) phases have also formed. All MMO samples were successfully reconstructed to the $Mg_{2-x}M_x/Al_1$ (M = Ca, Sr, Ba) layered double hydroxides (LDHs) in water at 50 °C for 6 h (pH 10). However, the spinel phases were not reconstructed and remained as impurity phases. Moreover, during the reconstruction process, a negligible amount of metal carbonates ($CaCO_3$, $SrCO_3$, and $BaCO_3$) have formed as well. Secondly, the MMO were also obtained by heating the reconstructed LDHs at the same temperatures and the phase composition, morphology, and surface properties of MMO were compared with obtained ones after initial annealing. It was demonstrated that the second time obtained Ca and Sr-substituted MMO samples contained more side phases. However, this was not the case for the Ba-substituted MMO samples, since both synthesis products obtained from precursor gels and by heating LDHs were composed of several crystalline phases. It was demonstrated for the first time that the microstructure of reconstructed MMO from sol–gel derived LDHs showed a "memory effect", i.e., the microstructural features of MMO were almost identical as was determined for LDHs. Besides, the microstructure of investigated samples was not dependent on the annealing temperature and substitution. The synthesized Mg(M)–Al MMO samples exhibited type IV isotherms independent of the annealing temperature. At higher pressure values, the H1 hystereses were detected, which are characteristic for the mesoporous (pore size in the range of 2–50 nm) materials. It was found that the pore size distributions obtained by the BJH method for the MMO specimens synthesized from the reconstructed Mg_2/Al_1 LDHs depended on both the synthesis temperature and nature of the substituent. The most narrow pore size distribution was determined for Sr-containing MMO (2.5–3.5 nm for the sample heat-treated at 800 °C). On the other hand, the sample with 5% mol of Ba and prepared at 950 °C had very broad pore size distribution. The pore diameter, wall thickness, and pore size distribution was found to be dependent on used synthesis method, heating temperature, and nature of alkali earth metal in the MMO host matrix.

Author Contributions: Formal Analysis, L.V., A.Z., A.I., and A.K.; Investigation, L.V., M.R., I.G.-P., A.Z., and V.P.; Resources, A.Z., A.I., and A.K.; Data Curation, L.V.; Writing—Original Draft Preparation, L.V., I.G.-P., and A.K.; Writing—Review and Editing, A.K.; Visualization, A.Z. and V.P.; Supervision, A.I. and A.K. All authors have read and agreed to the published version of the manuscript.

Funding: This work was supported by a Research grant N°CAMAT (No. S-LB-19-2) from the Research Council of Lithuania and Belarusian Republican Found for Fundamental Research (No. 19LITG-007).

Conflicts of Interest: The authors declare that they have no conflict of interest.

References

1. Li, F.; Duan, X. Applications of layered double hydroxides. In *Layered Double Hydroxides (Structure and Bonding)*; Mingos, D.M.P., Ed.; Springer-Verlag: Berlin/Heidelberg, Germany, 2006; pp. 193–223.
2. Sokol, D.; Klemkaite-Ramanauske, K.; Khinsky, A.; Baltakys, K.; Beganskiene, A.; Baltusnikas, A.; Pinkas, J.; Kareiva, A. Reconstruction effects on surface properties of Co/Mg/Al layered double hydroxide. *Mater. Sci. (Medžiagotyra)* **2017**, *23*, 144–149. [CrossRef]
3. Mishra, G.; Dash, B.; Pandey, S. Layered double hydroxides: A brief review from fundamentals to application as evolving biomaterials. *Appl. Clay Sci.* **2018**, *1539*, 172–186. [CrossRef]
4. Vieira, D.E.L.; Sokol, D.; Smalenskaite, A.; Kareiva, A.; Ferreira, M.G.S.; Vieira, J.M.; Brett, C.M.A.; Salak, A.N. Cast iron corrosion protection with chemically modified Mg-Al layered double hydroxides synthesized using a novel approach. *Surf. Coat. Technol.* **2019**, *375*, 158–163. [CrossRef]
5. Smalenskaite, A.; Pavasaryte, L.; Yang, T.C.K.; Kareiva, A. Undoped and Eu^{3+} doped magnesium-aluminium layered double hydroxides: Peculiarities of intercalation of organic anions and investigation of luminescence properties. *Materials* **2019**, *12*, 736. [CrossRef] [PubMed]
6. Li, Y.L.; Ma, J.; Yuan, Y.X. Enhanced adsorption of chromium by stabilized Ca/Al-Fe layered double hydroxide decorated with ferric nanoparticles. *Sci. Adv. Mater.* **2020**, *12*, 441–448. [CrossRef]
7. Zhang, Z.D.; Qin, J.Y.; Zhang, W.C.; Pan, Y.T.; Wang, D.Y.; Yang, R.J. Synthesis of a novel dual layered double hydroxide hybrid nanomaterial and its application in epoxy nanocomposites. *Chem. Eng. J.* **2020**, *381*, 122777. [CrossRef]
8. Sato, T.; Fujita, H.; Endo, T.; Shimada, M.; Tsunashima, A. Synthesis of hydrotalcite-like compounds and their physic-chemical properties. *Reactiv. Solids* **1988**, *5*, 219–228. [CrossRef]
9. Klemkaite, K.; Prosycevas, I.; Taraskevicius, R.; Khinsky, A.; Kareiva, A. Synthesis and characterization of layered double hydroxides with different cations (Mg, Co, Ni, Al), decomposition and reformation of mixed metal oxides to layered structures. *Centr. Eur. J. Chem.* **2011**, *9*, 275–282. [CrossRef]
10. Salak, A.N.; Tedim, J.; Kuznetsova, A.I.; Ribeiro, J.L.; Vieira, L.G.; Zheludkevich, M.L.; Ferreira, M.G.S. Comparative X-ray diffraction and infrared spectroscopy study of Zn-Al layered double hydroxides: Vanadate vs. nitrate. *Chem. Phys.* **2012**, *397*, 102–108. [CrossRef]
11. Meyn, M.; Beneke, K.; Lagaly, G. Anion exchange reactions of layered double hydroxides. *Inorg. Chem.* **1990**, *29*, 5201–5206. [CrossRef]
12. Newman, S.P.; Jones, W. Synthesis, characterization and applications of layered double hydroxides containing organic guests. *New J. Chem.* **1998**, *22*, 105–115. [CrossRef]
13. Olfs, H.W.; Torres-Dorante, L.O.; Eckelt, R.; Kosslick, H. Comparison of different synthesis routes for Mg-Al layered double hydroxides (LDH): Characterization of the structural phases and anion exchange properties. *Appl. Clay Sci.* **2009**, *43*, 459–464. [CrossRef]
14. Smalenskaite, A.; Vieira, D.E.L.; Salak, A.N.; Ferreira, M.G.S.; Katelnikovas, A.; Kareiva, A. A comparative study of co-precipitation and sol-gel synthetic approaches to fabricate cerium-substituted Mg/Al layered double hydroxides with luminescence properties. *Appl. Clay Sci.* **2017**, *143*, 175–183. [CrossRef]
15. Sokol, D.; Salak, A.N.; Ferreira, M.G.S.; Beganskiene, A.; Kareiva, A. Bi-substituted $Mg_3Al\text{-}CO_3$ layered double hydroxides. *J. Sol-Gel Sci. Technol.* **2018**, *85*, 221–230. [CrossRef]
16. Smalenskaite, A.; Salak, A.N.; Kareiva, A. Induced neodymium luminescence in sol-gel derived layered double hydroxides. *Mendeleev Commun.* **2018**, *28*, 493–494. [CrossRef]
17. Smalenskaite, A.; Kaba, M.M.; Grigoraviciute-Puroniene, I.; Mikoliunaite, L.; Zarkov, A.; Ramanauskas, R.; Morkan, I.A.; Kareiva, A. Sol-gel synthesis and characterization of coatings of Mg-Al layered double hydroxides (LDHs). *Materials* **2019**, *12*, 3738. [CrossRef]
18. Valeikiene, L.; Paitian, R.; Grigoraviciute-Puroniene, I.; Ishikawa, K.; Kareiva, A. Transition metal substitution effects in sol-gel derived $Mg_{3-x}M_x/Al_1$ (M = Mn, Co, Ni, Cu, Zn) layered double hydroxides. *Mater. Chem. Phys.* **2019**, *237*, 121863. [CrossRef]

19. Kovanda, F.; Grygar, T.; Dornicak, V. Thermal behaviour of Ni-Mn layered double hydroxide and characterization of formed oxides. *Solid State Sci.* **2003**, *5*, 1019–1026. [CrossRef]
20. Liu, X.W.; Wu, Y.L.; Xu, Y.; Ge, F. Preparation of Mg/Al bimetallic oxides as sorbents: Microwave calcination, characterization, and adsorption of Cr(VI). *J. Solid State Chem.* **2016**, *79*, 122–132. [CrossRef]
21. Vicente, P.; Perez-Bernal, M.E.; Ruano-Casero, R.J.; Ananias, D.; Almeida Paz, F.A.; Rocha, J.; Rives, V. Luminescence properties of lanthanide-containing layered double hydroxides. *Microp. Mesop. Mater.* **2016**, *226*, 209–220. [CrossRef]
22. Kryshtab, T.; Calderon, H.A.; Kryvko, A. Microstructure characterization of metal mixed oxides. *MRS Adv.* **2017**, *2*, 4025–4030. [CrossRef]
23. Bugris, V.; Adok-Sipiczki, M.; Anitics, T.; Kuzmann, E.; Homonnay, Z.; Kukovecz, A.; Konya, Z.; Sipos, P.; Palinko, I. Thermal decomposition and reconstruction of CaFe-layered double hydroxide studied by X-ray diffractometry and Fe-57 Mossbauer spectroscopy. *J. Molec. Struct.* **2015**, *1090*, 19–24. [CrossRef]
24. Millange, F.; Walton, R.I.; O'Hare, D. Time-resolved in situ X-ray diffraction study of the liquid-phase reconstruction of Mg-Al-carbonate hydrotalcite-like compounds. *J. Mater. Chem.* **2000**, *10*, 1713–1720. [CrossRef]
25. Li, L.; Qi, G.X.; Fukushima, M.; Wang, B.; Xu, H.; Wang, Y. Insight into the preparation of Fe_3O_4 nanoparticle pillared layered double hydroxides composite via thermal decomposition and reconstruction. *Appl. Clay Sci.* **2017**, *140*, 88–95. [CrossRef]
26. Bernardo, M.P.; Ribeiro, C. Zn-Al-based layered double hydroxides (LDH) active structures for dental restorative materials. *J. Mater. Res. Technol.* **2019**, *8*, 1250–1257. [CrossRef]
27. Elhalil, A.; Elmoubarki, R.; Machrouhi, A.; Sadiq, M.; Abdennouri, M.; Qourzal, S.; Barka, N. Photocatalytic degradation of caffeine by ZnO-ZnAl2O4 nanoparticles derived from LDH structure. *J. Environ. Chem. Eng.* **2017**, *5*, 3719–3726. [CrossRef]
28. Valente, J.S.; Lima, E.; Toledo-Antonio, J.A.; Cortes-Jacome, M.A.; Lartundo-Rojas, L.; Montiel, R.; Prince, J. Comprehending the thermal decomposition and reconstruction process of sol-gel MgAl layered double hydroxides. *J. Phys. Chem. C* **2010**, *114*, 2089–2099. [CrossRef]
29. Venugopal, B.R.; Shivakumara, C.; Rajamathi, M. A composite of layered double hydroxides obtained through random costacking of layers from Mg-Al and Co-Al LDHs by delamination-restacking: Thermal decomposition and reconstruction behavior. *Solid State Sci.* **2007**, *9*, 287–294. [CrossRef]
30. Chagas, L.H.; de Carvalho, G.S.G.; Carmo, W.R.D.; Gil, R.A.S.S.; Chiaro, S.S.X.; Leitao, A.A.; Diniz, R.; de Sena, L.A.; Achete, C.A. MgCoAl and NiCoAl LDHs synthesized by the hydrothermal urea hydrolysis method: Structural characterization and thermal decomposition. *Mater. Res. Bull.* **2015**, *64*, 207–215. [CrossRef]
31. Kim, B.K.; Gwak, G.H.; Okada, T.; Oh, J.M. Effect of particle size and local disorder on specific surface area of layered double hydroxides upon calcination-reconstruction. *J. Solid State Chem.* **2018**, *263*, 60–64. [CrossRef]
32. Seftel, E.M.; Ciocarlan, R.G.; Michielsen, B.; Meynen, V.; Mullens, S.; Cool, P. Insights into phosphate adsorption behavior on structurally modified ZnAl layered double hydroxides. *Appl. Clay Sci.* **2018**, *165*, 234–246. [CrossRef]
33. Lee, S.H.; Tanaka, M.; Takahashi, Y.; Kim, K.W. Enhanced adsorption of arsenate and antimonate by calcined Mg/Al layered double hydroxide: Investigation of comparative adsorption Check for mechanism by surface characterization. *Chemosphere* **2018**, *211*, 903–911. [CrossRef] [PubMed]
34. Kang, J.; Levitskaia, T.G.; Park, S.; Kim, J.; Varga, T.; Um, W. Nanostructured MgFe and CoCr layered double hydroxides for removal and sequestration of iodine anions. *Chem. Eng. J.* **2020**, *380*, 122408. [CrossRef]
35. Santos, R.M.M.; Tronto, J.; Briois, V.; Santilli, C.V. Thermal decomposition and recovery properties of ZnAl-CO_3 layered double hydroxide for anionic dye adsorption: Insight into the aggregative nucleation and growth mechanism of the LDH memory effect. *J. Mater. Chem. A* **2017**, *5*, 9998–10009. [CrossRef]
36. Cao, Y.; Wang, Y.X.; Zhang, X.Y.; Cai, X.G.; Li, Z.H.; Li, G.T. Facile synthesis of 3D Mg-Al layered double oxide microspheres with ultra high adsorption capacity towards methyl orange. *Mater. Lett.* **2019**, *257*, 126695. [CrossRef]
37. Belskaya, O.B.; Leont'eva, N.N.; Gulyaeva, T.I.; Cherepanova, S.V.; Talzi, V.P.; Drozdov, V.A.; Likholobov, V.A. Influence of a doubly charged cation nature on the formation and properties of mixed oxides MAlOx (M = Mg^{2+}, Zn^{2+}, Ni^{2+}) obtained from the layered hydroxide precursors. *Russ. Chem. Bull.* **2013**, *62*, 2349–2361. [CrossRef]

38. Zhao, Y.; Li, J.-G.; Fang, F.; Chu, N.; Ma, H.; Yang, X. Structure and luminescence behaviour of as-synthesized, calcined, and restored MgAlEu-LDH with high crystallinity. *Dalton Trans.* **2012**, *41*, 12175–12184. [CrossRef]
39. Ishikawa, K.; Garskaite, E.; Kareiva, A. Sol-gel synthesis of calcium phosphate-based biomaterials -A review of environmentally benign, simple and effective synthesis routes. *J. Sol-Gel Sci. Technol.* **2020**, *94*, 551–572. [CrossRef]

4 publikacija / 4th publication

Investigation of Structural and Luminescent Properties of Sol-Gel-Derived Cr-Substituted $Mg_3Al_{1-x}Cr_x$ Layered Double Hydroxides

L. Valeikiene, I. Grigoraviciute-Puroniene , A. Katelnikovas , A. Zarkov, A. Kareiva.

Molecules **26**, 1848 (2021)

DOI: 10.3390/molecules26071848

molecules

MDPI

Article

Investigation of Structural and Luminescent Properties of Sol-Gel-Derived Cr-Substituted $Mg_3Al_{1-x}Cr_x$ Layered Double Hydroxides

Ligita Valeikiene, Inga Grigoraviciute-Puroniene, Arturas Katelnikovas, Aleksej Zarkov * and Aivaras Kareiva

Institute of Chemistry, Vilnius University, Naugarduko 24, LT-03225 Vilnius, Lithuania; ligita.valeikiene@chgf.vu.lt (L.V.); inga.grigoraviciute@chf.vu.lt (I.G.-P.); arturas.katelnikovas@chf.vu.lt (A.K.); aivaras.kareiva@chgf.vu.lt (A.K.)

* Correspondence: aleksej.zarkov@chf.vu.lt

Abstract: In the present work, Cr-substituted $Mg_3Al_{1-x}Cr_x$ layered double hydroxides (LDHs) were synthesised through the phase conversion of sol-gel-derived mixed-metal oxides in an aqueous medium. The chromium substitution level in the range of 1 to 25 mol% was investigated. It was demonstrated that all synthesised specimens were single-phase LDHs. The results of elemental analysis confirmed that the suggested synthetic sol-gel chemistry approach is suitable for the preparation of LDHs with a highly controllable chemical composition. The surface microstructure of sol-gel-derived $Mg_3Al_{1-x}Cr_x$ LDHs does not depend on the chromium substitution level. The formation of plate-like agglomerated particles, which consist of hexagonally shaped nanocrystallites varying in size from approximately 200 to 300 nm, was observed. Optical properties of the synthesised $Mg_3Al_{1-x}Cr_x$ LDHs were investigated by means of photoluminescence. All Cr-containing powders exhibited characteristic emission in the red region of the visible spectrum. The strongest emission was observed for the sample doped with 5 mol% Cr^{3+} ions. However, the emission intensity of samples doped with 1–10 mol% Cr^{3+} ions was relatively similar. A further increase in the Cr^{3+} ion concentration to 25 mol% resulted in severe concentration quenching.

Keywords: layered double hydroxides; Mg_3Al_1; substitution effects; chromium; photoluminescence

Citation: Valeikiene, L.; Grigoraviciute-Puroniene, I.; Katelnikovas, A.; Zarkov, A.; Kareiva, A. Investigation of Structural and Luminescent Properties of Sol-Gel-Derived Cr-Substituted $Mg_3Al_{1-x}Cr_x$ Layered Double Hydroxides. *Molecules* **2021**, *26*, 1848. https://doi.org/10.3390/molecules26071848

Academic Editor: Eugene L. Kolychev

Received: 5 March 2021
Accepted: 23 March 2021
Published: 25 March 2021

1. Introduction

Layered double hydroxides (LDHs) are compounds composed of positively charged brucite-like layers with an interlayer gallery containing charge-compensating anions and water molecules. The metal cations occupy the centres of shared oxygen octahedra whose vertices contain hydroxide ions that connect to form infinite two-dimensional sheets [1–3]. The chemical formula of layered double hydroxides is expressed as $(M^{2+}{}_xM^{3+}{}_{1-x}(OH)_{2x}A{\cdot}zH_2O)$, where M^{2+} and M^{3+} are divalent and trivalent metal ions, respectively, and A^- is an intercalate anion that compensates the positive charge created by the partial substitution of M^{2+} by M^{3+} ions in brucite-type layers [1–3]. LDH structures containing Mg^{2+}, Zn^{2+}, Co^{2+}, Ni^{2+}, Cu^{2+} or Mn^{2+} ion as divalent cations and Al^{3+}, Cr^{3+}, Co^{3+}, Fe^{3+}, V^{3+}, Y^{3+} or Mn^{3+} ion as trivalent ones are known. LDHs with many different anionic species have been reported: both inorganic anions (carbonate, chloride, nitrate, sulphate, molybdate, phosphate, etc.) and organic anions (terephthalate, acrylate, lactate, etc.). LDHs are widely used as adsorbents, catalyst support precursors, anion exchangers, acid residue scavengers, flame retardants, osmosis membranes, sensors and others [4–12]. After calcination at temperatures from 300 to 600 °C, LDHs are converted to mixed-metal oxides (MMOs) with a high specific surface area and basic properties. The ability of MMOs to recover the original layered structure is a property known as the memory effect [4,9]. When MMOs are immersed in an aqueous solution that contains some anions, the layered structure can be recovered with those anions intercalated into the interlayer.

As mentioned before, chromium-containing LDHs have also been synthesised, and these compounds show interesting chemical and physical properties. For example, chromium-containing Mg-Cr and Ni-Cr LDHs have already been used as precursors to synthesise pillared derivatives with decavanadate anions without the use of any preswelling agent [13]. The decomposition products of these LDHs were successfully applied as adsorbents [14]. Zn-Cr LDH samples were synthesised using the classical co-precipitation approach from aqueous solution [15]. The adsorption capacities of the synthesised samples were investigated performing experiments with Indigo Carmine as the model of organic pollutant. Moreover, Zn-Cr and Zn-Cr LDHs, intercalated with the Keggin ion, showed a high adsorption capacity for effective removal of iron (II) from aqueous solution [16].

M(II)-Cr (M = Co, Ni, Cu and Zn) LDHs also show interesting photocatalytic properties and have been used for photocatalytic degradation of organic pollutants [17,18]. The decomposition products of different LDHs containing chromium have also been tested as catalysts [19,20]. It was also demonstrated that Mg-Cr LDHs containing composites can be used for the preparation of coatings that show optimal corrosion protection [21].

Considerable attention has been focused on incorporating different elements into LDH host layers to develop new functional materials that resemble designed optical properties. The effect of sensitising anions [22], multiwavelength luminescence [23], the size effect [24] and the influence of carboxylate [25] and terephtalate [26] on the optical properties of lanthanide-containing LDHs was investigated. Moreover, series of LDHs and mixed-metal oxides with different lanthanide cations were also prepared [27]. Smalenskaite et al. focused on the characterisation of LDHs doped with Tb^{3+} [28], Nd^{3+} [29] and Eu^{3+} [30]. Chromium was also used as a substituent in different LDHs for various reasons. For instance, Cr-substituted Mg-Al LDHs were successfully used as a catalyst in aldose-ketose isomerisation processes [31]. Mixed oxides, obtained by thermal decomposition of Cr-substituted LDHs, were studied in the reaction of hydrocarbon steam reforming for the production of hydrogen [32]. Rodriguez-Rivas et al. [33] recently suggested to use Cr-substituted Zn-Al LDHs as UV–VIS light photocatalysts for NO gas removal from the urban environment. Finally, the spectral emission of natural LDHs was studied by cathodo- and photoluminescence (PL) techniques [34]. It was concluded that the presence of Cr^{3+} ion activators induces characteristic PL emission peaks in the red-infrared region at 681, 688 and 696 nm linked to $^2E \rightarrow {}^4A_2$ transitions. However, the luminescent properties of Cr-doped or Cr-substituted Mg-Al LDHs have not been investigated so far to the best of our knowledge.

A sol-gel method based on in situ generation of mixed-metal chelates by complexing metal ions with various complexing agents in aqueous media was successfully used to prepare different monophasic inorganic compounds and nanostructures, such as biomaterials [35] and magnetic [36] and optical [37,38] materials. Previously, for the preparation of Mg-Cr and related LDHs, the non-aqueous sol-gel chemistry approach has been explored using metal alkoxides as starting materials [39,40]. We recently developed the indirect aqueous sol-gel method for the preparation of LDHs. We demonstrated that the synthesis of LDHs using this simple and environmentally benign method ensures the formation of homogeneous, monophasic samples having particles with a narrow size distribution [4,9,11,41]. It is well known that application of a synthesis method also depends on the chemical composition of the compound to be synthesised. The aim of this work was to synthesise $Mg_3Al_{1-x}Cr_x$ LDH samples for the first time using an aqueous sol-gel method and to investigate the effect of Cr^{3+} substitution on phase purity, morphological and luminescent properties of obtained end products. The luminescent properties of sol-gel-derived Cr-substituted Mg-Al LDHs was also investigated for the first time to the best of our knowledge.

2. Results and Discussion

The XRD patterns of Mg_3Al_1 and $Mg_3Al_{1-x}Cr_x$ LDHs with different chromium substitution levels (1–25 mol%) are shown in Figure 1. Characteristic diffraction peaks for

the LDH structure were observed at 2θ angles at ca. 11.5° (003), 23° (006) and 34.5° (009). Besides, two additional LDH peaks were clearly displayed at about 60.5° and 61.5°, which correspond to reflections from the (110) and (113) planes [4]. No diffraction lines attributable to the side phases could be observed in the XRD patterns of sol-gel-derived LDH samples. Less important reflections (015) and (018) visible at about 38–39° and 47–49°, respectively, were also attributed to the LDH phase. It is interesting to note that only 9 mol% of chromium was introduced to $Mg_3Al_{1-x}Cr_x$ LDHs when the impregnation method (adsorption) was used for the preparation [31]. It was also observed that aluminium substitution by chromium reduces the crystallinity of LDHs synthesised by the co-precipitation method [32].

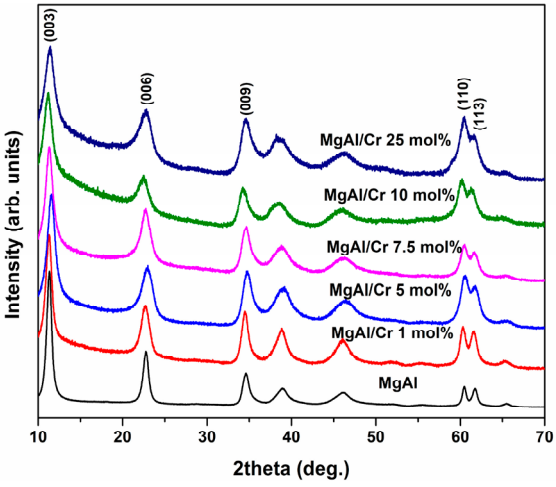

Figure 1. X-ray diffraction (XRD) patterns of Cr-substituted $Mg_3Al_{1-x}Cr_x$ LDHs.

The calculated values of d-spacing and lattice parameters of $Mg_3Al_{1-x}Cr_x$ LDHs are summarised in Table 1. As seen, both *d* values and lattice parameters slightly increased with increasing amounts of chromium in the LDH structure. This was expected, since a smaller Al^{3+} ion (0.535 Å, CN = 6) was monotonically replaced by a larger Cr^{3+} ion (0.615 Å, CN = 6) [42]. The calculated crystallite sizes of the Mg_3Al_1 and $Mg_3Al_{1-x}Cr_x$ LDHs were independent of the amount of chromium and varied in the range of 21.8–26.7 nm.

Table 1. The values of d-spacing and lattice parameters of $Mg_3Al_{1-x}Cr_x$ layered double hydroxides (LDHs) calculated by the Le Bail method.

Sample	d (003), Å	d (006), Å	d (110), Å	Lattice Parameters, Å	
				a	c
Mg-Al	7.6033	3.8017	1.5187	3.0374	22.8100
Mg-Al/Cr 1 mol%	7.7470	3.8735	1.5242	3.0484	23.2408
Mg-Al/Cr 5 mol%	7.7748	3.8876	1.5276	3.0551	23.3248
Mg-Al/Cr 7.5 mol%	7.8028	3.9015	1.5314	3.0627	23.4094
Mg-Al/Cr 10 mol%	7.8373	3.9187	1.5367	3.0733	23.5122
Mg-Al/Cr 25 mol%	7.8774	3.9475	1.5579	3.1158	23.6586

As seen from Table 1, the calculated lattice parameters also monotonically increased with increasing amounts of chromium: from 3.0374 to 3.1158 Å (a parameter) and from 22.8100 to 23.6586 Å (c parameter) with increasing amounts of chromium from 0% to 25%, respectively.

The FT-IR spectra of Cr-substituted $Mg_3Al_{1-x}Cr_x$ LDHs are presented in Figure 2.

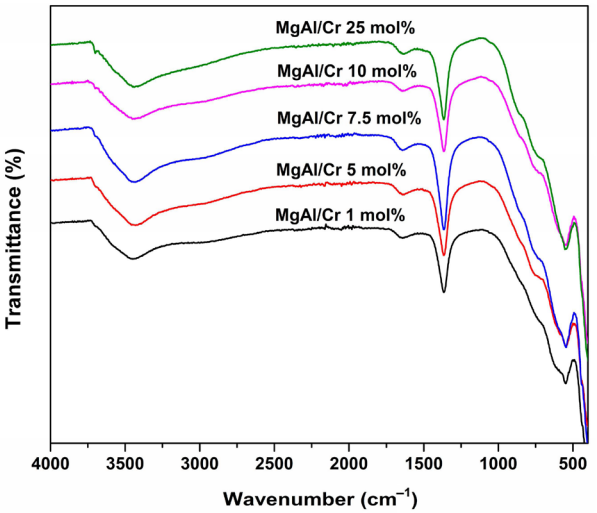

Figure 2. The Fourier transform infrared (FT-IR) spectra of Cr-substituted $Mg_3Al_{1-x}Cr_x$ LDHs.

Figure 2 clearly shows that all IR spectra were almost identical, i.e., independent of the chromium substitution level. The broad absorption bands visible in the range of 3650–3250 cm^{-1} could be attributed to the stretching vibrations of hydroxyl (-OH) groups and water molecules located between the layers in the LDH crystal structure [43]. The low-intensity bands observed at 1630–1600 cm^{-1} confirmed the presence of adsorbed molecular water on the surface of sol-gel-derived LDHs. The intense absorption bands located at about 1350 cm^{-1} could be attributed to the asymmetric vibration modes of carbonate ions (CO_3^{2-}) [43]. Finally, the pronounced absorption bands observed at about 600 and 480 cm^{-1} were attributable to metal–oxygen vibrations [11,43]. These results are in a good agreement with X-ray diffraction (XRD) analysis data confirming the formation of Cr-substituted $Mg_3Al_{1-x}Cr_x$ LDHs. Similar results were observed during FT-IR studies of sol-gel-derived $Mg_3Al_{1-x}Cr_x$ [4] or $Mg_{2-x}M_x/Al_1$ (M = Ca, Sr, Ba) [41] LDH samples.

SEM micrographs of Cr-substituted $Mg_3Al_{1-x}Cr_x$ LDHs prepared by the sol-gel method are depicted in Figure 3. Again, the surface microstructure of sol-gel-derived $Mg_3Al_{1-x}Cr_x$ LDHs did not depend on the chromium substitution level. Moreover, the characteristic features of LDHs could be observed in all presented SEM micrographs [4,9,11,28–30,41,43]. The formation of plate-like agglomerated particles, which consist of hexagonally shaped nanocrystallites varying in size from approximately 200 to 300 nm, was observed.

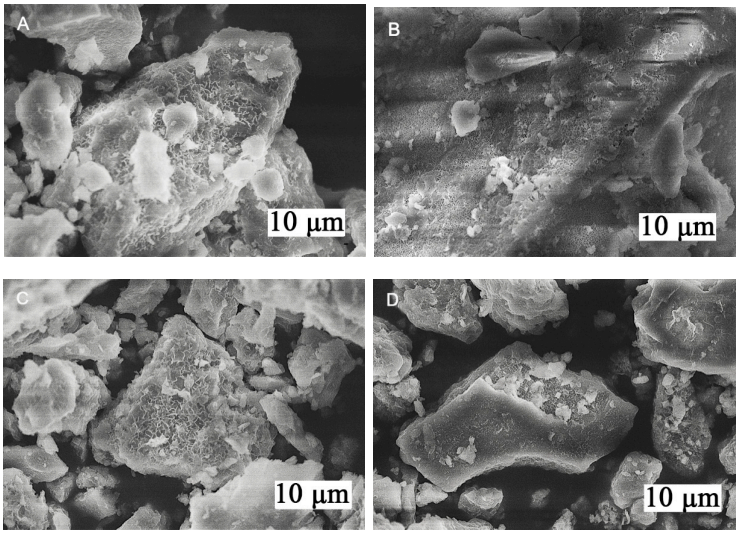

Figure 3. Scanning electron microscope (SEM) micrographs of Cr-substituted $Mg_3Al_{1-x}Cr_x$ LDHs. The amount of Cr in mol%: (**A**) 1, (**B**) 5, (**C**) 10 and (**D**) 25. The scale bars are the lengths of rectangles.

Elemental analysis of synthesised Cr-substituted $Mg_3Al_{1-x}Cr_x$ LDHs was performed prior to investigation of luminescent properties. ICP-OES and EDX were used for the determination of chromium, magnesium and aluminium in the synthesised LDH samples. The results of elemental analysis are presented in Table 2. The summarised results indicate that the molar ratios of Mg, Al and introduced amounts of Cr are in a good agreement with those obtained by both analysis methods and coincide with nominal ones.

Table 2. Inductively coupled plasma–optical emission spectrometry (ICP-OES) and the energy-dispersive X-ray (EDX) analysis results of elemental analysis of synthesised $Mg_3Al_{1-x}Cr_x$ LDHs (n is mole).

Sample	ICP-OES		EDX	
	n(Cr), %	n(Mg):n(Al + Cr)	n(Cr), %	n(Mg):n(Al + Cr)
Mg-Al/Cr 1 mol%	1.12	3:0.994	1.43	3:0.993
Mg-Al/Cr 5 mol%	5.39	3:0.990	7.22	3:1.06
Mg-Al/Cr 7.5 mol%	7.91	3:0.988	7.77	3:1.02
Mg-Al/Cr 10 mol%	10.5	3:0.997	12.9	3:0.875
Mg-Al/Cr 25 mol%	25.8	3:1.01	26.3	3:1.02

Thus, this study for the first time demonstrated that the previously developed sol-gel technique is suitable for the preparation of Cr-substituted LDHs.

The reflection spectra of $Mg_3Al_{1-x}Cr_x$ LDHs as a function of Cr^{3+} concentration are given in Figure 4a. All the spectra contained two broad absorption bands with maxima at ca. 550 and 380 nm. These bands could be assigned to the Cr^{3+} optical transitions of $^4A_{2g} \rightarrow {}^4T_{2g}(^4F)$ and $^4A_{2g} \rightarrow {}^4T_{1g}(^4F)$, respectively [44,45]. The increase in the Cr^{3+} concentration in the samples resulted in increased absorption.

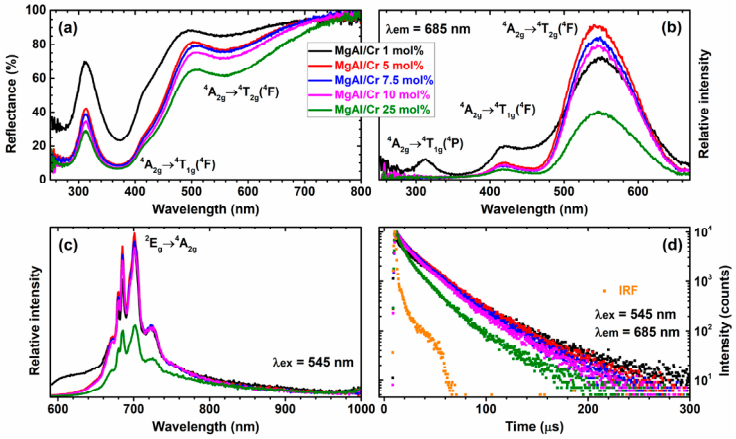

Figure 4. Reflection (**a**), excitation (**b**), emission (**c**) and photoluminescence (PL) emission decay curves (**d**) of $Mg_3Al_{1-x}Cr_x$ LDHs as a function of Cr^{3+} concentration. Instrument response function (IRF) in section (**d**) stands for instrument response function.

Excitation spectra (λ_{em} = 685 nm) of the synthesised specimens are shown in Figure 4b. Similar to the reflection spectra, there were several broad bands in the excitation spectra as well. One band possessed the maximum at ca. 545 nm and was attributed to the $^4A_{2g}\rightarrow{}^4T_{2g}(^4F)$ optical transition, whereas the other band peaked at ca. 420 nm and could be assigned to the $^4A_{2g}\rightarrow{}^4T_{1g}(^4F)$ optical transition of Cr^{3+} ions. It is interesting to note that excitation spectrum of the 1% Cr^{3+}-doped sample (Mg-Al/Cr 1 mol%) contained the third band at ca. 310 nm. This band arose from the $^4A_{2g}\rightarrow{}^4T_{1g}(^4P)$ transitions of Cr^{3+} ions.

Emission spectra of $Mg_3Al_{1-x}Cr_x$ LDHs samples are depicted in Figure 4c. There were several relatively sharp emission lines in the range of 660–740 nm that could be assigned to the $^2E_g\rightarrow{}^4A_{2g}$ optical transition of Cr^{3+} ions. The strongest emission was observed for the sample doped with 5% Cr^{3+} ions. Surprisingly, the highest intensity of the $^5D_0\rightarrow{}^7F_2$ transition for $Mg_3Al_{1-x}Ce_x$ LDHs was observed for the specimen with 0.05 mol% of Ce^{3+} [4]. It turned out that the emission intensity decreased with increasing concentration of Ce^{3+} up to 1 mol%. In the case of $Mg_3Al_{1-x}Nd_x$ LDHs, the luminescence of Nd^{3+} was observed only with intercalation of terephthalate in the interlayer spacing [29].

However, the emission intensity of samples doped with 1–10% Cr^{3+} was relatively similar. A further increase in the Cr^{3+} concentration to 25% resulted in severe concentration quenching. These results correlate with $Mg_3Al_{1-x}Cr_x$ LDHs' PL decay curves given in Figure 4d. The PL decay curves of samples doped with 1% to 10% Cr^{3+} were packed close together, indicating similar PL lifetime values. This was not, however, true for the PL decay curve of samples doped with 25% Cr^{3+}. This curve was much steeper, indicating lower PL lifetime values. The effective PL lifetime values were calculated according to the following equation [46]:

$$\tau_{eff} = \frac{\int_0^\infty I(t)tdt}{\int_0^\infty I(t)dt} \quad (1)$$

Here, *I(t)* is the PL intensity at the given time *t*. The obtained effective PL lifetime values (τ_{eff}) for 1%, 5%, 7.5%, 10% and 25% Cr^{3+}-doped samples were 23.0, 22.4, 20.6, 19.2 and 13.5 μs, respectively. Obviously, the τ_{eff} values gradually decreased with increasing Cr^{3+} concentration, which indicates that the internal efficiency of Cr^{3+} ions decreases as well. The results obtained clearly show that $Mg_3Al_{1-x}Cr_x$ LDHs are suitable for electro-

optical application. For instance, the material can be potentially applied as a red light-emitting diode (LED) [47]. Besides, these compounds show potential as imaging systems for biomedical applications.

3. Materials and Methods

3.1. Materials

For the synthesis of Cr-substituted $Mg_3Al_{1-x}Cr_x$ LDH samples, aluminium nitrate nonahydrate ($Al(NO_3)_3{\cdot}9H_2O$, 98.5%, Chempur, Plymouth, MI, USA), magnesium nitrate hexahydrate ($Mg(NO_3)_2{\cdot}6H_2O$), 99.0%, Chempur, Plymouth, MI, USA) and chromium nitrate nonahydrate ($Cr(NO_3)_3{\cdot}9H_2O$, 99.0%, Aldrich, Darmstadt, Germany) were used as starting materials. Citric acid ($C_6H_8O_7{\cdot}H_2O$, 99.5%, Chempur, Plymouth, MI, USA) and 1,2-ethanediol ($C_2H_6O_2$, 99.8%, Chempur, Plymouth, MI, USA) were used as complexing agents. The reconstruction of MMO powders to LDHs was performed in distilled water.

3.2. Synthesis

Cr-substituted $Mg_3Al_{1-x}Cr_x$ LDH samples (x = 0.0, 0.01, 0.05, 0.075, 0.1 and 0.25) were synthesised using $Al(NO_3)_3{\cdot}9H_2O$, $Mg(NO_3)_2{\cdot}6H_2O$ and $Cr(NO_3)_3{\cdot}9H_2O$. The aqueous solution of starting materials was mixed with 0.2 M solution of citric acid and 2 mL of 1,2-ethanediol under continuous stirring at 80 °C for 1 h. Next, the temperature of the magnetic stirrer was raised to 150 °C until complete evaporation of the solvent. The obtained gels were kept at 105 °C for 24 h. Mixed-metal oxides (MMOs) were obtained by calcination of the gels at 650 °C for 4 h. $Mg_3Al_{1-x}Cr_x$ LDHs were obtained by reconstruction of MMOs powders in distilled water at 50 °C for 6 h under stirring. The schematic representation of the sol-gel processing is illustrated in Figure 5.

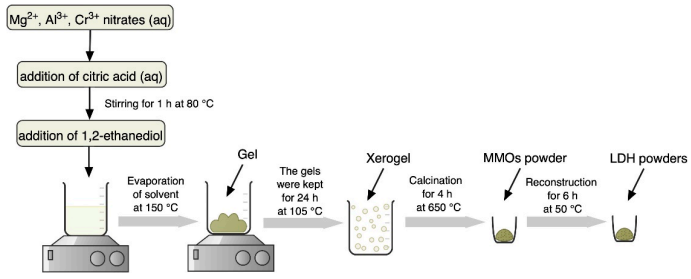

Figure 5. Schematic diagram of the sol-gel preparation of $Mg_3Al_{1-x}Cr_x$ layered double hydroxides (LDHs).

3.3. Characterisation

For characterisation of the phase purity of the synthesised materials, powder X-ray diffraction (XRD) analysis was performed in the 2θ range from 10° to 70° (step size of 0.02°) with a scanning speed of 2°/min using a MiniFlex II diffractometer (Rigaku, the Woodlands, TX, USA) (Cu Kα radiation). The size of crystallites was calculated by the Scherrer equation:

$$\tau = \frac{0.9\lambda}{B\cos\theta} \quad (2)$$

where τ is the mean crystallite size, λ is the X-ray wavelength, B is the line broadening of full width at half maximum (FWHM) intensity and θ is the Bragg angle. Fourier transform infrared (FT-IR) spectra were collected using an Alpha spectrometer (Bruker, Inc., Billerica, MA, USA). All spectra were recorded at ambient temperature in the range of 4000–480 cm^{-1}. The operational mode was transmittance (%). The morphology of synthesised LDH samples was investigated using a scanning electron microscope (SEM) (Hitachi SU-70, Tokyo, Japan). The energy-dispersive X-ray (EDX) analysis of the speci-

mens was performed using a SEM Hitachi TM 3000. The reflection, photoluminescence emission (PL) and excitation (PLE) spectra were recorded on an Edinburg Instruments FLS980 modular spectrometer (Edinburgh Instruments Ltd., Kirkton Campus, Livingstone UK). The spectrometer was equipped with a 450 W Xe lamp (Edinburgh Instruments Ltd., Kirkton Campus, Livingstone, UK) as an excitation source, a cooled (−20 °C) photomultiplier (Hamamatsu, Iwata, Japan) (R928P) and double-grating excitation and emission monochromators. Both excitation and emission spectra were corrected for the instrument spectral response. Elemental analysis of the synthesised samples was performed by inductively coupled plasma–optical emission spectrometry (ICP-OES) using an Optima 7000DV spectrometer (Perkin-Elmer, Waltham, MA, USA). The samples were dissolved in 5% nitric acid (HNO_3, Rotipuran® Supra 69%, Carl Roth) and diluted to an appropriate volume. Calibration solutions were prepared by an appropriate dilution of stock standard solutions (single-element ICP standards 1000 mg/L, Carl Roth, Karlsruhe, Germany).

4. Conclusions

In conclusion, $Mg_3Al_{1-x}Cr_x$ layered double hydroxides (LDHs) within the substitution range of chromium from 1 to 25 mol% were successfully synthesised for the first time by an aqueous sol-gel processing route. XRD analysis and FT-IR spectroscopy results confirmed that the synthesised $Mg_3Al_{1-x}Cr_x$ LDHs were predominant crystalline phases in the end products. The calculated values of d-spacing and lattice parameters of $Mg_3Al_{1-x}Cr_x$ LDHs slightly increased with increasing amounts of chromium. The sol-gel-derived $Mg_3Al_{1-x}Cr_x$ LDHs consisted of characteristic hexagonally shaped nanoparticles 200–300 nm in size regardless of the chromium substitution level. All Cr-containing powders exhibited characteristic emission in the red region of the visible spectrum. The major emission lines of $Mg_3Al_{1-x}Cr_x$ LDHs excited at 545 nm peaked in the red spectral region at 680–695 nm, originating from the $^2E_g \rightarrow {}^4A_2$ transition. The highest intensity of emission was observed for the $Mg_3Al_{1-x}Cr_x$ LDH specimen containing 5% of Cr^{3+}. With further increasing the chromium content up to 25%, concentration quenching was observed. Concentration quenching was also confirmed by the calculated PL effective lifetime values (τ_{eff}), which decreased from 22.4 μs for the 5% Cr^{3+}-doped sample to 13.5 μs for the 25% Cr^{3+}-doped sample.

Author Contributions: Conceptualisation, L.V. and A.K. (Aivaras Kareiva); methodology, L.V.; formal analysis, L.V., I.G.-P., A.Z. and A.K. (Arturas Katelnikovas); investigation, L.V., I.G.-P., A.Z. and A.K. (Arturas Katelnikovas); resources, A.K. (Aivaras Kareiva); writing—original draft preparation, L.V.; writing—review and editing, A.K. (Aivaras Kareiva); funding acquisition, A.K. (Aivaras Kareiva). All authors have read and agreed to the published version of the manuscript.

Funding: This work was supported by the research grant NEGEMAT (No. S-MIP-19-59) from the Research Council of Lithuania.

Institutional Review Board Statement: Not applicable.

Informed Consent Statement: Not applicable.

Data Availability Statement: Data is contained within the article.

Conflicts of Interest: The authors declare no conflict of interest.

Sample Availability: Samples of the compounds are available from the authors.

References

1. Mishra, G.; Dash, B.; Pandey, S. Layered double hydroxides: A brief review from fundamentals to application as evolving biomaterials. *Appl. Clay Sci.* **2018**, *153*, 172–186. [CrossRef]
2. Arrabito, G.; Bonasera, A.; Prestopino, G.; Orsini, A.; Mattoccia, A.; Martinelli, E.; Pignataro, B.; Medaglia, P.G. Layered Double Hydroxides: A Toolbox for Chemistry and Biology. *Crystals* **2019**, *9*, 361. [CrossRef]
3. Mohapatra, L.; Parida, K. A review on the recent progress, challenges and perspective of layered double hydroxides as promising photocatalysts. *J. Mater. Chem. A* **2016**, *4*, 10744–10766. [CrossRef]

4. Smalenskaite, A.; Vieira, D.E.L.; Salak, A.N.; Ferreira, M.G.S.; Katelnikovas, A.; Kareiva, A. A comparative study of co-precipitation and sol-gel synthetic approaches to fabricate cerium-substituted Mg-Al layered double hydroxides with luminescence properties. *Appl. Clay Sci.* **2017**, *143*, 175–183. [CrossRef]
5. Modrogan, C.; Caprarescu, S.; Dancila, A.M.; Orbulet, O.D.; Vasile, E.; Purcar, V. Mixed oxide-layered double hydroxides materials: Synthesis, characterization and efficient application for Mn^{2+} removal from synthetic wastewater. *Materials* **2020**, *13*, 4089. [CrossRef] [PubMed]
6. Shi, M.; Zhao, Z.; Song, Y.; Xu, M.; Li, J.; Yao, L. A novel heat-treated humic acid/MgAl-layered double hydroxide composite for efficient removal of cadmium: Fabrication, performance and mechanisms. *Appl. Clay Sci.* **2020**, *187*, 105482. [CrossRef]
7. Zhang, S.; Kano, N.; Mishima, K.; Okawa, H. Adsorption and Desorption Mechanisms of Rare Earth Elements (REEs) by Layered Double Hydroxide (LDH) Modified with Chelating Agents. *Appl. Sci.* **2019**, *9*, 4805. [CrossRef]
8. Soliman, E.R.; Kotp, Y.H.; Souaya, E.R.; Guindy, K.A.; Ibrahim, R.G.M. Development the sorption behavior of nanocomposite Mg/Al LDH by chelating with different monomers. *Compos. Part B Eng.* **2019**, *175*, 107131. [CrossRef]
9. Sokol, D.; Salak, A.N.; Ferreira, M.G.S.; Beganskiene, A.; Kareiva, A. Bi-substituted Mg3Al–CO3 layered double hydroxides. *J. Sol-Gel Sci. Technol.* **2018**, *85*, 221–230. [CrossRef]
10. Vieira, D.E.L.; Sokol, D.; Smalenskaite, A.; Kareiva, A.; Ferreira, M.G.S.; Vieira, J.M.; Salak, A.N. Cast iron corrosion protection with chemically modified Mg-Al layered double hydroxides synthesized using a novel approach. *Surf. Coat. Technol.* **2019**, *375*, 158–163. [CrossRef]
11. Valeikiene, L.; Paitian, R.; Grigoraviciute-Puroniene, I.; Ishikawa, K.; Kareiva, A. Transition metal substitution effects in sol-gel derived $Mg_{3-x}M_x/Al_1$ (M = Mn, Co, Ni, Cu, Zn) layered double hydroxides. *Mater. Chem. Phys.* **2019**, *237*, 121863. [CrossRef]
12. Szabados, M.; Adél Ádám, A.; Traj, P.; Muráth, S.; Baán, K.; Bélteky, P.; Kónya, Z.; Kukovecz, Á.; Sipos, P.; Pálinkó, I. Mechanochemical and wet chemical syntheses of CaIn-layered double hydroxide and its performance in a transesterification reaction compared to those of other Ca2M(III) hydrocalumites (M: Al, Sc, V, Cr, Fe, Ga) and Mg(II)-, Ni(II)-, Co(II)- or Zn(II)-based hydrotalcites. *J. Catal.* **2020**, *391*, 282–297. [CrossRef]
13. Kooli, F.; Rives, V.; Ulibarri, M.A. Preparation and Study of Decavanadate-Pillared Hydrotalcite-like Anionic Clays Containing Transition Metal Cations in the Layers. 2. Samples containing Magnesium-Chromium and Nickel-Chromium. *Inorg. Chem.* **1995**, *34*, 5122–5128. [CrossRef]
14. Kooli, F.; Martín, C.; Rives, V. FT-IR Spectroscopy Study of Surface Acidity and 2-Propanol Decomposition on Mixed Oxides Obtained upon Calcination of Layered Double Hydroxides. *Langmuir* **1997**, *13*, 2303–2306. [CrossRef]
15. Bouteraa, S.; Saiah, F.B.D.; Hamouda, S.; Bettahar, N. Zn-M-CO3 Layered Double Hydroxides (M=Fe, Cr, or Al): Synthesis, Characterization, and Removal of Aqueous Indigo Carmine. *Bull. Chem. React. Eng. Catal.* **2020**, *15*, 43–54. [CrossRef]
16. Oktrianty, M.; Palapa, N.R.; Mohadi, R.; Lesbani, A. Effective Removal of Iron (II) from Aqueous Solution by Adsorption using Zn/Cr Layered Double Hydroxides Intercalated with Keggin Ion. *J. Ecolog. Eng.* **2020**, *21*, 63–71. [CrossRef]
17. Mohapatra, L.; Parida, K.M. Zn–Cr layered double hydroxide: Visible light responsive photocatalyst for photocatalytic degradation of organic pollutants. *Sep. Purif. Technol.* **2012**, *91*, 73–80. [CrossRef]
18. Baliarsingh, N.; Parida, K.M.; Pradhan, G.C. Effects of Co, Ni, Cu, and Zn on Photophysical and Photocatalytic Properties of Carbonate Intercalated MII/Cr LDHs for Enhanced Photodegradation of Methyl Orange. *Ind. Eng. Chem. Res.* **2014**, *53*, 3834–3841. [CrossRef]
19. Tsyganok, A.I.; Inaba, M.; Tsunoda, T.; Uchida, K.; Suzuki, K.; Takehira, K.; Hayakawa, T. Rational design of Mg–Al mixed oxide-supported bimetallic catalysts for dry reforming of methane. *Appl. Catal. A Gen.* **2005**, *292*, 328–343. [CrossRef]
20. Nayak, S.; Pradhan, A.C.; Parida, K.M. Topotactic Transformation of Solvated MgCr-LDH Nanosheets to Highly Efficient Porous MgO/MgCr2O4 Nanocomposite for Photocatalytic H2 Evolution. *Inorg. Chem.* **2018**, *57*, 8646–8661. [CrossRef]
21. Liang, S.Y.; Ren, W.W.; Lin, W.X.; Zou, L.C.; Cui, X.P.; Chen, J.F. In-Situ Preparation of MgCr-LDH Nano-Layer on MAO Coating of Mg Alloy and Its Anti-Corrosion Mechanism. *Rare Metal Mater. Eng.* **2020**, *49*, 2830–2838.
22. Gunawan, P.; Xu, R. Lanthanide-Doped Layered Double Hydroxides Intercalated with Sensitizing Anions: Efficient Energy Transfer between Host and Guest Layers. *J. Phys. Chem. C* **2009**, *113*, 17206–17214. [CrossRef]
23. Domínguez, M.; Pérez-Bernal, M.E.; Ruano-Casero, R.J.; Barriga, C.; Rives, V.; Ferreira, R.A.S.; Carlos, L.D.; Rocha, J. Multiwavelength Luminescence in Lanthanide-Doped Hydrocalumite and Mayenite. *Chem. Mater.* **2011**, *23*, 1993–2004. [CrossRef]
24. Posati, T.; Costantino, F.; Latterini, L.; Nocchetti, M.; Paolantoni, M.; Tarpani, L. New Insights on the Incorporation of Lanthanide Ions into Nanosized Layered Double Hydroxides. *Inorg. Chem.* **2012**, *51*, 13229–13236. [CrossRef]
25. Zhang, Z.; Chen, G.; Liu, J. Tunable photoluminescence of europium-doped layered double hydroxides intercalated by coumarin-3-carboxylate. *RSC Adv.* **2014**, *4*, 7991–7997. [CrossRef]
26. Gao, X.; Lei, L.; Kang, L.; Wang, Y.; Lian, Y.; Jiang, K. Synthesis, characterization and optical properties of a red organic–inorganic phosphor based on terephthalate intercalated Zn/Al/Eu layered double hydroxide. *J. Alloys Compd.* **2014**, *585*, 703–707. [CrossRef]
27. Vicente, P.; Pérez-Bernal, M.E.; Ruano-Casero, R.J.; Ananias, D.; Almeida Paz, F.A.; Rocha, J.; Rives, V. Luminescence properties of lanthanide-containing layered double hydroxides. *Micropor. Mesopor. Mater.* **2016**, *226*, 209–220. [CrossRef]
28. Smalenskaite, A.; Salak, A.N.; Ferreira, M.G.S.; Skaudzius, R.; Kareiva, A. Sol-gel synthesis and characterization of hybrid inorganic-organic Tb(III)-terephthalate containing layered double hydroxides. *Opt. Mater.* **2018**, *80*, 186–196. [CrossRef]
29. Smalenskaite, A.; Salak, A.N.; Kareiva, A. Induced neodymium luminescence in sol-gel derived layered double hydroxides. *Mendeleev Commun.* **2018**, *28*, 493–494. [CrossRef]

30. Smalenskaite, A.; Pavasaryte, L.; Yang, T.C.K.; Kareiva, A. Undoped and Eu3+ Doped Magnesium-Aluminium Layered Double Hydroxides: Peculiarities of Intercalation of Organic Anions and Investigation of Luminescence Properties. *Materials* **2019**, *12*, 736. [CrossRef]
31. Shirotori, M.; Nishimura, S.; Ebitani, K. Genesis of a bi-functional acid–base site on a Cr-supported layered double hydroxide catalyst surface for one-pot synthesis of furfurals from xylose with a solid acid catalyst. *Catal. Sci. Technol.* **2016**, *6*, 8200–8211. [CrossRef]
32. Melo, F.; Morlanés, N. Study of the composition of ternary mixed oxides: Use of these materials on a hydrogen production process. *Catal. Today* **2008**, *133–135*, 374–382. [CrossRef]
33. Rodriguez-Rivas, F.; Pastor, A.; de Miguel, G.; Cruz-Yusta, M.; Pavlovic, I.; Sánchez, L. Cr3+ substituted Zn-Al layered double hydroxides as UV–Vis light photocatalysts for NO gas removal from the urban environment. *Sci. Total Environ.* **2020**, *706*, 136009. [CrossRef]
34. Correcher, V.; Garcia-Guinea, J. Cathodo- and photoluminescence emission of a natural Mg-Cr carbonate layered double hydroxide. *Appl. Clay Sci.* **2018**, *161*, 127–131. [CrossRef]
35. Ishikawa, K.; Garskaite, E.; Kareiva, A. Sol–gel synthesis of calcium phosphate-based biomaterials-A review of environmentally benign, simple, and effective synthesis routes. *J. Sol-Gel Sci. Technol.* **2020**, *94*, 551–572. [CrossRef]
36. Karoblis, D.; Zarkov, A.; Mazeika, K.; Baltrunas, D.; Niaura, G.; Beganskiene, A.; Kareiva, A. Sol-gel synthesis, structural, morphological and magnetic properties of BaTiO3–BiMnO3 solid solutions. *Ceram. Int.* **2020**, *46*, 16459–16464. [CrossRef]
37. Grigorjevaite, J.; Janulevicius, M.; Kruopyte, A.; Ezerskyte, E.; Vargalis, R.; Sakirzanovas, S.; Katelnikovas, A. Synthesis and optical properties of efficient orange emitting GdB5O9:Sm3+ phosphors. *J. Sol-Gel Sci. Technol.* **2020**, *94*, 80–87. [CrossRef]
38. Pakalniskis, A.; Marsalka, A.; Raudonis, R.; Balevicius, V.; Zarkov, A.; Skaudzius, R.; Kareiva, A. Sol-gel synthesis and study of praseodymium substitution effects in yttrium aluminium garnet Y3-xPrxAl5O12. *Opt. Mater.* **2021**, *111*, 110586. [CrossRef]
39. Jitianu, M.; Zaharescu, M.; Bălăsoiu, M.; Jitianu, A. The Sol-Gel Route in Synthesis of Cr(III)-Containing Clays. Comparison Between Mg-Cr and Ni-Cr Anionic Clays. *J. Sol-Gel Sci. Technol.* **2003**, *26*, 217–221. [CrossRef]
40. Saikia, P.; Gautam, A.; Goswamee, R.L. Synthesis of nanohybrid alcogels of SiO2 and Ni–Cr/Mg–Cr–LDH: Study of their rheological and dip coating properties. *RSC Adv.* **2016**, *6*, 112092–112102. [CrossRef]
41. Valeikiene, L.; Grigoraviciute-Puroniene, I.; Kareiva, A. Alkaline earth metal substitution effects in sol-gel–derived mixed metal oxides and Mg2-xMx/Al1 (M = Ca, Sr, Ba)–layered double hydroxides. *J. Austral. Ceram. Soc.* **2020**, *56*, 1531–1541. [CrossRef]
42. Shannon, R.D. Revised Effective Ionic Radii and Systematic Studies of Interatomic Distances in Halides and Chalcogenides. *Acta Crystallogr.* **1976**, *A32*, 751–767. [CrossRef]
43. Smalenskaite, A.; Sen, S.; Salak, A.N.; Ferreira, M.G.S.; Skaudzius, R.; Katelnikovas, A.; Kareiva, A. Sol-Gel Synthesis and Characterization of Non-Substituted and Europium-Substituted Layered Double Hydroxides Mg3/Al1-xEux. *Current Inorg. Chem.* **2016**, *6*, 149–154. [CrossRef]
44. Blasse, G.; Grabmaier, B.C. *Luminescent Materials*; Springer: Berlin, Germany, 1994; p. 232.
45. Yen, W.M.; Shionoya, S.; Yamamoto, H. *Fundamentals of Phosphors*; CRC Press: Boca Raton, FL, USA, 2007; p. 335.
46. Lahoz, F.; Martín, I.R.; Méndez-Ramos, J.; Núñez, P. Dopant distribution in a Tm3+-Yb3+ codoped silica based glass ceramic: An infrared-laser induced upconversion study. *J. Chem. Phys.* **2004**, *120*, 6180–6190. [CrossRef]
47. Zhu, L.L.; Hao, C.; Wang, X.H.; Guo, Y.N. Fluffy Cotton-Like GO/Zn-Co-Ni Layered Double Hydroxides Form from a Sacrificed Template GO/ZIF-8 for High Performance Asymmetric Supercapacitors. *ACS Sustain. Chem. Eng.* **2020**, *8*, 11618–11629. [CrossRef]

Vilnius University Press
9 Saulėtekio Ave., Building III, LT-10222 Vilnius
Email: info@leidykla.vu.lt, www.leidykla.vu.lt
Print run copies 20

Disertacijos anotacija

Naujų sluoksniuotų dvigubų hidroksidų sintezė, modifikavimas ir savybių tyrimas

Sluoksniuoti dvigubi hidroksidai (SDH) sulaukia didelio mokslininkų bendruomenės susidomėjimo dėl plačių taikymo galimybių katalizėje, fotochemijoje, elektrochemijoje, biomedicinos moksle, aplinkos apsaugoje, optikoje ir kt.. SDH priklauso anijoninių molžemių šeimai. Yra žinomi kaip hidrotalcito tipo junginiai, susidedantys iš teigiamą krūvį turinčių brusito ($Mg(OH)_2$) tipo sluoksnių. SDH bendra cheminė formulė gali būti užrašyta $[M^{2+}_{1-x}M^{3+}_x(OH)_2]^{x+}(A^{y-})_{x/y}\cdot zH_2O$, kurioje M^{2+} ir M^{3+} yra atitinkamai metalų katijonai, kurių oksidacijos laipsnis yra +2 ir +3. A^{y-} yra neorganinis (pvz., karbonatas, hidroksidas, nitratas, halogenidas, sulfatas, chromatas, vanadatas) arba organinis (pav. karbokslilatai ir kt.) anijonai, tarpsluoksnyje išsidėstęs kartu su vandens molekulėmis.

Termiškai skaidant SDH susidaro M^{2+} ir M^{3+} mišrūs metalų oksidai arba tų oksidų mišinys (MMO). MMO pasižymi dideliu paviršiaus plotu ir “atminties efektu” – unikalia savybe, kurios dėka, pašildžius MMO vandenyje, atsistato prieš terminį skaidymą buvusi sluoksniuota dvigubo hidroksido struktūra.

SDH sintetinamas įvairiais metodais. Dažniausiai naudojamas bendrojo nusodinimo metodas, kuris vykdomas sumaišant tirpiąsias metalų, sudarančių sluoksniuotą hidroksidą, druskas. Kita plačiai taikoma SDH sintezės technika yra anijonų mainų metodas, kurio metu tarpsluoksnyje esantis anijonas pakeičiamas kitu (vyksta intrerkaliacija). Dėl savo prigimtimi skirtingų anijonų įterpimo į SDH kristalinę struktūrą, keičiasi sluoksniuoto hidroksido cheminės ir fizikinės savybės. Daugybėje mokslinių publikacijų parodyta, kad zolių-gelių metodas yra labai patrauklus preparatyvinis sintezės būdas daugiakomponentėms medžiagoms gauti. Neseniai buvo sukurtas netiesioginis zolių-gelių sintezės metodas, leidžiantis pagaminti aukšto grynumo SDH. Sintezės zolių-gelių metodu gauti pradiniai pirmtakų geliai yra kaitinami 650 °C temperatūroje, o susidarę MMO yra atstatomi (rekonstruojami) dejonizuotame vandenyje 80 °C temperatūroje. Šis zolių-gelių

sintezės metodas, palyginti su bendrojo nusodinimo metodu, yra paprastesnis, gauti produktai yra homogeniškesni ir pasižymi aukštu kristališkumu.

Šio disertacinio darbo tikslas yra susintetinti naujus Mg/Al sluoksniuotus dvigubus hidroksidus ir, modifikuojant jų cheminę sudėtį, ištirti katijonų ir anijonų pakaitų įtaką galutinių produktų susidarymui bei gautų SDH savybėms. Šiam tikslui pasiekti buvo iškelti uždaviniai: Ištirti zolių-gelių metodu susintetintų $Mg_{3-x}M_x/Al_1$ (M = Mn, Co, Ni, Cu, Zn) SDH pakeitimo pereinamųjų metalų jonais galimybes.

Ištirti zolių-gelių metodu susintetintų $Mg_{2-x}M_x/Al_1$ (M = Ca, Sr, Ba) SDH ir atitinkamų MMO pakeitimo šarminių žemių metalų jonais galimybes. Ištirti susintetintų $Mg_{2-x}M_x/Al_1$ (M = Ca, Sr, Ba) SDH rekonstrukcijos ypatumus.

Ištirti ultragarso ir katijonų (Mn, Co, Ni, Cu, Zn) pakeitimo įtaką organinių anijonų (formiatas ($HCOO^-$), acetatas (CH_3COO^-), oksalatas ($C_2O_4^{2-}$), tartratas ($C_4H_6O_4^{2-}$) ir citratas ($C_6H_5O_7^{3-}$) įterpimo į Mg_3/Al_1 SDH struktūrą galimybėms.

Susintetinti $Mg_3Al_{1-x}Cr_x$ SDH mėginius zolių-gelių metodu ir ištirti Cr^{3+} poveikį gautų mėginių faziniam grynumui, morfologinėms ir liuminescencinėms savybėms.

Disertaciją sudaro įvadas, penki skyriai ir bendrosios išvados. Pirmame skyriuje aptariamos zolių-gelių metodu susintetintų $Mg_{3-x}M_x/Al_1$ (M = Mn, Co, Ni, Cu, Zn) SDH pakeitimo pereinamųjų metalų jonais galimybės. Antrame skyriuje analizuojami ištirtų zolių-gelių metodu susintetintų $Mg_{2-x}M_x/Al_1$ (M = Ca, Sr, Ba) SDH ir atitinkamų MMO pakeitimo šarminių žemių metalų jonais galimybės.Trečiame skyriuje kalbama apie susintetintų $Mg_{2-x}M_x/Al_1$ (M = Ca, Sr, Ba) SDH rekonstrukcijos ypatumus. Ketvirtame skyriuje aptariama ultragarso ir katijonų (Mn, Co, Ni, Cu, Zn) pakeitimo įtaka organinių anijonų (formiatas ($HCOO^-$), acetatas (CH_3COO^-), oksalatas ($C_2O_4^{2-}$), tartratas ($C_4H_6O_4^{2-}$) ir citratas ($C_6H_5O_7^{3-}$) įterpimo į Mg_3/Al_1 SDH struktūrą galimybėms. Penktame skyriuje aptariamas ir ištirtas Cr^{3+} poveikis susintetintų $Mg_3Al_{1-x}Cr_x$ SDH mėginių zolių-gelių metodu gautų mėginių faziniam grynumui, morfologinėms ir liuminescencinėms savybėms.

Šio darbo naujumas ir originalumas: Buvo ištirtos zolių-gelių sintezės metodu susintetintų pereinamųjų metalų $Mg_{3-x}M_x/Al_1$ (M = Mn, Co, Ni, Cu, Zn) SDH, šarminių žemių metalų $Mg_{2-x}M_x/Al_1$ (M = Ca, Sr, Ba) SDH (ir atitinkamų MMO) pakeitimo galimybės. Išanalizuoti Mg(M)–Al (M = Ca, Sr, Ba) MMO rekonstrukcijos

ypatumai. Ištirta ultragarso ir katijonų (Mn, Co, Ni, Cu, Zn) pakeitimo įtaka organinių anijonų (formiato ($HCOO^-$), acetato (CH_3COO^-), oksalato ($C_2O_4^{2-}$), tartrato ($C_4H_6O_4^{2-}$) ir citrato ($C_6H_5O_7^{3-}$)) į Mg_3/Al_1 SDH struktūrą įterpimui. Pirmą kartą zolių-gelių metodu buvo susintetinti $Mg_3Al_{1-x}Cr_x$ SDH mėginiai. Ištirta Cr^{3+} įtaka gautų mėginių faziniam grynumui, morfologinėms ir liuminescencinėms savybėms.

Pagrindiniai disertacijos rezultatai paskelbti 4 moksliniuose straipsniuose, rezultatai viešinti 7 mokslinėse konferencijose.

Dissertation annotation

Synthesis of new layered double hydroxides, modification and investigation of properties

Recently layered double hydroxides (LDHs) have attracted substantial attention due to a wide range of important application areas, e.g. catalysis, photochemistry, electrochemistry, magnetization, biomedical science, environmental applications, and optics. A general chemical formula of the LDHs can be expressed as $[M^{2+}_{1-x}M^{3+}_{x}(OH)_2]^{x+}(A^{y-})_{x/y}\cdot zH_2O$, where M^{2+} (Mg, Zn, Co, Ni, Cu, Mn, . . .) and M^{3+} (Al, Ga, Cr, Co, Fe, V, Y, Mn, . . .) are divalent and trivalent metal cations, respectively, and A^{y-} is an intercalated anion which is located in the interlayer spaces along with water molecules and compensates the positive charge created by the partial substitution of M^{2+} by M^{3+} in a positively charged metal hydroxide layers. LDHs exhibit excellent ability to adopt organic and inorganic anions.

LDHs can be fabricated by different synthesis methods. The most common preparation technique is co-precipitation method starting from soluble salts of the metals. The most common second technique for the preparation of LDHs is anion-exchange. The indirect sol-gel synthesis route for the preparation of LDHs recently was also developed. The synthesized precursor gels were converted to the mixed metal oxides (MMO) by heating the gels at 650 °C. The LDHs were fabricated by reconstruction of MMO in deionized water at 80 °C. The proposed sol-gel synthesis route for LDHs showed some benefits over the co-precipitation method such as simplicity, high homogeneity and good crystallinity of the end synthesis products, effectiveness, cost efficiency and suitability for different systems.

The aim of this PhD thesis was to synthesize new Mg-Al-based layered double hydroxides by modifying its chemical composition, to investigate cation and anion substitution effects on the formation of the end products and to investigate properties of obtained LDHs. To achieve this, the main tasks were formulated as follows: To investigate transition metal substitution effects in $Mg_{3-x}M_x/Al_1$ (M = Mn, Co, Ni, Cu, Zn) LDHs synthesized using the sol-gel chemistry approach. To investigate alkaline earth metal substitution effects in sol-gel derived $Mg_{2-x}M_x/Al_1$ (M = Ca, Sr, Ba) LDHs

and related mixed-metal oxides. To investigate the reconstruction peculiarities of sol-gel derived $Mg_{2-x}M_x/Al_1$ (M = Ca, Sr, Ba) LDHs. To investigate the influence of ultrasound and cation substitution (Mn, Co, Ni, Cu, Zn) on the intercalation of organic anions (formate ($HCOO^-$), acetate (CH_3COO^-), oxalate ($C_2O_4^{2-}$), tartrate ($C_4H_6O_4^{2-}$) and citrate ($C_6H_5O_7^{3-}$)) to the structure of Mg_3/Al_1 LDHs. To synthesize the $Mg_3Al_{1-x}Cr_x$ LDH samples using an aqueous sol-gel method and investigate effect of Cr^{3+} substitution on phase purity, morphological and luminescent properties of obtained end products.

The dissertation contains: introduction, five chapters and general conclusions. The first chapter investigates effect of transition metal substitution in $Mg_{3-x}M_x/Al_1$ (M = Mn, Co, Ni, Cu, Zn) LDHs synthesized using the sol-gel chemistry approach.

Iinvestigation of alkaline earth metal substitution effects in sol-gel derived $Mg_{2-x}M_x/Al_1$ (M = Ca, Sr, Ba) LDHs and related mixed-metal oxides is in the second chapter.

Results of the reconstruction peculiarities of sol-gel derived $Mg_{2-x}M_x/Al_1$ (M = Ca, Sr, Ba) LDHs are analyzed in the third chapter.

The influence of ultrasound and cation substitution (Mn, Co, Ni, Cu, Zn) on the intercalation of organic anions (formate ($HCOO^-$), acetate (CH_3COO^-), oxalate ($C_2O_4^{2-}$), tartrate ($C_4H_6O_4^{2-}$) and citrate ($C_6H_5O_7^{3-}$)) to the structure of Mg_3/Al_1 LDHs is discussed in the fourth chapter.

Analysis of the $Mg_3Al_{1-x}Cr_x$ LDH samples using an aqueous sol-gel method and investigation of ther effect of Cr^{3+} substitution on phase purity, morphological and luminescent properties of obtained end products are in the fifth chapter.

The novelty and originality of PhD thesis. The transition metal substitution effects in $Mg_{3-x}M_x/Al_1$ (M = Mn, Co, Ni, Cu, Zn) LDHs synthesized by sol-gel synthesis method were investigated. The alkaline earth metal substitution effects in $Mg_{2-x}M_x/Al_1$ (M = Ca, Sr, Ba) LDHs synthesized by sol-gel synthesis method were investigated. The reconstruction peculiarities of sol-gel derived $Mg_{2-x}M_x/Al_1$ (M = Ca, Sr, Ba) LDHs by changing proceeding conditions were investigated. The chromium-substituted

$Mg_3Al_{1-x}Cr_x$ LDH samples were fabricated using an aqueous sol-gel method and luminescent properties of obtained specimens were investigated.

The main results of the thesis were published in 4 scientific publications, the results were presented in 7 scientific conferences.